



UNIVERSIDADE FEDERAL DE SANTA CATARINA  
CENTRO DE CIÊNCIAS FÍSICAS E MATEMÁTICAS  
PROGRAMA DE PÓS-GRADUAÇÃO EM OCEANOGRAFIA

Antônia Pamela Yhaohannah de Lima

**AVALIAÇÃO DA CIRCULAÇÃO SUPERIOR DO ATLÂNTICO SUL, BASEADA  
EM MEDIÇÕES DIRETAS E MODELOS DE CIRCULAÇÃO**

Florianópolis  
2020

Antônia Pamela Yhaohannah de Lima

**AVALIAÇÃO DA CIRCULAÇÃO SUPERIOR DO ATLÂNTICO SUL, BASEADA  
EM MEDIÇÕES DIRETAS E MODELOS DE CIRCULAÇÃO**

Dissertação submetida ao Programa de Pós-Graduação  
em Oceanografia da Universidade Federal de Santa  
Catarina para a obtenção do título de mestre em  
oceanografia.

Orientador: Prof. Antonio Fernando Härter Fetter Filho,  
Dr.

Florianópolis

2020

**Ficha de identificação da obra elaborada pelo autor,  
através do Programa de Geração Automática da Biblioteca Universitária da UFSC.**

de Lima, Antônia Pamela Yhaohannah  
Avaliação da circulação superior do Atlântico Sul, baseada  
em medições diretas e modelos de circulação / Antônia Pamela  
Yhaohannah de Lima ; orientador, Antonio Fernando Härter  
Fetter Filho, 2020.  
88 p.

Dissertação (mestrado) - Universidade Federal de Santa  
Catarina, Centro de Ciências Físicas e Matemáticas,  
Programa de Pós-Graduação em Oceanografia, Florianópolis,  
2020.

Inclui referências.

1. Oceanografia. 2. Circulação de larga escala. 3.  
Variações sazonal e interdecadal. 4. Célula de Revolvimento  
Meridional do Atlântico. 5. Corrente do Brasil. I. Härter  
Fetter Filho, Antonio Fernando . II. Universidade Federal  
de Santa Catarina. Programa de Pós-Graduação em  
Oceanografia. III. Título.

Antônia Pamela Yhaohannah de Lima

**AVALIAÇÃO DA CIRCULAÇÃO SUPERIOR DO ATLÂNTICO SUL, BASEADA  
EM MEDIÇÕES DIRETAS E MODELOS DE CIRCULAÇÃO**

O presente trabalho em nível de mestrado foi avaliado e aprovado por banca examinadora composta pelos seguintes membros:

Prof. Renato Ramos Silva, Dr.

Universidade Federal de Santa Catarina

Jose Antonio Moreira Lima, Dr.

Centro de Pesquisa e Desenvolvimento Leopoldo Américo Miguêz de Mello

Certificamos que esta é a **versão original e final** do trabalho de conclusão que foi julgado adequado para obtenção do título de mestre em oceanografia.

---

Coordenação do Programa de Pós-Graduação

---

Prof. Antonio Fernando Härter Fetter Filho, Dr.

Orientador

Florianópolis, 2020

## AGRADECIMENTOS

À minha mãe Rose Lima, por ser meu alicerce nesta vida e pelo apoio incondicional às minhas decisões pessoais e profissionais. Por ter me ensinado a perseverar diante dos obstáculos e desafios, a lidar com as consequências das minhas escolhas e acima de tudo aprender com elas.

À Rafaela Cristiny, pelo companheirismo e paciência. Por todo incentivo, conselhos e suporte (psicológico e emocional), sua presença foi fundamental na fase de finalização do trabalho.

Aos amigos/irmãos Nirllem, Preta, Karine, Joice, Carina, Layse, Ana Beatriz, Eduardo, Karlla, Bella, Eva, Ary e Herbert, que apoiaram e possibilitaram minha vinda para Florianópolis, sempre me aconselhando e me mantendo firme no alcance dos meus objetivos.

Aos também oceanógrafos Gabriela, Leandro e Thiago, pelas discussões oceanográficas e de vida, que me acresceram como profissional e como ser humano.

Ao meu orientador, Prof. Antonio Fetter, por todos os ensinamentos, oportunidades, paciência, conversas e discussões. Por sempre acreditar no meu potencial e me incentivar a ser uma profissional melhor, sem sua participação essa pesquisa não teria acontecido.

Aos professores e doutores Antonio Klein, Arthur Antonio Machado, Jose Antonio Lima, Ricardo Matano, Renato Ramos e Luis Felipe Mendonça, por me auxiliar na construção e evolução das diversas fases dessa pesquisa.

Aos integrantes do Laboratório de Dinâmica dos Oceanos e do PPGOCEANO, por toda troca de conhecimento, apoio psicológico e hora do café, durante os últimos anos. Em especial, a Bruna, Micael, Theia, Cesar, Luana, Isadora, Pedro e Ana Paula. Cada conversa e revisão, tornaram este trabalho mais fácil.

Aos amigos e familiares que me acompanharam, torcendo pelo meu sucesso e se solidarizando com todas as dificuldades encontradas. Em especial aos meus avós e minhas tias Nilda e Creuza.

À Agência Nacional de Petróleo, Gás Natural e Biocombustíveis (ANP) e Petrobras pelo suporte financeiro através do Projeto “Monitoramento Sismológico e Oceanográfico de um Segmento na Margem Sudeste do Brasil: Norte da Bacia de Santos ao Sul da Bacia do Espírito Santo”.

Ao Programa de Pós-graduação em Oceanografia pelo suporte na minha formação como Mestre em Oceanografia.

“É o grau de comprometimento que determina o sucesso, não o número de seguidores.”  
(LUPIN, 2007)

## RESUMO

A circulação oceânica no Oceano Atlântico Sul (OAS) é caracterizada por inúmeras singularidades não encontradas em nenhuma outra bacia, o transporte de calor em direção ao equador dentro do Giro Subtropical do Atlântico Sul (GSAS) é uma dessas singularidades e caracteriza o braço superior da Célula de Revolvimento Meridional do Atlântico (CRMA). Para o Brasil, a Corrente de Contorno Oeste (CCO) desse giro é de grande interesse, uma vez que a dinâmica da circulação oceânica na costa leste do país é dominada por seu fluxo. As águas transportadas dentro do giro resultam das trocas de calor e sal com os oceanos Austral, Índico e Pacífico, portanto, as massas de água que constituem o ramo superior da CRMA são produto dessa mistura. Diante desse cenário, foram investigadas no presente trabalho as variabilidades das camadas que constituem a circulação superior, formadas pela Água de Superfície (AS), Água Central do Atlântico Sul (ACAS) e Água Intermediária Antártica (AIA), e os padrões nas variações espaciais e sazonais na velocidade da componente meridional e no transporte de volume (TV) da Corrente do Brasil (CB). Campos de médias mensais de dois produtos de reanálise de modelagem numérica e dados medidos *in situ* por fundeios oceanográficos e flutuadores Argo foram utilizados nas investigações. Para a análise de massa d'água os dados foram separados em dois períodos, de 1993 a 2001 e de 2002 a 2012, sendo o Argo analisado apenas no segundo período devido a disponibilidade dos dados, enquanto para a análise da CB o período completo de 1993-2012 foi abordado. A intensidade das variáveis velocidade e transporte foi maior durante a primavera e o verão em 23°S, em decorrência de mudanças sazonais na circulação atmosférica, na posição da bifurcação da Corrente Sul Equatorial e a presença de células de recirculação ao longo da CB. Os resultados sustentaram ainda a existência de variabilidades espaciais e temporais nas massas d'água do OAS, na velocidade meridional e no transporte de volume da CB. Tendências de aquecimento e salinização sobre o OAS e o aumento no volume da ACAS e da AIA influenciam de forma negativa o transporte dentro da CRMA e consequentemente no transporte de águas do Atlântico Sul para o Atlântico Norte.

**Palavras-chave:** Circulação de larga escala. Variações sazonal e interdecadal. Célula de Revolvimento Meridional do Atlântico. Corrente do Brasil. Massas d'água.

## ABSTRACT

The ocean circulation in the South Atlantic Ocean (SAO) is characterized by numerous singularities not found in any other basin, the heat transport towards equator within the South Atlantic Subtropical Gyre (SASG) is one of these singularities and characterizes the upper arm of the Atlantic Meridional Overturning Circulation (AMOC). For Brazil, the Western Boundary Current (WBC) of this tour is of great interest, since the dynamics of ocean circulation on the country's east coast is dominated by its flow. The waters transported within the gyre result from heat and salt exchanges with the Southern, Indian and Pacific oceans, therefore, the water bodies that constitute the upper branch of AMOC are the product of this mixture. In view of this scenario, the variability of the layers that constitute the upper circulation, formed by Surface Water (SW), South Atlantic Central Water (SACW) and Antarctic Intermediate Water (AAIW), and patterns in spatial variations, were investigated in the present work. and seasonal in the speed of the southern component and in the volume transport (VT) of the Brazil Current (BC). Fields of monthly averages of two numerical modeling reanalysis products and data measured in *in situ* by oceanographic anchorages and ARGO floats were used in the investigations. For the water mass analysis the data were separated into two periods, from 1993 to 2001 and from 2002 to 2012, with ARGO being analyzed only in the second period due to data availability, while for the BC analysis the complete period from 1993 to 2012 was addressed. The intensity of the speed and transport variables was higher during spring and summer at 23°S, due to seasonal changes in atmospheric circulation, in the position of the bifurcation of the South Equatorial Current, and the presence of recirculation cells along the BC. The results also supported the existence of spatial and temporal variability in the water bodies of the SAO, and in the southern speed and in the volume transport of the BC. Trends in warming and salinization over the SAO and the increase in the volume of SACW and in the AAIW would negatively influence transport within the AMOC and consequently in the transport of water from the South Atlantic to the North Atlantic.

**Keywords:** Large-scale Circulation. Seasonal and interdecadal variations. Atlantic Meridional Overturning Circulation. Brazil Current. Water masses.

## LISTA DE FIGURAS

Figura 1 – Mapa da área de estudo localizada na Bacia de Campos, com demarcação da posição dos fundeios oceanográficos .....	25
Figura 2 – Diagramas de Taylor das componentes U e V do HYCOM ( <b>a</b> e <b>b</b> ) e do GLORYS ( <b>c</b> e <b>d</b> ).....	26
Figura 3 – Média mensal da componente meridional para o HYCOM ( <b>a</b> e <b>b</b> ) e para o GLORYS ( <b>c</b> e <b>d</b> ). As linhas tracejadas coloridas representam os valores de velocidade para os anos de 1993–2012, a linha contínua em preto representa a mediana e a linha contínua em vermelho representa a média desses dados.....	27
Figura 4 – Histogramas de ocorrências do centro do jato da Corrente do Brasil (CB) por longitude, para as duas reanálises (HYCOM e GLORYS: a, b, c e d), no período de 1993–2012. Os limites utilizados na identificação da ocorrência do jato da CB foram 37,5°W e 38,5°W, para as latitudes de 22°S e 23°S, respectivamente .....	28
Figura 5 – Série temporal do transporte de volume da Corrente do Brasil, calculado pelo método “dos contornos” e “das caixas” nas latitudes 22°S e 23°S para dados do HYCOM e do GLORYS ( <b>a</b> , <b>b</b> , <b>c</b> e <b>d</b> ) .....	30
Figura 6 – Média mensal do transporte de volume para o HYCOM ( <b>a</b> e <b>b</b> ) e para o GLORYS ( <b>c</b> e <b>d</b> ). As linhas tracejadas coloridas representam os valores de transporte para os anos de 1993–2012, a linha contínua em preto representa a mediana e a linha contínua em vermelho representa a média desses dados.....	31
Figure 7 – Average circulation in the South Atlantic Subtropical Gyre for the period from 1993 to 2012, obtained from the reanalysis data from GLORYS. The colors indicate the surface temperature of the sea, varying from 12°C (dark blue) to 28°C (dark red), for the analyzed period. The zonal and meridional components of the current velocity are represented by vectors (arrows in black), and the main currents that form the SASG in the study area, represented by the arrows in white, are Brazil Current (BC), Benguela Current (BeC) and the Southern Branch of the South Equatorial Current (SECs) .....	39
Figure 8 – Location of transects over the South Atlantic Ocean, where $\theta$ -S diagrams and longitudinal sections of temperature and salinity were developed, depending on the depth. The black and red lines refer to the area of the $\theta$ -S vertical profile sections, made for all longitudes in the 3 selected latitudes. (A) west transect at	

10°S, (B) east transect at 10°S, (C) west transect at 20°S, (D) east transect at 20°S, (E) west transect at 30°S, and (F) east transect at 30°S. The pink and blue lines represent the longitudinal sections at 35°W (SEC_35°W) and 5°E (SEC_5°E), respectively.....	42
Figure 9 – Interannual variability of data from HYCOM (HYC), GLORYS (GLO), and ARGO (ARG), for the annual average of the periods 1993–2001 (P1) and 2002–2012 (P2), represented in vertical profiles for temperature relation (°C) versus salinity for each longitude, of the sectors of the South Atlantic Ocean (SAO). The SAO was divided into six sections, nominally represented by (A) west group at 10°S, (B) east group at 10°S, (C) west group at 20°S, (D) east group at 20°S, (E) west group at 30°S and (F) east group at 30°S .....	45
Figure 10 – Representation of temperature (°C) (solid black line) for data from HYCOM (HYC), GLORYS (GLO), and ARGO (ARG), during the periods 1993–2012 (P20) and 2002–2012 (P2), represented in sectors of the South Atlantic Ocean (SAO). The SAO was divided into six sections, nominally represented by (A) west group at 10°S, (B) east group at 10°S, (C) west group at 20°S, (D) east group at 20°S, (E) west group at 30°S and (F) east group at 30°S. The continuous lines in cyan represent the linear trend (°C.decade <sup>-1</sup> ) of the data from the period 1993 to 2012, and the continuous lines in red represent the trend (°C.decade <sup>-1</sup> ) for the period of validity of ARGO (2002–2012), with the blue dashed lines representing the statistical significance of the data.....	48
Figure 11 – The same represented in Figure 10, for the salinity data (PSU.decada <sup>-1</sup> ).....	51
Figure 12 – Longitudinal sections of average temperature (°C) in 35°W (Brazilian coast) and 5°E (African coast), for the data of HYCOM (HYC), GLORYS (GLO) and ARGO (ARG), during the periods of 1993–2001 (P1) and 2002–2012 (P2), divided into annual average (panels of line 1), summer (panels of line 2), autumn (panels of line 3), winter (panels of line 4), and spring (line 5 panels). Dashed lines show the potential density of the interface between Surface Water (SW) and South Atlantic Central Water (SACW) (25.7kg.m <sup>-3</sup> ), between SACW and Antarctic Intermediate Water (AAIW) (26.8kg.m <sup>-3</sup> ), and between AAIW and North Atlantic Deep Water (27.5kg.m <sup>-3</sup> ).....	55
Figure 13 – The same as in Figure 12, for PSU salinity data .....	58
Figure 14 – Representation of the bias for the longitudinal sections of temperature (°C) and salinity at 35°W (Brazilian coast) and 5°E (African coast), data from HYCOM	

(HYC) about ARGO and GLORYS (GLO) about ARGO, during the period between 2002–2012, divided into annual average (panels of line 1), summer (panels of line 2), autumn (panels of line 3), winter (panels of line 4), and spring (line 5 panels). Dashed lines show the potential density of the interface between Surface Water (SW) and South Atlantic Central Water (SACW) ( $25.7\text{kg.m}^{-3}$ ), between SACW and Antarctic Intermediate Water (AAIW) ( $26.8\text{kg.m}^{-3}$ ), and between AAIW and North Atlantic Deep Water ( $27.5\text{kg.m}^{-3}$ ) .....	60
Figure 15 – Representation of interface depth between Surface Water and South Atlantic Central Water, for data from HYCOM (HYC), GLORYS (GLO), and ARGO (ARG), during the periods 1993–2001 (P1) and 2002–2012 (P2), divided into annual (panels of line 1), summer (panels of line 2), autumn (panels of line 3), winter (panels of line 4), and spring (panels of line 5) averages .....	63
Figure 16 – The same as in Figure 15 for the interface between the South Atlantic Central Water and the Antarctic Intermediate Water. ....	64
Figure 17 – The same as in Figure 15 for the interface between Antarctic Intermediate Water and North Atlantic Deep Water.....	65
Figure 18 – Representation of the South Atlantic Central Water layer thickness, for data from HYCOM (HYC), GLORYS (GLO), and ARGO (ARG), during the periods 1993–2001 (P1) and 2002–2012 (P2), divided into annual (panels of line 1), summer (panels of line 2), autumn (panels of line 3), winter (panels of line 4), and spring (panels of line 5) averages.....	66
Figure 19 – The same as in Figure 18 for the thickness of the Antarctic Intermediate Water layer .....	68
Figure 20 – Average time series of average volume ( $\times 10^{14}$ ) in $\text{m}^3$ , of each water mass for the South Atlantic. For data from HYCOM (continuous line in black), GLORYS (continuous line in red) and ARGO (continuous line in blue), during the periods 1993–2001 (panels on the left), for reanalysis, and 2002–2012 (panels on the right), for both types of data. The first row of panels shows the results for Surface Water (SW), the second row of panels shows the results for South Atlantic Central Water (SACW), and the third row of panels shows the results for Antarctic Intermediate Water (AAIW). The dashed lines represent the linear trend ( $\text{m}^3.\text{decade}^{-1}$ ), with 95% statistical significance, of the data from HYCOM, GLORYS, and ARGO, respectively. ....	70

## LISTA DE TABELAS

Table 1 – Trend values (TD) of temperature (in $^{\circ}\text{C}.\text{decade}^{-1}$ ), for the data of HYCOM, GLORYS, and ARGO, during the periods of 1993–2012 (P20) and 2002–2012 (P2), in sectors of the South Atlantic Ocean (SAO). The SAO was divided into six sections, nominally represented by (A) west group at $10^{\circ}\text{S}$ , (B) east group at $10^{\circ}\text{S}$ , (C) west group at $20^{\circ}\text{S}$ , (D) east group at $20^{\circ}\text{S}$ , (E) west group at $30^{\circ}\text{S}$ and (F) east group at $30^{\circ}\text{S}$ . The trends were calculated for each water mass of the upper circulation of the SAO, represented by Surface Water (SW), South Atlantic Central Water (SACW), and Antarctic Intermediate Water (AAIW).....	50
Table 2 – The same shown in Table 1, for the salinity data ( $\text{PSU}.\text{decada}^{-1}$ ) ..	52
Table 3 – Values of mean temperature differences (in $^{\circ}\text{C}$ ) between two cross-sections (at $35^{\circ}\text{W}$ and $5^{\circ}\text{E}$ ), on the western and eastern borders of the South Atlantic Ocean (SAO). The data are from the HYCOM and GLORYS reanalyses, and ARGO floats, during the periods 1993–2001 (P1) and 2002–2012 (P2). The analyzes were divided into annual, summer, autumn, winter and spring averages for each period. Also, they were calculated for each water mass of the upper circulation of the SAO, represented by Surface Water (SW), South Atlantic Central Water (SACW), and Antarctic Intermediate Water (AAIW).....	54
Table 4 – The same as in Table 3, for PSU salinity data.....	57
Table 5 – Representation of the Root Mean Square Error for the longitudinal sections of temperature ( $^{\circ}\text{C}$ ) and salinity (PSU) in $35^{\circ}\text{W}$ (Brazilian coast) and $5^{\circ}\text{E}$ (African coast), from HYCOM data in comparison with ARGO, and GLORYS with ARGO, during the period between 2002–2012, divided into annual, summer, autumn, winter, and spring averages .....	62
Table 6 – Average volume values (in $\times 10^{14}\text{m}^3$ ) for the South Atlantic Ocean (SAO). The data are from the HYCOM and GLORYS reanalyses, and ARGO floats, during the periods 1993–2001 (P1) and 2002–2012 (P2). The analyzes were divided for each water mass of the upper circulation of the SAO, represented by Surface Water (SW), South Atlantic Central Water (SACW), and Antarctic Intermediate Water (AAIW).....	70

## LISTA DE ABREVIATURAS E SIGLAS

ACAS	Água Central do Atlântico Sul
AS	Água de Superfície
AIA	Água Intermediária Antártica
APAN	Água Profunda do Atlântico Norte
ASAS	Anticiclone Subtropical do Atlântico Sul
CRMA	Célula de Revolvimento Meridional do Atlântico
COG	Circulação Oceânica Global
CBM	Confluência Brasil-Malvinas
CBe	Corrente da Benguela
CA	Corrente das Agulhas
CM	Corrente das Malvinas
CCO	Corrente de Contorno Oeste
CAS	Corrente do Atlântico Sul
CB	Corrente do Brasil
CNB	Corrente Norte do Brasil
CSE	Corrente Sul Equatorial
GSAS	Giro Subtropical do Atlântico Sul
HN	Hemisfério Norte
HS	Hemisfério Sul
MA	Massas d'água
M. Caixa	Método das Caixas
M. Cont.	Método dos Contornos
OAN	Oceano Atlântico Norte
OAS	Oceano Atlântico Sul
PD	Passagem de Drake
SCB	Sistema Corrente do Brasil
TV	Transporte de Volume
VA	Vazamento das Agulhas

## LISTA DE ABREVIATURAS E SIGLAS (ARTIGO)

AAIW	Antarctic Intermediate Water
AL	Agulhas Leakage
AMOC	Atlantic Meridional Overturning Circulation
BC	Brazil Current
BeC	Benguela Current
CFSR	Climate Forecast System Reanalysis
DP	Drake Passage
GLORYS	Global Ocean Reanalysis and Simulations
HYCOM	Hybrid Coordinate Ocean Model
ISAS	<i>In Situ</i> Analysis System
LPO	<i>Laboratoire de Physique des Océans</i>
NAO	North Atlantic Ocean
NCAR	National Center for Atmospheric Research
NCEP	National Centers for Environmental Prediction
NCODA	Marine Coupled Ocean Data Assimilation
NEMO	Nucleus for European Modeling of the Ocean
RMSE	Root Mean Square Error
SAC	South Atlantic Current
SACW	South Atlantic Central Water
SAM2	<i>Système d'Assimilation Mercator version 2</i>
SAO	South Atlantic Ocean
SASG	South Atlantic Subtropical Gyre
SEC	South Equatorial Current
SECs	Southern Branch of the South Equatorial Current
SO-ARGO	Argo Observing Service
SW	Surface Water
TD	Trend
TEOS-10	Thermodynamic Equation of Seawater-2010

## SUMÁRIO

<b>1</b>	<b>INTRODUÇÃO .....</b>	<b>17</b>
1.1	OBJETIVOS.....	20
1.1.1	Objetivo Geral.....	20
1.1.2	Objetivos Específicos.....	21
<b>VARIABILIDADE ESPACIAL E TEMPORAL DA CORRENTE DO BRASIL</b>		
<b>NA BACIA DE CAMPOS</b>		
<b>2</b>	<b>INTRODUÇÃO .....</b>	<b>23</b>
<b>3</b>	<b>OBJETIVOS .....</b>	<b>24</b>
<b>4</b>	<b>METODOLOGIA.....</b>	<b>24</b>
<b>5</b>	<b>RESULTADOS .....</b>	<b>25</b>
<b>6</b>	<b>CONCLUSÃO.....</b>	<b>32</b>
<b>7</b>	<b>AGRADECIMENTOS .....</b>	<b>33</b>
	<b>REFERÊNCIAS.....</b>	<b>34</b>
<b>SPATIAL AND TEMPORAL VARIABILITY OF WATER MASSES IN THE</b>		
<b>UPPER CIRCULATION OF THE SOUTH ATLANTIC</b>		
<b>8</b>	<b>INTRODUCTION .....</b>	<b>36</b>
<b>9</b>	<b>DATA AND METHODS.....</b>	<b>39</b>
<b>10</b>	<b>RESULTS AND DISCUSSION.....</b>	<b>43</b>
10.1	SPATIAL AND INTERANNUAL VARIABILITY OF SAO WATER MASSES...	43
10.2	SPATIAL AND SEASONAL VARIABILITY IN LONGITUDINAL SECTIONS	53
10.3	INTERFACE DEPTHS AND LAYER THICKNESS OF WATER MASSES.....	62
<b>11</b>	<b>CONCLUSIONS.....</b>	<b>73</b>
	<b>ACKNOWLEDGMENT .....</b>	<b>74</b>

<b>12</b>	<b>REFERENCES .....</b>	<b>75</b>
	<b>CONCLUSÃO.....</b>	<b>79</b>
	<b>REFERÊNCIAS.....</b>	<b>82</b>
	<b>ANEXO A - Comprovante de submissão na revista <i>Ocean Dynamics</i>.....</b>	<b>88</b>

## 1 INTRODUÇÃO

Os oceanos atuam como importantes reguladores do clima, ao armazenar e transportar calor, através das correntes marinhas (THOMPSON; RAHMSTORF, 2009). Essas correntes são formadas por dois principais processos, que em conjunto caracterizam a Circulação Oceânica Global (COG), induzida em superfície pelos ventos e em profundidade pelas diferenças de temperatura e salinidade (POND; PICKARD, 1983). Em função desses diferentes processos de formação dos fluxos, a COG é dividida em duas componentes, conhecidas como circulação dirigida pelo vento e circulação termohalina.

Os processos da circulação do oceano superior são controlados pela fricção da atmosfera com a superfície da água, gerando fluxos de convergência e divergência de massas na camada de Ekman (TALLEY, 2002). Essa interação oceano-atmosfera faz com que os campos das correntes oceânicas sejam de modo geral similares aos campos de vento, exceto pela presença das barreiras continentais (BROWN et al., 2001). Na circulação profunda, os fluxos são formados pela diferença de densidade entre as massas d'água (MA), em consequência do resfriamento das águas de superfície nos polos, que afundam e migram em direção ao equador (BROWN et al., 2001).

A circulação superior de cinco das maiores bacias oceânicas é dominada por feições de larga escala conhecidas como giros subtropicais (PEDLOSKY, 1990). Em sua origem, essas feições são uma resposta do oceano ao cisalhamento dos alísios e dos ventos de oeste (ROSSBY, 1999). Uma vez que o movimento das águas superficiais é à direita do vento no Hemisfério Norte (HN) e à esquerda do vento no Hemisfério Sul (HS), o sentido do fluxo desses giros é oposto para cada hemisfério, e anticiclônico em ambos (RODRIGUES, 2015).

As características do conjunto de correntes que formam esses giros são assimétricas, sendo fluxos estreitos, quentes e intensos, nas fronteiras oeste dos oceanos e largos, frios e lentos, nas fronteiras leste (TALLEY, 2002). No HS, o Giro Subtropical do Atlântico Sul (GSAS) é a feição correspondente para o Oceano Atlântico Sul (OAS), formada pela Corrente do Brasil (CB), pela Corrente do Atlântico Sul (CAS), pela Corrente da Benguela (CBe) e pela Corrente Sul Equatorial (CSE) (MARCELLO et al., 2018).

A CB tem origem ao sul de 10°S e flui ao longo da costa leste do continente sul-americano, caracterizando a Corrente de Contorno Oeste (CCO) do GSAS (STRAMMA, 1991). O fluxo da CB termina no encontro com a Corrente das Malvinas (CM) em aproximadamente 38°S, na região conhecida como Confluência Brasil-Malvinas (CBM), gerando intensas

instabilidades vorticiais de mesoescala (MAAMAATUAIAHUTAPU et al., 1999; SILVEIRA et al., 2000). A leste da Confluência as águas que se afastam da costa são transportadas pela CAS em direção ao continente africano. Nessa região, a CAS converge com a CBe através da Bacia do Cabo, transportando águas frias e salinas em direção ao equador (STRAMMA; PETERSON, 1990; MARCELLO et al., 2018). A borda norte do GSAS é formada então pelo fluxo em direção a noroeste das águas que saem da CBe, entram no braço sul da CSE e migram em direção à costa brasileira, fechando o giro subtropical (RODRIGUES et al., 2007).

Nesse cenário, a CB destaca-se em âmbito regional para a costa brasileira, uma vez que os processos de circulação no domínio dessa corrente interferem em setores relevantes para o país, por exemplo, economicamente a circulação oceânica é de grande interesse para a segurança das atividades de extração na indústria petrolífera (BILÓ et al., 2014). A dimensão do fluxo das correntes que formam o Sistema Corrente do Brasil (SCB), compreende cerca de 3000m de coluna d'água (SILVEIRA et al., 2000) e o transporte realizado por elas, envolve MA com características distintas e altera a circulação sobre a plataforma e o talude continental brasileiro (CAMPOS et al., 2000; VIANA et al., 2002).

Esses fluxos estão submetidos à intensa atividade de mesoescala dessa CCO. A disposição de vórtices ciclônicos sucedidos por anticiclônicos na CB, evidentes nas observações por imagens de satélites realizadas por Garfield (1990), suscitam a proeminente característica meandrante do SCB. Em determinadas regiões esses vórtices são desconectados do eixo principal da corrente proporcionando a formação de anéis, que são transportados sobre o Oceano Atlântico e aprisionam águas com propriedades distintas das circundantes (MANO et al., 2009). A formação de meandros é reportada no estudo de Campos, Gonçalves e Ikeda (1995) como produto dos gradientes topográficos e da abrupta mudança na linha de costa brasileira.

Outro importante sistema de mesoescala dentro para a circulação do GSAS são os Anéis que se desprendem na Retroflexão da Corrente das Agulhas (CA), conhecido como Vazamento das Agulhas (VA). Segundo Guerra et al. (2018) esses anéis migram em direção a oeste e interferem no transporte do SCB e de acordo com Beal et al. (2011) a entrada desses anéis impacta também a intensidade da Célula de Revolvimento Meridional do Atlântico (CRMA).

O transporte de calor em direção ao equador dentro do GSAS caracteriza o braço superior da CRMA (RINTOUL, 1991; MIGNAC et al., 2018). O padrão global do sistema oceano-atmosfera carrega água do equador em direção aos polos. Em contrapartida, a existência desse ramo da CRMA é uma compensação à exportação de água fria do Oceano Atlântico Norte

(OAN), caracterizada pela intrusão da Água Profunda do Atlântico Norte (APAN) dentro do GSAS, em profundidades elevadas (HOLFORT; SIEDLER, 2001; MCDONAGH; KING, 2005).

As águas transportadas dentro do OAS resultam das trocas de calor e sal com os oceanos Austral, Índico e Pacífico, portanto, as MA que constituem o ramo superior da CRMA são produto dessa mistura (GARZOLI; MATANO, 2011; MIGNAC et al., 2018). O vazamento dos anéis na região do VA é responsável pela conexão Indo-Atlântica e a Passagem de Drake (PD) é a via Pacífico-Atlântica (GORDON, 1986; RINTOUL, 1991; DE RUIJTER et al., 1999; RÜHS et al., 2019). A intrusão e a redistribuição dessas águas no OAS modificam as propriedades das MA transportadas no giro subtropical. Como consequência, gera variabilidades em diferentes escalas espaciais e temporais, que a longo prazo podem alterar também as características da CRMA (GARZOLI; MATANO, 2011).

Stramma e England (1999) dividem a distribuição vertical dessas massas em circulação superior e profunda, determinando esquematicamente a formação e a circulação delas dentro do GSAS. Em superfície, águas quentes e salinas são formadas nas regiões tropicais e subtropicais e circulam em subsuperfície após sofrerem subducção, caracterizando a camada de mistura no OAS (TOMCZAK; GODFREY, 1994).

Abaixo da Água de Superfície (AS), a coluna d'água é ocupada pela Água Central do Atlântico Sul (ACAS) formada na região da CBM. Essa MA é transportada pela CAS em direção a costa africana, onde grande parte do seu fluxo entra na CBe e consecutivamente na CSE, migrando em direção a costa brasileira. A bifurcação da CSE transporta parte da ACAS em direção ao equador, com a Corrente Norte do Brasil (CNB), e parte em direção a CBM novamente, sendo carregada pela CB. Na região do Vazamento das Agulhas, as propriedades dessa massa d'água são redistribuídas, devido a intrusão das águas centrais mais quentes e mais salina do Oceano Índico.

A base da circulação superior definida no trabalho de Stramma e England (1999) é formada pela Água Intermediária Antártica (AIA), que de acordo com Talley (1996) tem origem na região superficial da camada circumpolar, na porção norte da PD. Assim como a ACAS, a AIA entra na CAS e segue o mesmo fluxo que a MA sobreposta a ela. No entanto, a latitude da bifurcação da CSE ao nível de profundidade da AIA ocorre mais ao sul, em cerca de 25°S, em comparação ao nível da ACAS, no qual a bifurcação ocorre em cerca de 20°S (RODRIGUES et al., 2007). Na circulação profunda, o fluxo predominante é o transporte da APAN, formada em altas latitudes no OAN (HOLFORT; SIEDLER, 2001).

Como visto, a circulação oceânica no OAS é caracterizada por inúmeras singularidades não encontradas em nenhuma outra bacia (GORDON, 1988). Investigações nas últimas décadas buscaram aprofundar o conhecimento sobre as características únicas dessa circulação (por exemplo, STRAMMA; ENGLAND, 1999; RODRIGUES et al., 2010; MARCELLO et al., 2018). Contudo, muitas lacunas ainda permanecem em aberto em relação aos padrões que controlam os processos no OAS. O comportamento das MA, quanto à sua distribuição espacial e temporal e as variabilidades em diferentes escalas, é um campo amplo nesse sentido (BRYDEN et al., 2003; THRESHER et al., 2014; TIM et al., 2018; CAPUANO et al., 2018). Diante do cenário de troca de calor e sal do OAS com os oceanos adjacentes, muito ainda precisa ser investigado para entender as variações no volume de cada massa d'água, os processos que controlam primordialmente essas variações e as consequências dessa distribuição na COG.

Além disso, a presença da CB na costa sudeste brasileira é de grande interesse regionalmente para o Brasil, uma vez que a dinâmica da circulação oceânica na costa leste do país é dominada por seu fluxo. Portanto, o avanço no conhecimento sobre as características da CB contribui, regionalmente, no desenvolvimento de setores sociais e econômicos e ampara a implantação de políticas ambientais adequadas.

Tendo em vista esses cenários, a proposta do presente trabalho foi investigar as variabilidades de calor e sal do OAS em escalas espaciais e temporais, com foco em identificar alterações no volume das massas de água que apresentem potencial capacidade de alterar a circulação atual do GSAS e os processos da CRMA à longo prazo. Bem como, investigar padrões nas variações espaciais e sazonais na velocidade da componente meridional e no transporte de volume (TV) da Corrente do Brasil, com o intuito de expandir os conhecimentos sobre essa CCO ao largo da costa leste brasileira.

## 1.1 OBJETIVOS

### **1.1.1 Objetivo Geral**

O objetivo do presente trabalho foi investigar tendências de variabilidades de calor e sal no Oceano Atlântico Sul em escalas espaciais e temporais. Em adição, também foi proposto investigar padrões nas variações espaciais e sazonais na velocidade da componente meridional e no transporte de volume (TV) da Corrente do Brasil.

### **1.1.2 Objetivos Específicos**

Os objetivos específicos propostos são:

- Avaliar a aplicação de produtos de reanálises na caracterização das massas d'água do OAS.
- Identificar alterações no volume das massas de água que apresentem potencial capacidade de alterar a circulação atual do GSAS e os processos da CRMA à longo prazo.
- Calcular o transporte através de dois métodos distintos, identificando as principais diferenças no resultado entre ambos e avaliar qual o melhor método para o cálculo do TV.

Antônia Pamela Yhaohannah de Lima

**VARIABILIDADE ESPACIAL E TEMPORAL DA CORRENTE DO BRASIL NA  
BACIA DE CAMPOS**

Esta seção é destinada a apresentação do trabalho científico desenvolvido e apresentado no XIII Simpósio sobre Ondas, Marés, Engenharia Oceânica e Oceanografia por Satélite.

Florianópolis  
2020

## RESUMO

Este trabalho apresenta padrões de variabilidade na velocidade da corrente e no transporte de volume, no domínio da Corrente do Brasil na Bacia de Campos, através dos produtos de reanálise *Hybrid Coordinate Ocean Model* (HYCOM) e *Global Ocean Reanalysis and Simulations* (GLORYS), para 22°S e 23°S. As reanálises foram comparadas a 6 meses de dados obtidos *in situ*, para o ano de 1993. O transporte de volume foi calculado através de dois métodos distintos, nomeados como métodos dos contornos e das caixas. Espacialmente, o TV aumenta em 23°S, consequência da existência de células de recirculação ao longo da CB e pela incorporação de anéis das Agulhas na altura de Cabo Frio. Sazonalmente, a intensidade das variáveis velocidade e transporte é maior durante a primavera e o verão, em decorrência de mudanças sazonais na circulação atmosférica e na posição da bifurcação da Corrente Sul Equatorial.

**Palavras chave:** Transporte de volume. Sazonalidade. Cabo de São Tomé e Cabo Frio.

## 2 INTRODUÇÃO

As Correntes de Contorno Oeste desempenham papel fundamental no balanço de calor do planeta, caracterizadas por fluxos estreitos, quentes e intensos, constituem os ramos oeste dos giros subtropicais que transportam MA aquecidas na região equatorial em direção aos polos (BROWN et al., 2001). No Hemisfério Sul, a CCO associada ao Giro Subtropical do Atlântico Sul, é formada por um complexo sistema de correntes que flui ao largo da costa leste do Brasil, dominado em superfície pela Corrente do Brasil.

Essa porção do território brasileiro incorpora a bacia sedimentar de Campos, área reconhecida por sua importância para a indústria petrolífera do país, sendo responsável por cerca de 60% da produção e 90% das reservas de óleo e gás nacional (ANP, 2016). Intrínseca a essa atividade, existe a preocupação com a segurança das plataformas e estruturas utilizadas na exploração deste recurso, que estão sujeitas à dinâmica da circulação oceânica.

Portanto, o avanço no conhecimento sobre as características da CB contribui, não somente, para aprofundar as investigações climáticas globais, mas, regionalmente, para auxiliar na implantação de projetos adequados na exploração do petróleo ao largo do sudeste do Brasil.

### 3 OBJETIVOS

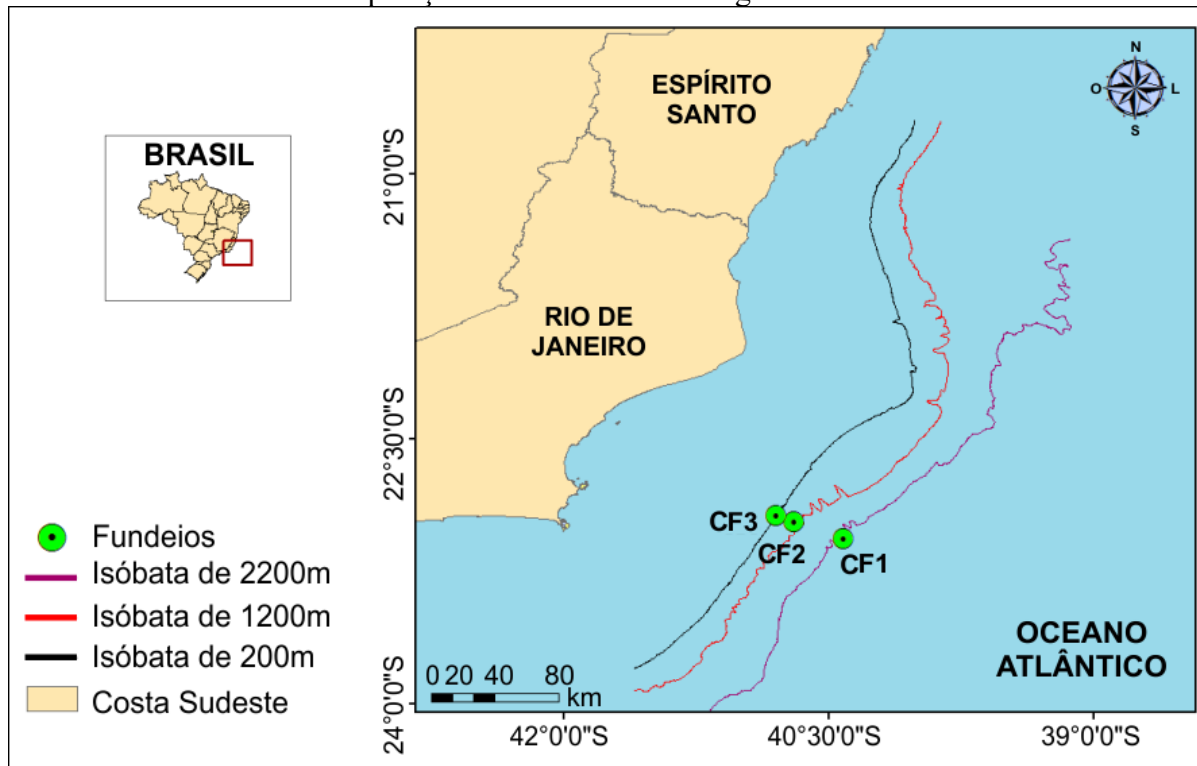
Investigar padrões nas variações espaciais e sazonais na velocidade da componente meridional e no transporte de volume da Corrente do Brasil, com foco nas radiais de 22°S e 23°S (Bacia de Campos), ao longo de duas décadas (1993–2012), a partir de dados de reanálise.

### 4 METODOLOGIA

Análises estatísticas foram feitas a partir de diagramas de Taylor (TAYLOR, 2001), entre os produtos de reanálise HYCOM e GLORYS e dados de correntógrafos distribuídos em 3 fundeios oceanográficos, localizados na Bacia de Campos (Figura 1). Para essa análise e elaboração dos diagramas foram calculados os valores de desvio padrão e coeficiente de correlação, de cada conjunto de dado.

Uma vez que o TV, é função da velocidade da corrente, os diagramas foram estimados para as componentes U e V da velocidade, em 6 níveis de profundidade (P 100m, P 173m, P 240m, P 375m, P 880m e P 1980m), no período de 6 meses durante o ano de 1993. Os níveis de profundidade foram determinados, de acordo com a distribuição dos correntógrafos nas linhas de fundeio. Das reanálises foram escolhidos os pontos mais próximos as coordenadas geográficas e as profundidades dos correntógrafos.

Figura 1 – Mapa da área de estudo localizada na Bacia de Campos, com demarcação da posição dos fundeios oceanográficos.



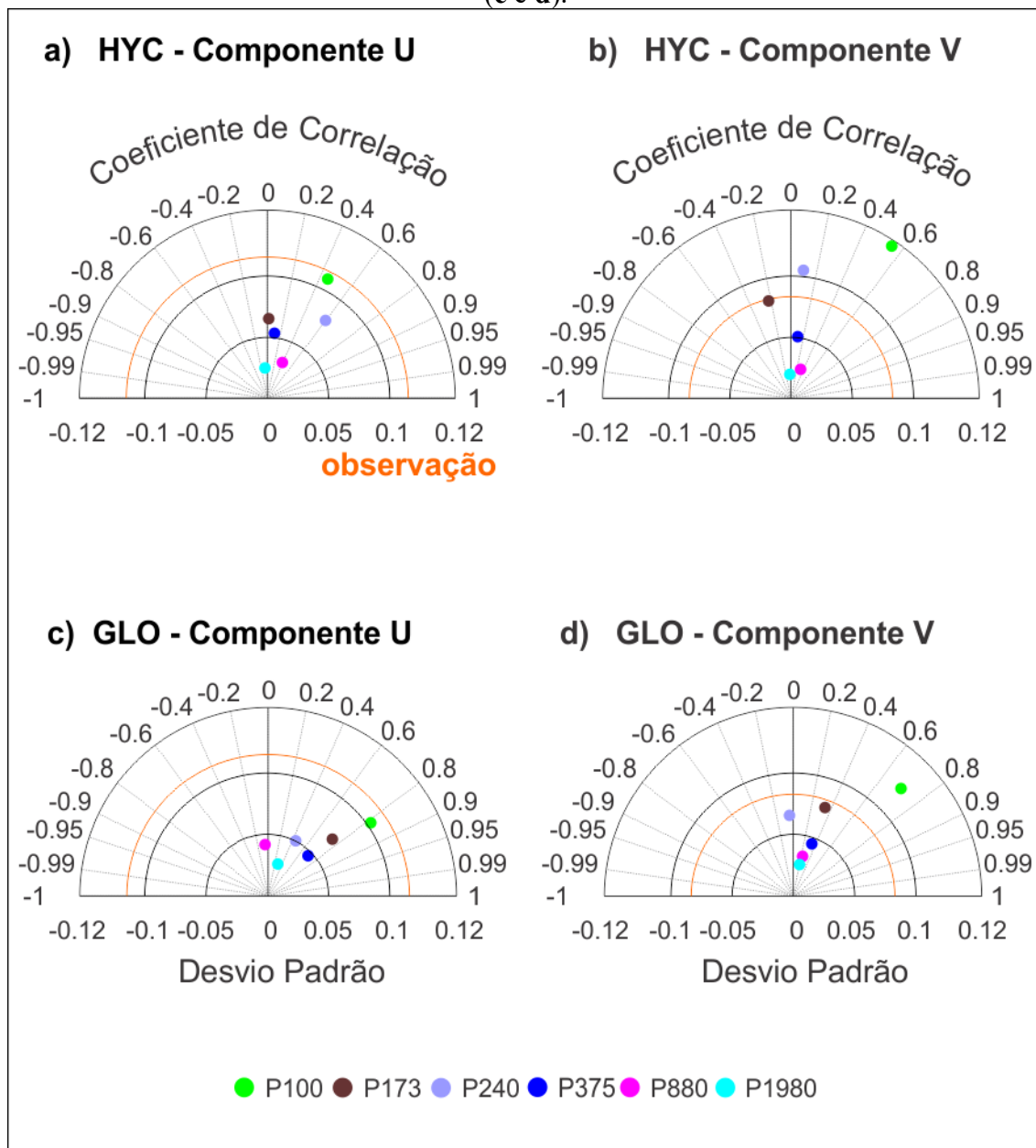
Fonte: A autora (2019).

Posteriormente, foram geradas séries temporais de velocidade meridional de corrente, com cobertura temporal de 20 anos a partir dos dois produtos de reanálise. O transporte de volume foi então obtido através de dois métodos propostos por Lima (1997), denominados “método dos contornos” (M. Cont.) e “método das caixas” (M. Caixa). Ambos fundamentos na integração da velocidade onde a componente meridional é negativa.

## 5 RESULTADOS

Nos diagramas de Taylor (Figura 2a, 2b, 2c e 2d), as duas reanálises representaram melhor os dados observados nos níveis mais superficiais. Os dados mais profundos (P1980) do HYCOM resultaram em correlação negativa ( $r=-0,05$  para a componente U e  $r=-0,08$  para a componente V), no entanto, para a componente meridional a correlação em P100 foi equivalente a  $r=0,55$  e o desvio padrão em P173 foi igual ao observado nos dados *in situ* ( $0,08\text{m.s}^{-1}$ ).

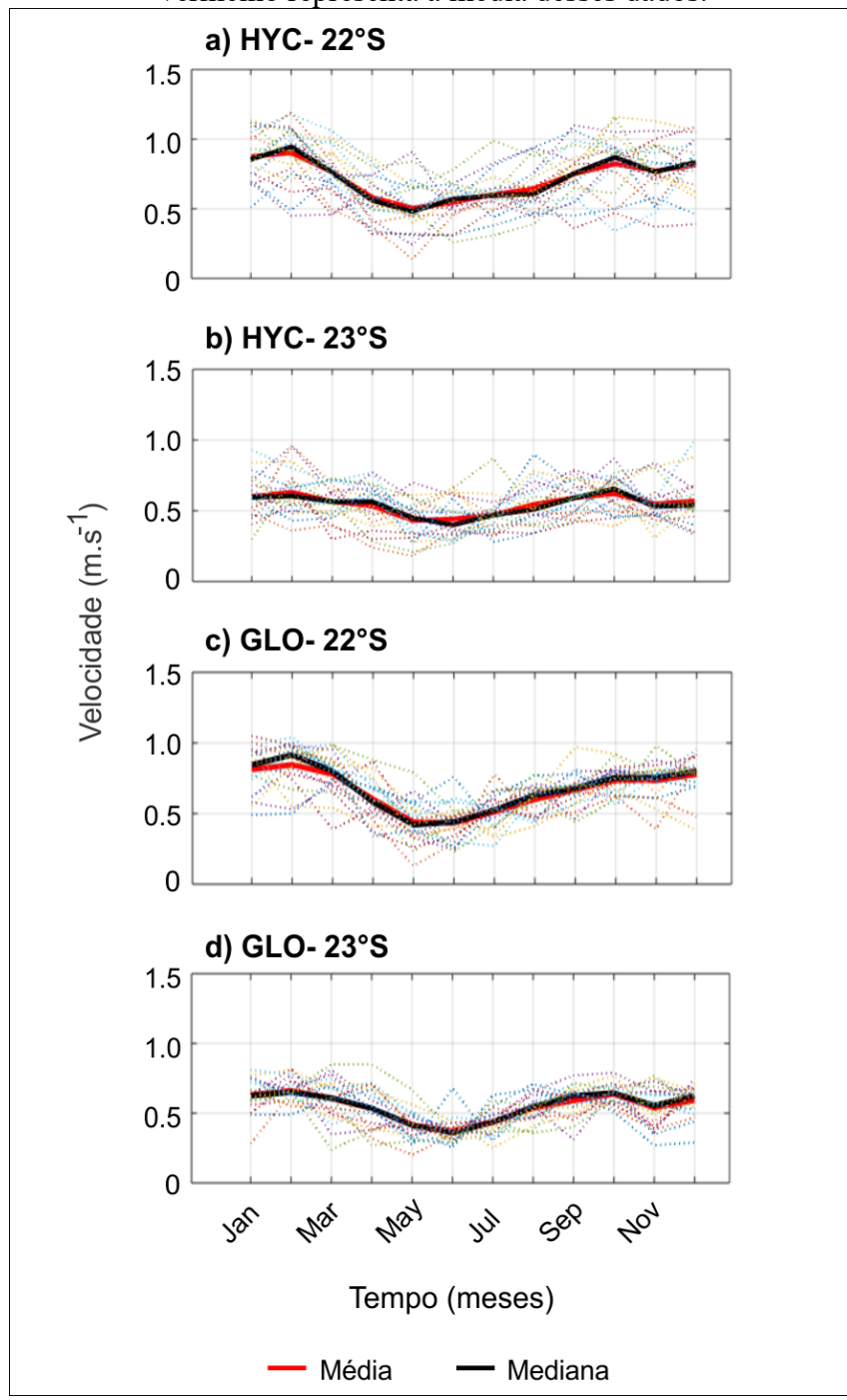
Figura 2 – Diagramas de Taylor das componentes U e V do HYCOM (a e b) e do GLORYS (c e d).



Fonte: A autora (2019).

O GLORYS apresentou melhor coeficiente de correlação ( $r$ ) para as duas componentes da velocidade, igual a  $r=0,81$  (U) e  $r=0,70$  (V), e o desvio padrão mais semelhante ao dado observado foi registrado em P173 ( $0,07\text{m.s}^{-1}$ ). Os resultados das médias mensais (Figura 3a, 3b, 3c e 3d) de velocidade da corrente apresentaram ciclo anual definido, com aumento durante o verão e a primavera. Para o HYCOM os valores negativos máximos que caracterizam o centro do jato da CB, foram equivalentes à  $-0,96\text{m.s}^{-1}$  ( $22^{\circ}\text{S}$ ) e  $-0,75\text{m.s}^{-1}$  ( $23^{\circ}\text{S}$ ), para o GLORYS foram iguais à  $-0,93\text{m.s}^{-1}$  ( $22^{\circ}\text{S}$ ) e  $-0,69\text{m.s}^{-1}$  ( $23^{\circ}\text{S}$ ).

Figura 3 – Média mensal da componente meridional para o HYCOM (**a** e **b**) e para o GLORYS (**c** e **d**). As linhas tracejadas coloridas representam os valores de velocidade para os anos de 1993–2012, a linha contínua em preto representa a mediana e a linha contínua em vermelho representa a média desses dados.

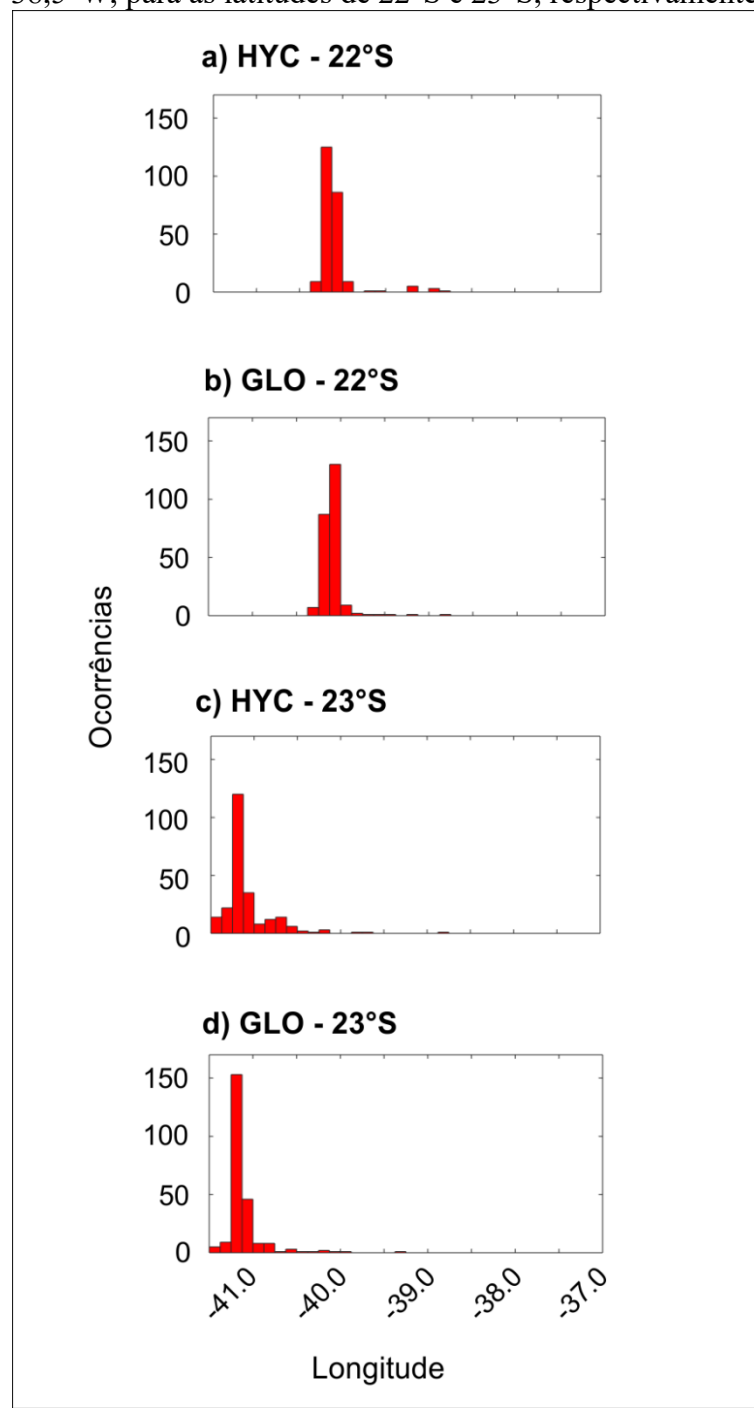


Fonte: A autora (2019).

Em 22°S o centro do jato esteve bem organizado sobre a quebra da plataforma e no talude continental na maioria das ocorrências, 148 vezes sobre a longitude de 40,25°W para o HYCOM (Figura 4a) e 143 vezes na longitude de 40°W para o GLORYS (Figura 4b). Em 23°S,

o cenário é de “espalhamento”, em consequência da busca mudança na orientação da linha de costa em Cabo Frio, nessa radial o centro do jato esteve sobre a longitude 41°W em 61 das ocorrências nos dados do HYCOM (Figura 4c) e sobre 40,75°W em 83 das ocorrências nos dados do GLORYS (Figura 4d).

Figura 4 – Histogramas de ocorrências do centro do jato da Corrente do Brasil (CB) por longitude, para as duas reanálises (HYCOM e GLORYS: **a, b, c e d**), no período de 1993–2012. Os limites utilizados na identificação da ocorrência do jato da CB foram 37,5°W e 38,5°W, para as latitudes de 22°S e 23°S, respectivamente.

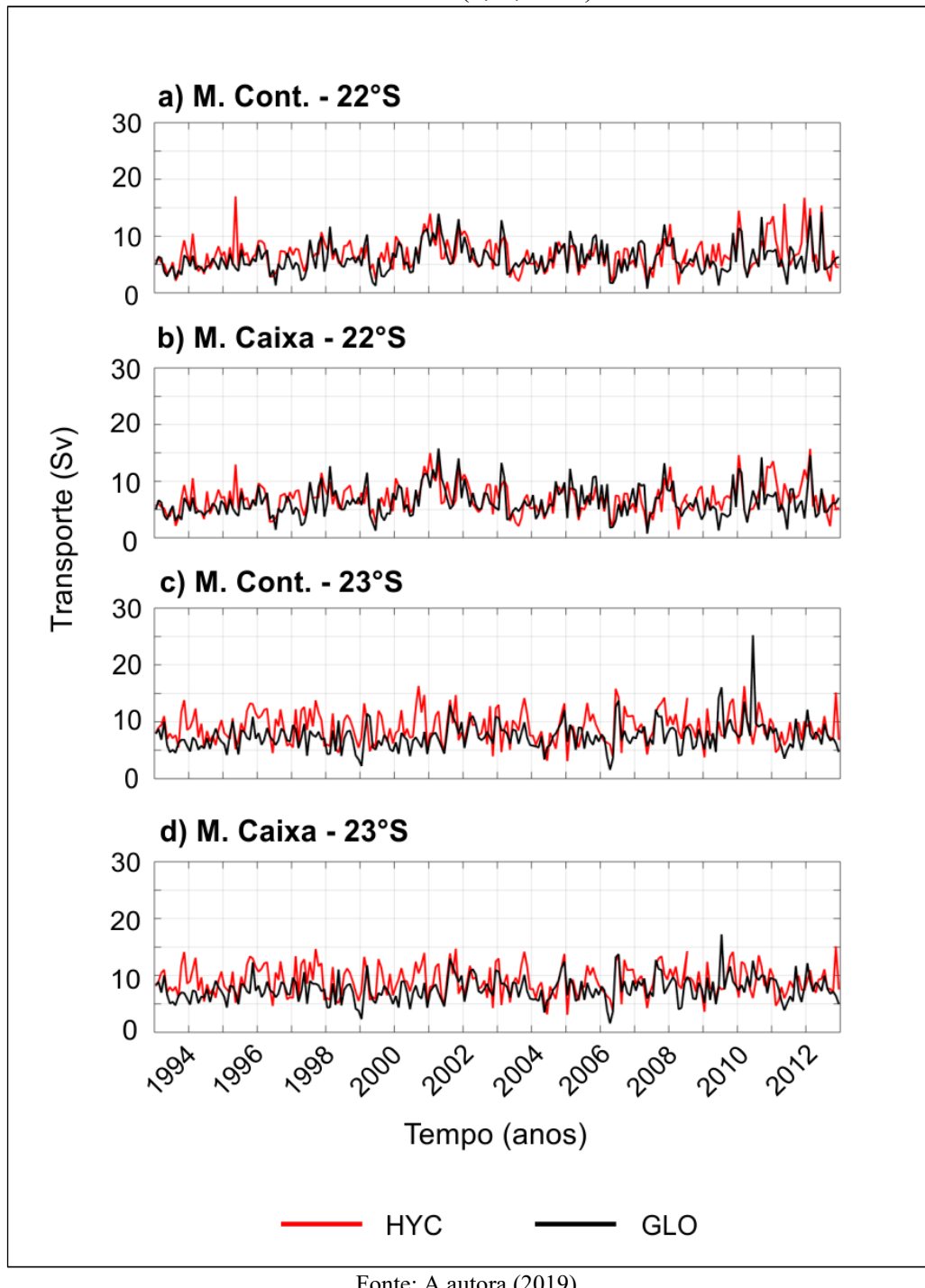


Fonte: A autora (2019).

As estimativas de TV (Figura 5a, 5b, 5c e 5d) calculadas pelos dois métodos foram semelhantes. A maior discrepância entre os dados foi registrada em períodos de intensa atividade de mesoescala, aferida através da presença de picos de máximo transporte de volume. Além disso, a ocorrência da passagem desses sistemas também foi verificada através de imagens de elevação da superfície do mar.

Em 22°S esses sistemas foram bem representados pelos dados do HYCOM nos anos de 1995 e 2011, em 23°S o HYCOM registrou essa atividade no ano 2000 e os dados do GLORYS registraram picos em 2009 e 2010. Independente da radial ou do modelo, a utilização do método dos contornos favoreceu a observação da passagem desses sistemas, em vista da abordagem proposta pelo método, de localizar o centro do jato da CB a partir da posição da velocidade meridional negativa máxima.

Figura 5 – Série temporal do transporte de volume da Corrente do Brasil, calculado pelo método “dos contornos” e “das caixas” nas latitudes 22°S e 23°S para dados do HYCOM e do GLORYS (a, b, c e d).

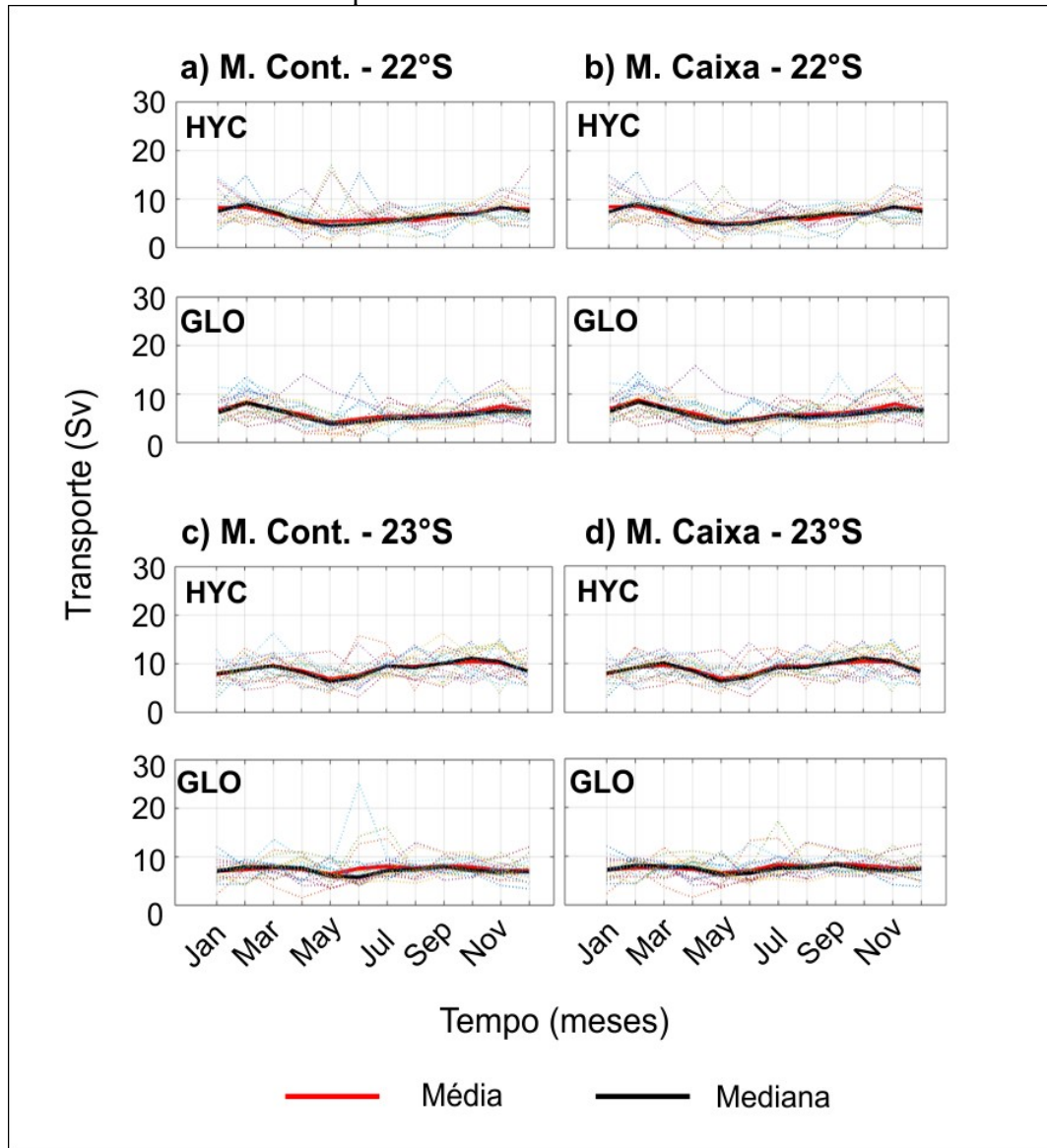


Fonte: A autora (2019).

Na comparação das médias mensais (Figura 6a, 6b, 6c e 6d), a magnitude do transporte para 23°S foi superior. O máximo registrado para a latitude de Cabo Frio foi igual a 12,13Sv (HYCOM) e na latitude do Cabo de São Tomé foi de 8,90Sv (HYCOM). Sazonalmente, os maiores valores de TV foram observados durante o verão (GLORYS) e a primavera (HYCOM), e mínimos predominaram no outono e no inverno. Para os dois modelos o método das caixas

verificou o máximo volume nas médias mensais, equivalentes à: 8,90Sv (HYCOM) e 8,78Sv (GLORYS) em 22°S, e 12,13Sv (HYCOM) e 10,42Sv (GLORYS) em 23°S.

Figura 6 – Média mensal do transporte de volume para o HYCOM (**a** e **b**) e para o GLORYS (**c** e **d**). As linhas tracejadas coloridas representam os valores de transporte para os anos de 1993–2012, a linha contínua em preto representa a mediana e a linha contínua em vermelho representa a média desses dados.



Fonte: A autora (2019).

Vários estudos anteriores já apresentaram o incremento do transporte de volume da CB fluindo para sul ao longo do talude continental brasileiro (STRAMMA et al., 1990, MÜLLER et al., 1998, SCHMID; MAJUMDER, 2018). O estudo da variabilidade sazonal do transporte da CB é objeto de dois artigos recentes (SCHMID; MAJUMDER, 2018, GOES et

al., 2019), cujos resultados são bastante similares aos obtidos neste estudo. Em comparação aos resultados obtidos por Schmid e Majumder, foram obtidas diferenças no transporte de volume da ordem de 2Sv e 3Sv, para 22°S e 23°S, respectivamente. Em relação ao estudo de Goes et al., as diferenças foram cerca de 2Sv.

Em adição a estes, Guerra et al. (2018) apontam que anéis provenientes do Vazamento das Agulhas alcançam a CB e alteram o volume transportado e destacam uma ocorrência na região de Cabo Frio. O ciclo anual definido com máximos na primavera e no verão, pode ser explicado pelo aumento da intensidade dos ventos de N-NE do Anticiclone Subtropical do Atlântico Sul (ASAS) durante essas estações (DERECZYNISKY et al., 2009), associada a migração da bifurcação da CSE ao nível da ACAS, mais a norte no verão e mais a sul no inverno (RODRIGUES et al., 2007).

## 6 CONCLUSÃO

O presente trabalho investigou, através dos produtos de reanálise HYCOM e GLORYS, durante o período de 20 anos (1993–2012), padrões nas variações espaciais e sazonais na velocidade da componente meridional e no transporte de volume da Corrente do Brasil, ao largo da região sudeste brasileira.

A partir dos resultados e dos trabalhos já realizados, foram apontadas duas principais causas para a existência do ciclo anual do transporte da CB, identificado na região estudada, e para as variações espaciais ao longo do seu fluxo. Uma das possibilidades é a variação anual do rotacional do vento, causado pelo deslocamento sazonal da posição do ASAS, responsável pelo GSAS. Esta variabilidade sazonal do ASAS é discutida em Reboita et al. (2019).

Outra possibilidade, está relacionada as alterações no volume transportado, devido a existência de células de recirculação ao longo da CB e pela incorporação de Anéis das Agulhas na altura de Cabo Frio. Além disso, a intensidade das variáveis velocidade e transporte também pode estar sendo alterada durante a primavera e o verão, em decorrência das mudanças sazonais na circulação atmosférica e na posição da bifurcação da CSE.

Uma vez identificado o ciclo anual da CB, estudos posteriores podem ser desenvolvidos, com o objetivo de investigar as principais forçantes responsáveis pela ocorrência desses ciclos sazonais. Correlacionando, estas alterações as variações associadas ao rotacional do vento e a migração do ASAS e da bifurcação da CSE.

## 7 AGRADECIMENTOS

À ANP/PETROBRAS pelo desenvolvimento do termo de cooperação com a Universidade Federal de Santa Catarina (UFSC), no âmbito do projeto “Rede de Caracterização e Modelagem Geológica de Reservatórios – CARMOD Petrobras. Monitoramento Sismológico e Oceanográfico de um Segmento na Margem Sudeste do Brasil: Norte da Bacia de Santos ao Sul da Bacia do Espírito Santo”. Bem como, ao suporte do Centro de Pesquisa e Desenvolvimento Leopoldo Américo Miguêz de Mello – CENPES, na realização do presente trabalho.

## REFERÊNCIAS

- AGÊNCIA NACIONAL DO PETRÓLEO, GÁS NATURAL E BIOCOMBUSTÍVEIS (ANP). **Anuário Estatístico do Petróleo, Gás Natural e Biocombustíveis**. Rio de Janeiro: ANP, 2016. 264 p.
- BROWN, E. *et al.* **Ocean Circulation**. Oxford: Butterworth-Heinemann, 2001. p. 79-142.
- DERECHYNSKY, C. P., OLIVEIRA, J. S., MACHADO, C. O. Climatologia da precipitação no município do Rio de Janeiro. **Revista Brasileira de Meteorologia**, v. 24, n. 1, p. 24-38, 2009.
- GOES, M. *et al.* Long-Term Monitoring of the Brazil Current Transport at 22° S from XBT and Altimetry Data: Seasonal, Interannual, and Extreme Variability. **Journal of Geophysical Research: Oceans**, v. 124, p. 3645-3663, 2019.
- GUERRA, L. A. A; PAIVA, A. M., CHASSIGNET, E. P. On the translation of Agulhas rings to the western South Atlantic Ocean. **Deep Sea Research Part I: Oceanographic Research Papers**, v. 139, p. 104-113, 2018.
- LIMA, J. A. M. Oceanic circulation on the Brazilian Shelf- break and Slope at 22°S. 1997. 164 f. Tese (Doutorado em Matemática Aplicada) - University of New South Wales, Kensington.
- MÜLLER, T. *et al.* Direct measurements of western boundary currents off Brazil between 20°S and 28°S. **Journal of Geophysical Research**, v. 103, p. 5429-5437, 1998.
- REBOITA, M. S. *et al.* The South Atlantic Subtropical Anticyclone: Present and Future Climate. **Frontiers in Earth Science**, v. 7, p. 1-8, 2019.
- RODRIGUES, R. R.; ROTHSTEIN, L. M.; WIMBUSH, M. Seasonal variability of the South Equatorial current bifurcation in the Atlantic Ocean. **Journal of Physical Oceanography**, v. 37, p. 16-30, 2007.
- SCHMID, C.; MAJUMDER, S. Transport variability of the Brazil Current from observations and a data assimilation model. **Ocean Science**, v. 14, p. 417-436, 2018.
- STRAMMA, L.; IKEDA, Y.; PETERSON, R. G. Geostrophic transport in the Brazil Current region north of 20°S. **Deep-Sea Research**, v. 37, n. 1A, p. 1875-1886, 1990.
- TAYLOR, K. E. Summarizing multiple aspects of model performance in a single diagram. **Journal of Geophysical Research**, v. 106, p. 7183-7192, 2001.

Antônia Pamela Yhaohannah de Lima

**SPATIAL AND TEMPORAL VARIABILITY OF WATER MASSES IN THE UPPER  
CIRCULATION OF THE SOUTH ATLANTIC**

Esta seção é destinada a apresentação do artigo científico desenvolvido e submetido a revista *Ocean Dynamics*, como parte dos requisitos para a obtenção do grau de mestre em Oceanografia pela Universidade Federal de Santa Catarina.

Florianópolis

2020

## ABSTRACT

This work investigates spatial and temporal trends and variability, of the layers that constitute the upper circulation of the South Atlantic Ocean (SAO), formed by Surface Water (SW), South Atlantic Central Water (SACW) and Antarctic Intermediate Water (AAIW). Monthly average fields of numerical modeling reanalysis products and data measured in *in situ* (ARGO data) were analyzed in this research. Given the proposal, the following questions were addressed: 1) Are the heat and salt variability in spatial and temporal scales similar in the two decades analyzed in the SAO? 2) Is there a trend to change the volume of water masses that can influence the current circulation of the South Atlantic Subtropical Gyre and influence the processes of the Atlantic Meridional Overturning Circulation (AMOC) in the long term? If so, what mechanism would be the main driver of this process? 3) Are global reanalyses of high-resolution ocean circulation capable of reproducing the variability observed in *in situ* data in the South Atlantic? Monthly averages were separated into two periods, from 1993 to 2001 and from 2002 to 2012, with ARGO being analyzed only in the second period, due to data availability. The results supported the existence of spatial and temporal variability, with greater variability in the processes during the second decade. Trends in warming and salinization over the SAO and the increase in the volume of SACW and AAIW would negatively influence transport within the AMOC and consequently the transport of water from SAO to the North Atlantic Ocean (NAO).

**Keywords:** Large-scale circulation. Seasonal and interdecadal variations. Atlantic Meridional Overturning Circulation. Numerical Modeling. ARGO floats.

## 8 INTRODUCTION

Subtropical gyres are large-scale features that dominate global circulation at medium latitudes (PEDLOSKY, 1990). They are formed by a set of surface ocean currents, driven by overlying anticyclonic wind systems (BROWN et al., 2001). Present in five ocean basins, the subtropical gyres play a fundamental role in the transport of heat, and consequently, in the climatic balance of the planet (ROEMMICH et al., 2016). The South Atlantic Subtropical Gyre (SASG) is the feature corresponding to the South Atlantic Ocean (SAO), consisting mainly of the Brazil Current (BC), the South Atlantic Current (SAC), the Benguela Current (BeC) and the South Equatorial Current (SEC) (MARCELLO et al., 2018).

BC originates in the south of 10°S and flows along the east coast of the South American continent, characterizing the western boundary of the SASG (STRAMMA, 1991). The flow of the BC ends at the encounter with the Malvinas Current at approximately 38°S, in the region known as the Brazil-Malvinas Confluence, generating intense mesoscale vortical instabilities (MAAMAATUAIAHUTAPU et al., 1999; SILVEIRA et al., 2000). To the east of Confluence, the waters that move away from the coast are transported by SAC towards the African continent. In this region, SAC converges with BeC through the Cape Basin, transporting cold and saline waters towards the equator (STRAMMA; PETERSON, 1990; MARCELLO et al., 2018). The northern edge of the SASG is then formed by the flow towards the northwest of the waters that leave the BeC, enter the southern branch of the SEC and migrate towards the Brazilian coast, closing the subtropical gyre (RODRIGUES et al., 2007).

The heat transport towards the equator within the SASG characterizes the upper branch of the Atlantic Meridional Overturning Circulation (AMOC) (RINTOUL, 1991; MIGNAC et al., 2018). In contrast, the existence of this branch of AMOC is a compensation for the export of cold water from the North Atlantic Ocean (NAO), characterized by the intrusion of North Atlantic Deep Water into the SASG, at higher depths (HOLFORT; SIEDLER, 2001; McDONAGH; KING, 2005).

The waters transported within the SAO result from heat and salt exchanges with the Southern, Indian and Pacific oceans, therefore, the water masses that constitute the upper branch of AMOC are the product of this mixture (GARZOLI; MATANO, 2011; MIGNAC et al., 2018). The Leakage of the Rings in the region of the Retroflexion of the Agulhas Current, or simply Agulhas Leakage (AL), is responsible for the Indo-Atlantic connection and the Drake Passage (DP) is the Pacific-Atlantic route (GORDON, 1986; RINTOUL, 1991; DE RUIJTER et al., 1999; RÜHS et al., 2019). The intrusion and redistribution of these waters in the SAO modify the properties of the water masses transported in the subtropical gyre. Consequently, it generates variability in different spatial and temporal scales, which in the long run can also alter the characteristics of AMOC (GARZOLI; MATANO, 2011).

As seen, the oceanic circulation in the SAO is characterized by numerous singularities not found in any other basin (GORDON, 1988). Investigations in recent decades have sought to deepen knowledge about the unique characteristics of this circulation (for example, STRAMMA; ENGLAND, 1999; RODRIGUES et al., 2010; MARCELLO et al., 2018). However, many gaps remain open regarding the standards that control the processes in SAO. The behavior of water masses, regarding their spatial and temporal distribution and the

variability at different scales, is a broad field in this sense (BRYDEN et al., 2003; THRESHER et al., 2014; TIM et al., 2018; CAPUANO et al., 2018). Given the scenario of heat and salt exchange of the South Atlantic with the adjacent oceans, much remains to be investigated to understand the variations in the volume of each water mass, the processes that primarily control these variations and the consequences of this distribution in the global circulation.

The general scheme proposed by Stramma and England (1999) divides the vertical distribution of these masses in superior and deep circulation. Based on this scheme, the variability of the layers that constitute the upper circulation, formed by Surface Water (SW), South Atlantic Central Water (SACW) and Antarctic Intermediate Water (AAIW), were investigated in the present work. To contribute to the determination of possible patterns of variability and trends in the SAO, this study investigates seasonal and interannual variations, as well as analyzes of the spatial distribution of each of these water masses. For this, were used different datasets from numerical model reanalysis products (two decades of temporal coverage), generated by the *Hybrid Coordinate Ocean Model* (HYCOM) and by the *Global Ocean Reanalysis and Simulations* (GLORYS), and data from ARGO floats (a decade of temporal coverage).

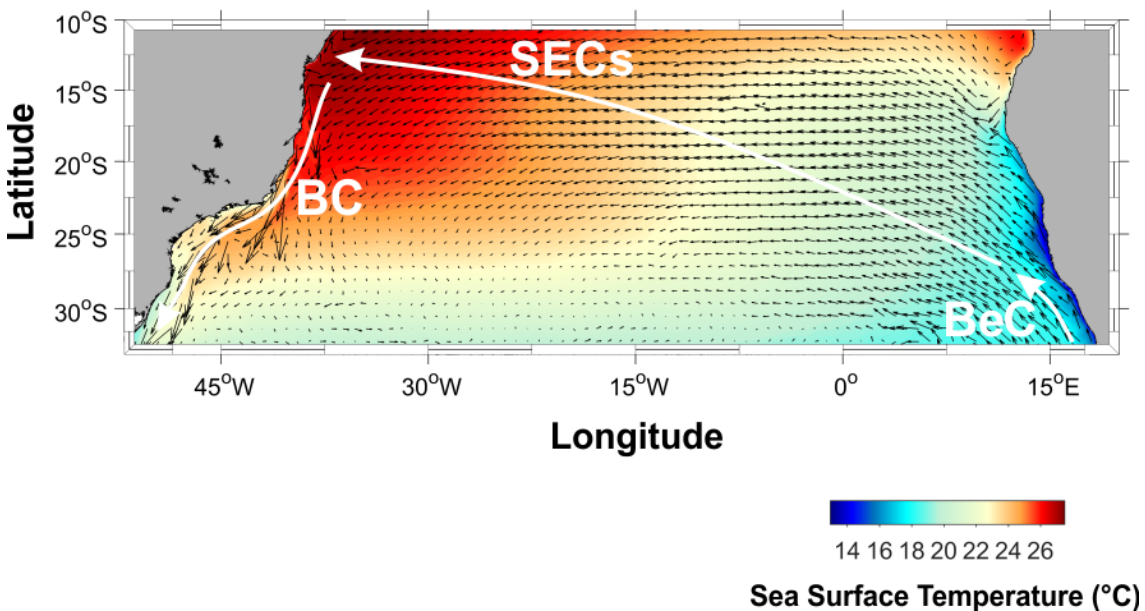
Numerical modeling has been an effective alternative, representing the meso and large-scale processes of global ocean circulation, over the past few decades (GABIOUX et al., 2013). Storto et al. (2019) highlight that the ocean reanalyses obtained from these models is an important tool for monitoring changes and variability in the oceans. In the South Atlantic, investigations into the variability in AMOC and water masses have been made possible in several studies, such as those by Hazeleger and Drijfhout (2006), Rimaud et al. (2012), and Mignac et al. (2018), due to the efforts made in the development of these products.

In this context and based on the proposed objective, we sought to answer the following questions: 1) Are the heat and salt variability in SAO, in spatial and temporal scales, similar in the two decades analyzed? 2) Is there a trend to change the volume of water masses, which can influence the current circulation of SASG and AMOC processes in the long term? If so, what mechanism would be the main driver of this process? 3) Are global reanalyses data of high-resolution ocean circulation capable of reproducing the variability observed in *in situ* data from the South Atlantic?

## 9 DATA AND METHODS

The investigations on the circulation in the SASG (Figure 7) and the variability of the water masses over the SAO, were made from three sets of temperature ( $\theta$ ) and salinity (S) data, which correspond to the reanalysis products and the *in situ* data. This approach made it possible to compare estimated data (numerical modeling) and measured data. The sources and characteristics of each data set used are described below.

Figure 7 – Average circulation in the South Atlantic Subtropical Gyre for the period from 1993 to 2012, obtained from the reanalysis data from GLORYS. The colors indicate the surface temperature of the sea, varying from 12°C (dark blue) to 28°C (dark red), for the analyzed period. The zonal and meridional components of the current velocity are represented by vectors (arrows in black), and the main currents that form the SASG in the study area, represented by the arrows in white, are Brazil Current (BC), Benguela Current (BeC) and the Southern Branch of the South Equatorial Current (SECs).



The choice of reanalysis was based on the methodology of Lima et al. (2016), who consider three main aspects for the selection of the reanalysis product: spatial resolution with the ability to represent mesoscale events (50–500km), time series that represent the seasonal and interannual variability of the water masses, and the ability to assimilate data.

The first product evaluated was the *Hybrid Coordinate Ocean Model* (HYCOM), a high-resolution eddy-permitting model, which numerically solves the primitive equations of ocean dynamics using a hybrid vertical coordinate including isopycnal coordinates for the open

ocean and sigma coordinates for the platform and coastal regions (CHASSIGNET et al., 2009). The model presents data assimilation through the *Marine Coupled Ocean Data Assimilation* (NCODA) system, which behaves similarly to an optimal multivariate interpolation technique, where the atmospheric forcing comes from the National Centers for Environmental Prediction and Climate Forecast System Reanalysis (NCEP/CFSR) (LIMA et al., 2016).

The configuration for the data assimilation is based on a horizontal resolution of  $1/12^\circ$ , in a grid type "Arakawa C", distributed in 40 vertical levels (0–5000m) provided in-depth coordinates, with temporal coverage from 1993 to 2012 (HYCOM, 2017). The download and more information about the configuration of this data can be found on the HYCOM portal (<https://www.hycom.org/>).

The second product of numerical modeling used was the reanalysis data set generated by the *Global Ocean Reanalysis and Simulations* (GLORYS), that is the result of different sources of oceanic records, processed by several groups such as the National Centers for Environmental Prediction and National Center for Atmospheric Research (NCEP/NCAR) and the European Space Agency (SOTO-NAVARRO; CRIADO-ALDEANUEVA, 2012). The horizontal resolution of GLORYS is  $1/12^\circ$ , with 50 vertical levels (0.5–5500m), for the period from 1993 to 2016, using an "Arakawa C" type grid, and the model is eddy-permitting for mesoscale (SOTO-NAVARRO; CRIADO-ALDEANUEVA, 2012; LIMA et al., 2016).

GLORYS reanalysis is based on the ORCA025 configuration and version 3.1 of the Nucleus for European Modeling of the Ocean (NEMO), with atmospheric forcing fields from ERA-Interim (LIMA et al., 2016). The data assimilation technique for the model is the *Système d'Assimilation Mercator version 2* (SAM2) (MERCATOR OCEAN, 2017). The download of this data and more information about GLORYS configuration can be accessed on the COPERNICUS portal (<http://marine.copernicus.eu/services-portfolio/access-to-products/>).

The *In Situ Analysis System* (ISAS) is a tool developed and maintained by the *Laboratoire de Physique des Océans* (LPO) within the *Argo Observing Service* (SO-ARGO), to synthesize temperature and salinity data from the ARGO profiles in a field grid through interpolation. The data is optimally interpolated in a grid with a horizontal resolution of  $1/2^\circ$  and 152 vertical levels, between 1 and 2000m deep. The last ISAS update, named ISAS15, was computed with ISAS-Version 7 (GAILLARD et al., 2016) and the reference climatology ISAS13, with oceanic properties represented in monthly averages for the period from 2002 to 2015.

In this study, data from the interpolated ARGO profilers (ISAS15) were used as a reference *in situ* data set for the HYCOM and GLORYS reanalyses. It should be noted that the

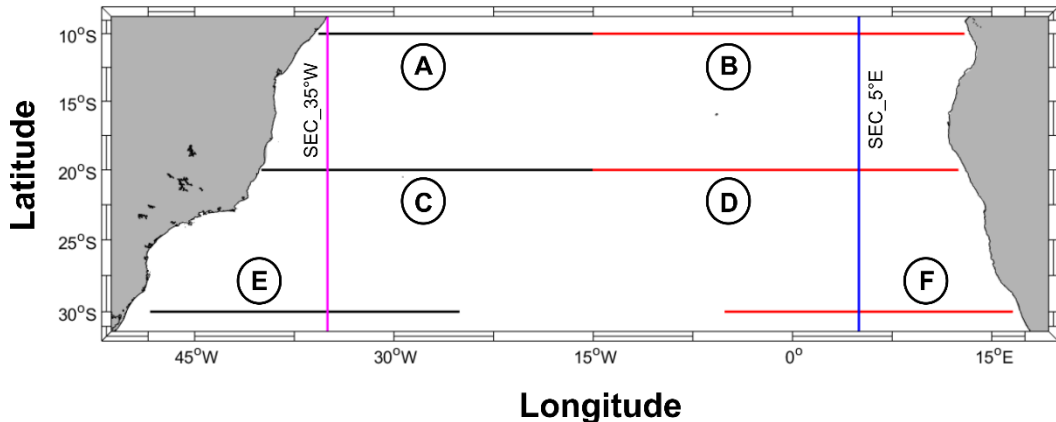
ARGO profiles are part of the set of temperature and salinity records assimilated to generate these two reanalyses products, as well as data from CTD, XBT, buoys, and moorings. However, as the focus of this work was not the validation of numerical models, it was decided to use the results of ISAS15 only as a comparative subsidy for reanalysis, considering that no other database measured *in situ* has the same spatial and temporal coverage than those made available by the ARGO project. From approach, it was expected to obtain approximate results between the reanalysis data and the data measured *in situ*.

Thus, two individual analyzes were performed, one for the pre-ARGO period (1993–2001) or first period (P1) and the other for the period when ARGO was active (2002–2012) or the second period (P2), covering the two decades of data made available by numerical modeling. For the second investigation, the ARGO *in situ* temperature data was transformed into potential temperature, just like the format of the reanalysis “output” data, based on the method available on the *Thermodynamic Equation of Seawater-2010* (TEOS-10) (<http://www.teos-10.org/>).

The investigations of spatial variability in the behavior of water masses were carried out through the analysis of  $\theta$ -S diagrams, longitudinal sections of temperature and salinity, and the delimitation of the depths of interface ( $z_{itf}$ ) between the water masses in the SAO. All analyzes were performed in a similar way for the two defined periods.

For the elaboration of the diagrams, the SAO was divided into six groups: (A) west group at 10°S, (B) east group at 10°S, (C) west group at 20°S, (D) east group at 20°S, (E) west group at 30°S and (F) east group at 30°S (Figure 8). In this way, vertical  $\theta$ -S relation profiles at each longitude were represented for the SAO sectors.

Figure 8 – Location of transects over the South Atlantic Ocean, where  $\theta$ -S diagrams and longitudinal sections of temperature and salinity were developed, depending on the depth. The black and red lines refer to the area of the  $\theta$ -S vertical profile sections, made for all longitudes in the 3 selected latitudes. (A) west transect at 10°S, (B) east transect at 10°S, (C) west transect at 20°S, (D) east transect at 20°S, (E) west transect at 30°S, and (F) east transect at 30°S. The pink and blue lines represent the longitudinal sections at 35°W (SEC\_35°W) and 5°E (SEC\_5°E), respectively.



As for in-depth analysis of the thermohaline structure, it was decided to work with two longitudinal sections of  $\theta$  and S, one closer to the Brazilian coast at 35°W (SEC\_35°W) and another closer to the African coast (SEC\_5°E) (Figure 8). In the second period, in addition to plotting the longitudinal sections in the original resolution of the data, the products of the reanalysis were interpolated to a grid of 1/2° horizontal resolution, and the ARGO data were interpolated to the vertical levels of HYCOM and GLORYS. Thus, it was possible to calculate the Bias and Root Mean Square Error (RMSE) between the numerical modeling data and the data measured in *in situ*.

In the location of the interface depths, specific values of potential density ( $\sigma$ ) were used, associated with the limits between water masses. The density was calculated from the temperature and salinity data and the representative indices were the same used in the study by Pereira et al. (2014) for the SAO. This work assumes that values of  $\sigma=25.7\text{kg.m}^{-3}$  separate Tropical Water from SACW, here this value will be accepted for the separation between SW and SACW ( $z_{\text{itf}_{\text{SW}}\text{SACW}}$ ), with  $\sigma=26.8\text{kg.m}^{-3}$  for the interface between SACW and AAIW ( $z_{\text{itf}_{\text{SACW}}\text{AAIW}}$ ), and  $\sigma=27.5\text{kg.m}^{-3}$  for the interface between AAIW and NADW ( $z_{\text{itf}_{\text{AAIW}}\text{NADW}}$ ).

The identification of the interface depths was also used in the calculation of the thicknesses ( $\Delta$ ) of the water masses SW, SACW, and AAIW. The surface water thickness ( $\Delta_{\text{sw}}$ ) was assumed to be equivalent to the interface depth value between SW and SACW, while for SACW and AAIW they were calculated as indicated in Equations 1 and 2, respectively.

$$\Delta_{\text{SACW}} = z_{\text{-itf}}_{\text{SACW-AAIW}} - z_{\text{-itf}}_{\text{SW-SACW}} \quad (1)$$

$$\Delta_{\text{AAIW}} = z_{\text{-itf}}_{\text{AAIW-NADW}} - z_{\text{-itf}}_{\text{SACW-AAIW}} \quad (2)$$

Temporal variability was grouped into two types: seasonal variation and interannual variation. Seasonal variations were obtained by subdividing all spatial analyzes into average seasons of summer (January, February, and March), autumn (April, May, and June), winter (July, August, and September), spring (October, November, and December) and annual average. On the other hand, to study the interannual variations analyzes made using the  $\theta$ -S diagram were used, describing vertical profiles of the  $\theta$ -S relationship in each longitude within the sectors indicated above, using averages for each year analyzed. Another analysis aimed to investigate interannual variability was the calculation of monthly average time series of the volume values of each water mass.

## 10 RESULTS AND DISCUSSION

### 10.1 SPATIAL AND INTERANNUAL VARIABILITY OF SAO WATER MASSES

During the two periods (P1 and P2), HYCOM and GLORYS reanalysis data showed that Surface Waters ( $\sigma \leq 25.7 \text{ kg.m}^{-3}$ ) are warmer and more saline at  $10^{\circ}\text{S}$ , for the sectors A and B (Figure 9 – panels in rows 1 and 2). Since the other latitudes are located to the south, the position around the equator latitude is responsible for the highest values.

In the western sector of the SAO at  $10^{\circ}\text{S}$  (A, figure 9), the spatial variability of the SW in the GLORYS data is greater than in the HYCOM data, during the periods P1 and P2. Evaluating only the second decade (P2), the data measured in *in situ* by ARGO was more similar to HYCOM reanalysis, because of the reduced spatial variability in the floating data. On the other hand, during P2 the two reanalyses presented interannual variability greater than the variance of the ARGO data, during P2.

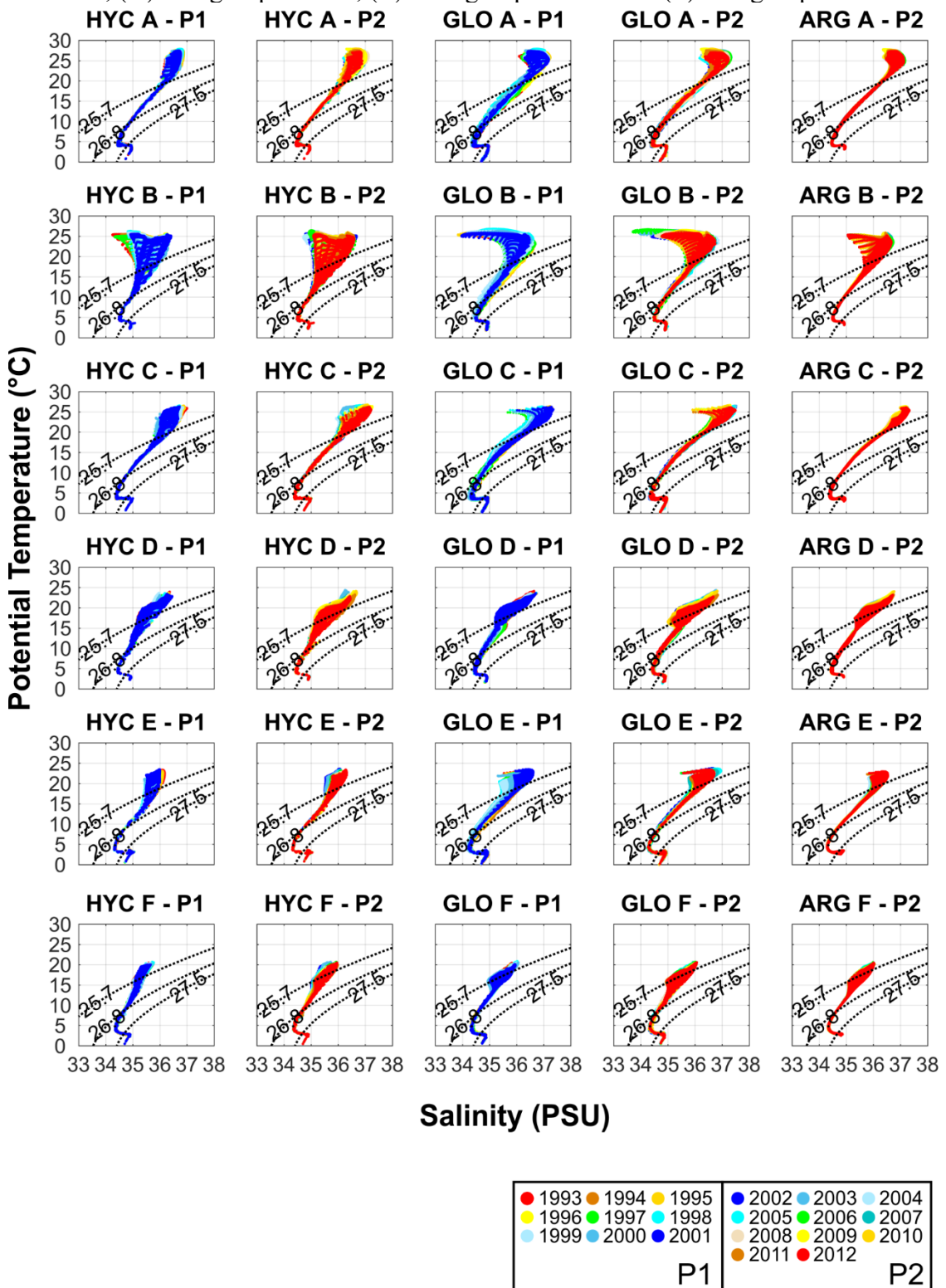
For the eastern sector of the SAO at  $10^{\circ}\text{S}$  (B, figure 9), the spatial and interannual variability of the SW increased in both types of data (reanalysis and measured in *in situ*). In this

region the horizontal gradients of temperature and salinity are higher due to the presence of the Angola Gyre and the Angola-Benguela Front (LASS et al., 2000), the lack of similar structures in sector A, resulted in different characteristics in the comparison of the two sectors (A and B).

Similar to sector A, in sector B the GLORYS data also showed greater spatial variability than HYCOM in P1 and P2, for the SW. The spatial variability of the floats in the second decade was also not as high as pointed out in the GLORYS data, resembling HYCOM data. About interannual variability, the two models overestimated the results compared to ARGO.

Also, in sector A there was little spatial variability of ACAS ( $25.7\text{kg.m}^{-3} < \sigma \leq 26.8\text{ kg.m}^{-3}$ ) in the two reanalyses during P1, and in the two types of data in the P2 period. In sector B, the spatial variability increased, mainly at the top of this water mass, and just as in the west of the SAO, the greatest interannual variability occurred in P1 in the GLORYS data. In the other results, the interannual differences were smaller or did not occur.

Figure 9 – Interannual variability of data from HYCOM (HYC), GLORYS (GLO), and ARGO (ARG), for the annual average of the periods 1993–2001 (P1) and 2002–2012 (P2), represented in vertical profiles for temperature relation ( $^{\circ}\text{C}$ ) versus salinity for each longitude, of the sectors of the South Atlantic Ocean (SAO). The SAO was divided into six sections, nominally represented by (A) west group at  $10^{\circ}\text{S}$ , (B) east group at  $10^{\circ}\text{S}$ , (C) west group at  $20^{\circ}\text{S}$ , (D) east group at  $20^{\circ}\text{S}$ , (E) west group at  $30^{\circ}\text{S}$  and (F) east group at  $30^{\circ}\text{S}$ .



In sector C, located west of the SAO at 20°S (Figure 9 – panels in row 3), the spatial variability in the reanalysis data was greater compared to sector A, in the two analysis periods (P1 and P2). However, for the same region (C), the data from the ARGO floats showed less spatial variability than in A, during P2.

For the P1 period, the interannual variability of GLORYS data was greater than the interannual variability in HYCOM. In P2, all results showed little interannual variability, mainly in the data from GLORYS and ARGO floats. The assimilation of ARGO data into numerical modeling data from the 21st century onwards, contributed to changes in the θ-S variability, by adding realistic values to the results obtained and the products generated (HUANG et al., 2008).

On the east side of the SAO at 20°S (D, figure 9), the spatial variability was greater than in the region adjacent to the Brazilian coast (C) for the same latitude. Longitudinal differences in D (Figure 9 – panels in row 4) were smaller than in B, but were representative for SW at 20°S, due to the presence of the Front formed by the meeting of the Angola Current and BeC in this region (COLBERG; REASON, 2006).

In interannual variability, the results were similar for reanalysis during P1. The biggest differences observed occurred from 1998 to 2000 in the HYCOM data. In P2, in 1998, the small variability of HYCOM remained around the other analyzed data, but in general, the interannual variability of the reanalysis was similar to the *in situ* data.

Most of the SACW spatial variability in D, as in B, occurred at the top of the layer, near the interface between the SW and the SACW. Due to the ocean-atmosphere interaction, the exchange processes that occur in the SW, promote a layer with greater spatial and interannual variability, in comparison to the deeper layers, as demonstrated over the decades by Walin (1982), Donners et al. (2005), and Goes et al. (2018). GLORYS better represented this variability in sector D, when compared to what was observed in the *in situ* data.

At 30°S, in the western region of the SAO (Figure 9 – panels in row 5), little interannual variability was observed in the HYCOM data during P1, compared to the GLORYS results for the same region. During P2, the behavior of the two reanalyses was the opposite, with greater interannual variability in the HYCOM data. In terms of spatial variability, GLORYS coincided better with what was observed in the ARGO data, which showed few spatial differences in the second decade analyzed.

According to Pedlosky (1990), the reduction in temperature and salinity of latitudes, as they approach the poles, alters the intensity of exchanges driven by atmospheric conditions

in the surface layer of the ocean, causing the reduction in variability observed in the data at 30°S.

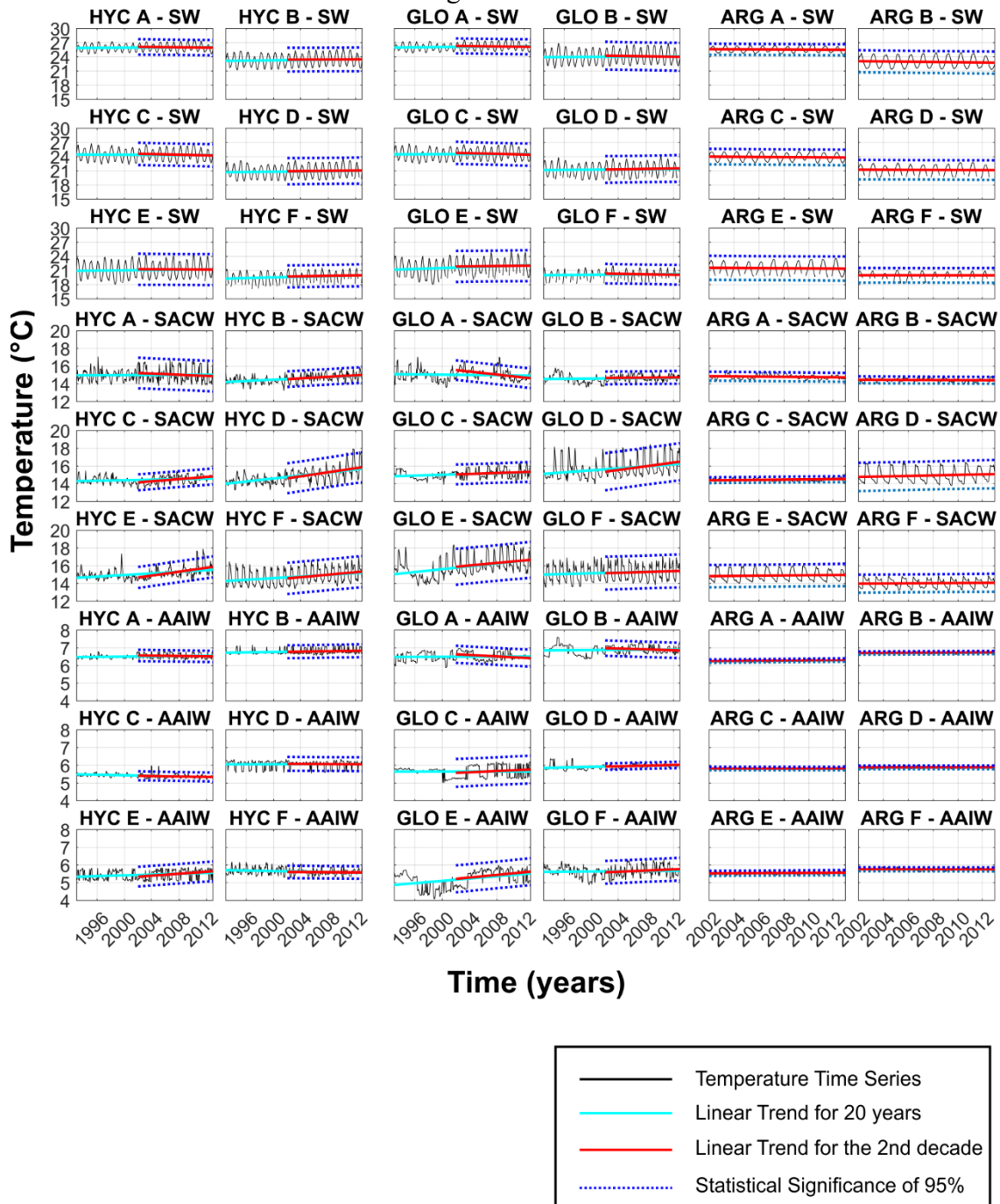
In sector F (Figure 9 – panels in row 6), the interannual variability of the two reanalyses was similar during P1 and the spatial variability was greater in GLORYS. In P2, the interannual differences were greater in HYCOM and spatially similar in the two reanalyses, due to the little interannual and spatial variability of the ARGO data, GLORYS better represented what was observed by the floats.

The reduction of the values of  $\theta$  and S at high latitudes in the Southern Hemisphere, causes a reduction in the thickness of the SW layer, as discussed later in this work. As a result of this reduction, the top of the SACW layer becomes more susceptible to the processes of ocean-atmosphere interaction, by transferring flow along the water column. As a result of this aspect, the behavior of SACW at 30°S, was similar to what has been described for SW in all analyses.

In all analyzes AAIW ( $26.8\text{kg.m}^{-3} < \sigma < 27.5\text{kg.m}^{-3}$ ) was represented by a minimum of salinity in the curve of the  $\theta$ -S diagram. In this layer, considerable spatial and interannual variability was not observed in any of the sectors or periods, as occurred in the layers above this water mass.

In addition to the  $\theta$ -S diagrams, Figures 10 and 11 show the variations in temperature and salinity data, in the sectors in which the SAO was divided. Linear trend lines (by decade) were generated separately for the full 20-year period (P20), and only for the ARGO term, highlighting the interdecadal differences of these variables in each water mass.

Figure 10 – Representation of temperature ( $^{\circ}\text{C}$ ) (solid black line) for data from HYCOM (HYC), GLORYS (GLO), and ARGO (ARG), during the periods 1993–2012 (P20) and 2002–2012 (P2), represented in sectors of the South Atlantic Ocean (SAO). The SAO was divided into six sections, nominally represented by (A) west group at  $10^{\circ}\text{S}$ , (B) east group at  $10^{\circ}\text{S}$ , (C) west group at  $20^{\circ}\text{S}$ , (D) east group at  $20^{\circ}\text{S}$ , (E) west group at  $30^{\circ}\text{S}$  and (F) east group at  $30^{\circ}\text{S}$ . The continuous lines in cyan represent the linear trend ( $^{\circ}\text{C}.\text{decade}^{-1}$ ) of the data from the period 1993 to 2012, and the continuous lines in red represent the trend ( $^{\circ}\text{C}.\text{decade}^{-1}$ ) for the period of validity of ARGO (2002–2012), with the blue dashed lines representing the statistical significance of the data.



Time series and  $\theta$  and S trends in Figures 10 and 11 showed that heating and salinization in SW and SACW predominated during P20, while cooling and salinization of SW and heating and salinization of SACW predominated in P2. In the AAIW, the reanalysis data disagreed with each other in most sectors for P20. As for P2, heating and refreshing predominated.

The warming of the oceans in recent decades was addressed in the study by Roemmich et al. (2015) as a trend since 1951, equivalent to about  $0.1^{\circ}\text{C}.\text{decade}^{-1}$ . However, the authors point out that in the period between 1998 and 2013 there were no significant upward trends in the Sea Surface Temperature values, as a result of the cooling in the Eastern Equatorial Pacific Ocean (La Niña). In deeper waters (100–500m), heating anomalies were observed and related to El Niño variability.

According to Curry et al. (2003), the evaporation and precipitation ratio ( $E - P$ ) in latitudes above  $25^{\circ}\text{S}$  is pointed out as the main cause of salinization of the upper layers of the ocean. They also stated that the trend values for positive salinity for these areas are of the order of 0.004PSU, similar to the values obtained in this work through the reanalysis data (Table 1).

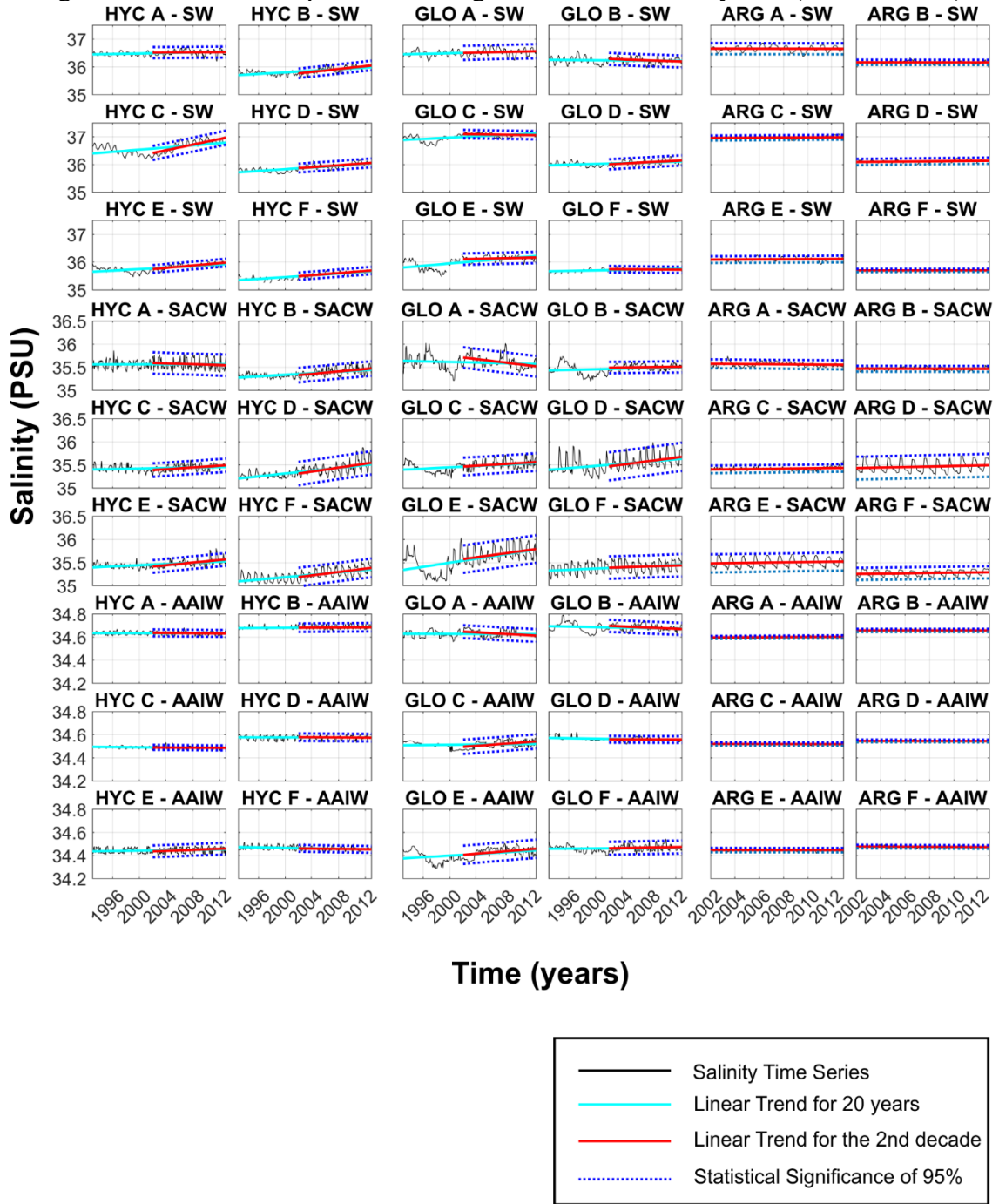
In the SAO surface layer, HYCOM's P20 trends pointed to greater warming and salinization in sectors east of the South Atlantic, while GLORYS trends pointed to sectors west of the Atlantic (Tables 1 and 2). Since there are no data measured in *in situ* for comparison during the first decade of the 20 years analyzed, it was not possible to state clearly which representation is the true one, based only on these data.

Table 1 – Trend values (TD) of temperature (in  $^{\circ}\text{C}.\text{decade}^{-1}$ ), for the data of HYCOM, GLORYS, and ARGO, during the periods of 1993–2012 (P20) and 2002–2012 (P2), in sectors of the South Atlantic Ocean (SAO). The SAO was divided into six sections, nominally represented by (A) west group at 10°S, (B) east group at 10°S, (C) west group at 20°S, (D) east group at 20°S, (E) west group at 30°S and (F) east group at 30°S. The trends were calculated for each water mass of the upper circulation of the SAO, represented by Surface Water (SW), South Atlantic Central Water (SACW), and Antarctic Intermediate Water (AAIW).

<b>Latitude (°S)</b>	<b>Sector</b>	<b>Water mass</b>	<b>HYCOM</b>		<b>GLORYS</b>		<b>ARGO</b>
			<b>TD P20 (°C)</b>	<b>TD P2 (°C)</b>	<b>TD P20 (°C)</b>	<b>TD P2 (°C)</b>	<b>TD P2 (°C)</b>
10	A	SW	0.002	-0.005	0.004	-0.006	-0.004
10	B	SW	0.005	0.002	0.003	-0.007	-0.009
20	C	SW	-0.002	-0.010	0.001	-0.011	-0.005
20	D	SW	0.005	0.004	0.004	0.007	-0.003
30	E	SW	0.005	-0.002	0.016	0.005	-0.005
30	F	SW	0.011	0.007	0.004	-0.007	-0.001
10	A	SACW	0.011	0.007	-0.002	-0.028	-0.004
10	B	SACW	0.001	-0.010	0.002	0.002	-0.002
20	C	SACW	0.012	0.014	0.007	0.008	0.004
20	D	SACW	0.005	0.020	0.019	0.034	0.010
30	E	SACW	0.028	0.037	0.027	0.024	0.004
30	F	SACW	0.015	0.036	0.007	0.007	0.003
10	A	AAIW	0.015	0.023	0.000	-0.007	0.002
10	B	AAIW	0.001	-0.002	0.001	-0.004	0.001
20	C	AAIW	0.002	0.002	0.000	0.006	0.000
20	D	AAIW	-0.003	-0.002	0.003	0.003	0.000
30	E	AAIW	0.000	-0.001	0.011	0.012	0.001
30	F	AAIW	0.004	0.009	0.001	0.005	0.000

According to the  $E - P$  distribution map, referred to in various literature, as in the studies by Schmitt (1995), Curry et al. (2003), and Lagerloef et al. (2010), the western border of the SAO is characterized by high salinity values in the superficial layers since, in this area, evaporation is superior to precipitation. However, for P2, the ARGO floats showed greater cooling in the sectors adjacent to the Brazilian coast than in the sectors adjacent to the African coast, and that the salinity trend (Figure 11) did not diverge between the two. In this aspect, the HYCOM data was better than the GLORYS data.

Figure 11 – The same represented in Figure 10, for the salinity data ( $\text{PSU} \cdot \text{decade}^{-1}$ ).



In the HYCOM temperature trends for SACW during P20, sectors A, C, and E, were in a warming process higher by at least  $0.01^\circ\text{C} \cdot \text{decade}^{-1}$  when compared to sectors B, D and F, being the largest difference in  $\theta$  trend between the Brazilian and African coasts. On the other hand, in GLORYS this behavior occurred only in sectors E and F, while in D the trend was greater than in C, and in A there was cooling and in B, heating.

These differences between reanalyses were also identified in the salinity trend (Table 2), HYCOM recorded greater salinization in all sectors on the east side of the OAS (B, D, and F). For GLORYS, only sector D presented greater salinization (compared to C), with refreshment in A and salinization in B, and greater salinization in E than in F.

Table 2 – The same shown in Table 1, for the salinity data ( $\text{PSU} \cdot \text{decada}^{-1}$ ).

<b>Latitude (°S)</b>	<b>Sector</b>	<b>Water mass</b>	<b>HYCOM</b>		<b>GLORYS</b>		<b>ARGO</b>
			<b>TD P20 (PSU)</b>	<b>TD P2 (PSU)</b>	<b>TD P20 (PSU)</b>	<b>TD P2 (PSU)</b>	<b>TD P2 (PSU)</b>
10	A	SW	0.002	0.001	0.002	0.002	0.000
10	B	SW	0.005	0.009	-0.001	-0.003	0.000
20	C	SW	0.006	0.017	0.004	-0.001	0.001
20	D	SW	0.005	0.006	0.002	0.004	0.001
30	E	SW	0.004	0.007	0.007	0.002	0.001
30	F	SW	0.005	0.006	0.002	-0.001	0.000
10	A	SACW	0.000	-0.001	-0.001	-0.006	-0.001
10	B	SACW	0.003	0.004	0.001	0.000	0.000
20	C	SACW	0.001	0.003	0.002	0.003	0.001
20	D	SACW	0.005	0.007	0.004	0.006	0.002
30	E	SACW	0.002	0.005	0.007	0.007	0.001
30	F	SACW	0.004	0.006	0.002	0.002	0.001
10	A	AAIW	0.000	0.000	0.000	-0.001	0.000
10	B	AAIW	0.000	0.000	0.000	-0.001	0.000
20	C	AAIW	0.000	0.000	0.000	0.001	0.000
20	D	AAIW	0.000	0.000	0.000	0.000	0.000
30	E	AAIW	0.000	0.001	0.001	0.002	0.000
30	F	AAIW	0.000	0.000	0.000	0.000	0.000

SACW region in P2 trends from θ and S, showed that the GLORYS results were better than the HYCOM results, when compared to the ARGO data. From the records of the floats, a trend of cooling and refreshing of the Brazilian coast was observed in 10°S, and a heating and salinization trend in other latitudes were identified. For the African coast, the greatest trend of warming and salinization occurred at 20°S.

The data encountered was the biggest trend of heating and salinization among the data measured in *in situ*, being at 20°S on the African coast at 20°S, and at 30°S heating and salinization on the west side of SAO.

The Agulhas Current Ring Leak, in the Retroflexion region, is responsible for the entry of warmer and saline waters on the east side of the South Atlantic. According to Goes et al. (2014), two main factors may be responsible for this heating and salinization of the SAO. First, the expansion of the SASG and the consequent increase in the mixing of the waters of the

Agulhas within the South Atlantic. Second, the strengthening of the west winds and the increase in the AL, causing the entry of waters at higher depths at the level of SACW and AAIW.

Following, HYCOM data showed, for the most part, that the AAIW heating trends for the Brazilian coast during P1 and P2, while for the African coast there were heating trends in P1 and cooling in P2. On the other hand, the GLORYS data showed an AAIW heating process in both sectors and for both periods, except at 10°S latitude during P2. Comparatively, in most cases, the float data pointed to the same observed in GLORYS, with the reservations that lower trend values were verified for sectors C, D, and F ( $-0.00003^{\circ}\text{C}.\text{decade}^{-1}$ ,  $0.00004^{\circ}\text{C}.\text{decade}^{-1}$  and  $-0.0002^{\circ}\text{C}.\text{decade}^{-1}$ , respectively).

Salinity trends were similar for HYCOM and GLORYS, with values approximately equal to 0, in most sectors. During P2, very low values were repeated for ARGO in all sectors, in the order of  $-2 \times 10^{-4}^{\circ}\text{C}.\text{decade}^{-1}$ . For GLORYS, negative trend values were observed in A and B, and an increase in salinity was recorded in E. In HYCOM only sector E showed a positive trend value, the other values were approximately equal to 0.

According to Schmidtko and Johnson (2012), temperature variations in the AAIW are related to variations in the Southern Annular Mode and the Sea Surface Temperature, close to the main areas of formation of this water mass, especially during the winter. However, in some cases in the SAO, this variation may result from the entry of Indian Ocean waters into the Atlantic Ocean, through the AL.

These variabilities can alter the ventilation of the waters at the base of the thermocline in subtropical regions, as well as reduce the oxygenation of deep waters, a region in which AAIW plays an important role in this subject (SCHMIDTKO; JOHNSON, 2012).

The differences in the entry of waters from the Pacific and Southern Oceans, in contrast to the Indian Ocean, are pointed out by Yao et al. (2017) as the main cause for the refreshing of the intermediate waters in the SAO. The authors suggest that the entry of less saline water from the regions of origin of the AAIW, where precipitation is greater than evaporation, promotes a decrease in salinity in the AAIW within the SAO.

## 10.2 SPATIAL AND SEASONAL VARIABILITY IN LONGITUDINAL SECTIONS

From the surface to the base of the mixture layer, annual average temperatures and salinity (Figure 12 – panels in rows 1 and 2) were observed higher on the west side of the South Atlantic ( $35^{\circ}\text{W}$ ), compared to the east side ( $5^{\circ}\text{E}$ ) (Tables 3 and 4).

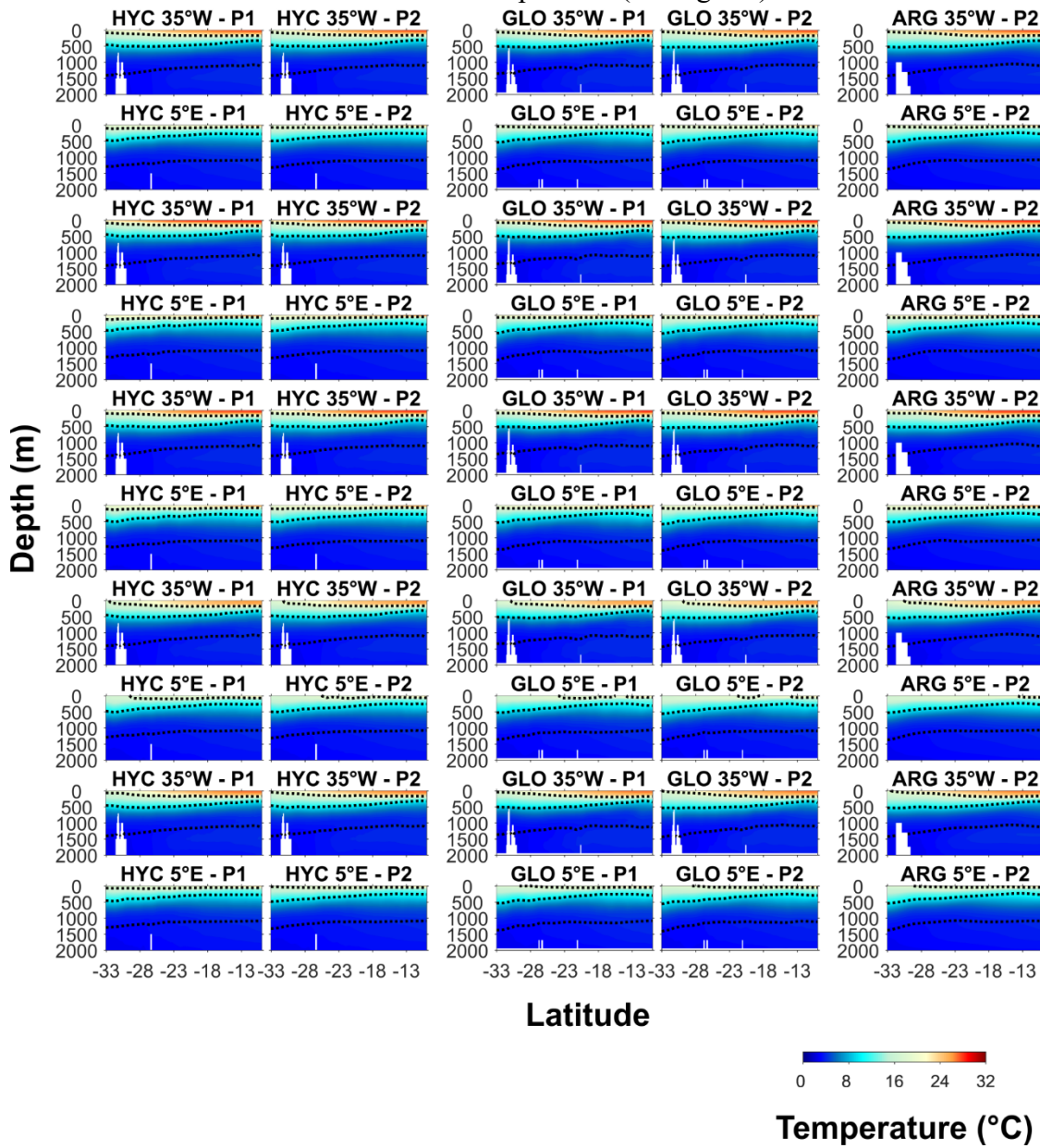
The analysis of seasonal averages showed differences of up to 4.23°C and 0.82PSU for HYCOM data, and 3.79°C and 0.75PSU for GLORYS data, during P1 between the west side and east side of the SAO. For P2, the differences in  $\theta$  increased for the two reanalyses (5.45°C and 4.01°C) while the salinity decreased for HYCOM (0.80PSU) and increased for GLORYS (0.85PSU). In comparison to the ARGO data, temperature differences were better represented by GLORYS (glorys-argo=0.4°C) and salinity differences by HYCOM (hycom-argo=0PSU).

Table 3 – Values of mean temperature differences (in °C) between two cross-sections (at 35°W and 5°E), on the western and eastern borders of the South Atlantic Ocean (SAO). The data are from the HYCOM and GLORYS reanalyses, and ARGO floats, during the periods 1993–2001 (P1) and 2002–2012 (P2). The analyzes were divided into annual, summer, autumn, winter and spring averages for each period. Also, they were calculated for each water mass of the upper circulation of the SAO, represented by Surface Water (SW), South Atlantic Central Water (SACW), and Antarctic Intermediate Water (AAIW).

Water mass	Period	HYCOM		GLORYS		ARGO
		$\theta_{35^{\circ}\text{W}-5^{\circ}\text{E}}$ P1 (°C)	$\theta_{35^{\circ}\text{W}-5^{\circ}\text{E}}$ P2(°C)	$\theta_{35^{\circ}\text{W}-5^{\circ}\text{E}}$ P1 (°C)	$\theta_{35^{\circ}\text{W}-5^{\circ}\text{E}}$ P2 (°C)	$\theta_{35^{\circ}\text{W}-5^{\circ}\text{E}}$ P2 (°C)
SW	Annual	3.89	1.83	3.62	3.78	3.24
SW	Summer	3.69	4.16	3.29	3.22	2.54
SW	Autumn	3.45	5.45	3.11	3.37	2.78
SW	Winter	3.93	3.85	3.78	3.75	1.93
SW	Spring	4.23	3.11	3.79	4.01	3.61
SACW	Annual	0.53	0.30	0.34	0.67	0.51
SACW	Summer	0.62	0.50	0.36	0.83	0.61
SACW	Autumn	0.74	-0.98	0.76	1.08	0.85
SACW	Winter	0.20	-0.28	-0.62	-0.72	-0.47
SACW	Spring	0.18	0.22	-0.57	-0.07	0.05
AAIW	Annual	-0.58	-0.49	-0.69	-0.46	-0.34
AAIW	Summer	-0.53	-0.41	-0.67	-0.46	-0.37
AAIW	Autumn	-0.57	-0.44	-0.71	-0.45	-0.38
AAIW	Winter	-0.46	-0.50	-0.68	-0.44	-0.32
AAIW	Spring	-0.61	-0.48	-0.70	-0.41	-0.35

The differences between 35°W and 5°E, mainly during spring and winter, showed the cold and less saline winter waters (the result of the flows from the Southern Ocean), which enter the SAC and are partly transported by BeC, in region adjacent to the African coast at 5°E (STRAMMA; ENGLAND, 1999). This flow accentuates the divergences existing between the two cross-sections during this season and its influence remains until spring, resulting in the discrepancies found.

Figure 12 – Longitudinal sections of average temperature ( $^{\circ}\text{C}$ ) in  $35^{\circ}\text{W}$  (Brazilian coast) and  $5^{\circ}\text{E}$  (African coast), for the data of HYCOM (HYC), GLORYS (GLO) and ARGO (ARG), during the periods of 1993–2001 (P1) and 2002–2012 (P2), divided into annual average (panels of line 1), summer (panels of line 2), autumn (panels of line 3), winter (panels of line 4), and spring (line 5 panels). Dashed lines show the potential density of the interface between Surface Water (SW) and South Atlantic Central Water (SACW) ( $25.7\text{kg.m}^{-3}$ ), between SACW and Antarctic Intermediate Water (AAIW) ( $26.8\text{kg.m}^{-3}$ ), and between AAIW and North Atlantic Deep Water ( $27.5\text{kg.m}^{-3}$ ).



The SACW level, or the layer below the mixing zone, SACW level, the main characteristic that differentiated the west side and east side of the SAO, were the depths occupied by this water mass at latitudes between  $28^{\circ}\text{S}$  and  $13^{\circ}\text{S}$ . West of the SAO the SACW base reached depths of up to 520m and migrated to 250m in the northernmost latitudes. To the

east of the SAO, the lower limit of this body of water was 400m, displacing up to 225m in the northernmost latitudes.

Seasonally, the outcrop of SACW on the surface was the most prominent aspect between the two regions. In both longitudinal sections, in the results of the two reanalyses, and the ARGO data for P2, SACW reached the surface during the winter. However, this Resurgence event was spatially greater on the east side of the SAO, occupying latitudes between 14°S and 33°S, while on the west side the latitudes were restricted between 30°S and 33°S, both results from the ARGO floats.

The Resurgence phenomenon was better represented in the GLORYS data during the two periods analyzed, compared to the ARGO product. For P1, HYCOM did not show the Upwelling process in any 35°W season, although this was evident in the GLORYS data during the winter in both sections. However, for 5°E, the two reanalyses agreed in one aspect, the two results suggested that the Upwelling occupies larger areas during P2.

Resurgence events are common to winter seasons on the western and eastern borders of the South Atlantic (FENNEL, 1999; SILVEIRA et al., 2000). The intensity of this process was greater in the eastern portion of the SAO, due to the extension of the Benguela Upwelling System, characterized as one of the largest Upwelling Systems in the global oceans (SHILLINGTON et al., 2006).

The differences between  $\theta$  and S in the SACW were not as high as in the superficial layer, in none of the analyzed periods. However, the greatest results for divergences between 35°W and 5°E all occurred in the fall, in both periods and for both types of data, as can be seen in Table 3 for temperature and Table 4 for salinity.

In the seasons of higher temperature (summer and autumn) the differences between the two borders of the SAO, increase due to the transport performed by BC (WU et al., 2012). The flow of the BC, over the Brazilian continental slope transports from the surface up to about 500m, warm and saline waters from the equator towards the poles (STRAMMA, 1991). On the eastern border of the SAO, the flow of cold water towards the equator through BeC, compensates for the heat transport from the equator to the south pole. These temperature differences are evident in the most superficial layers, mainly during the hottest and coldest seasons.

Table 4 – The same as in Table 3, for PSU salinity data.

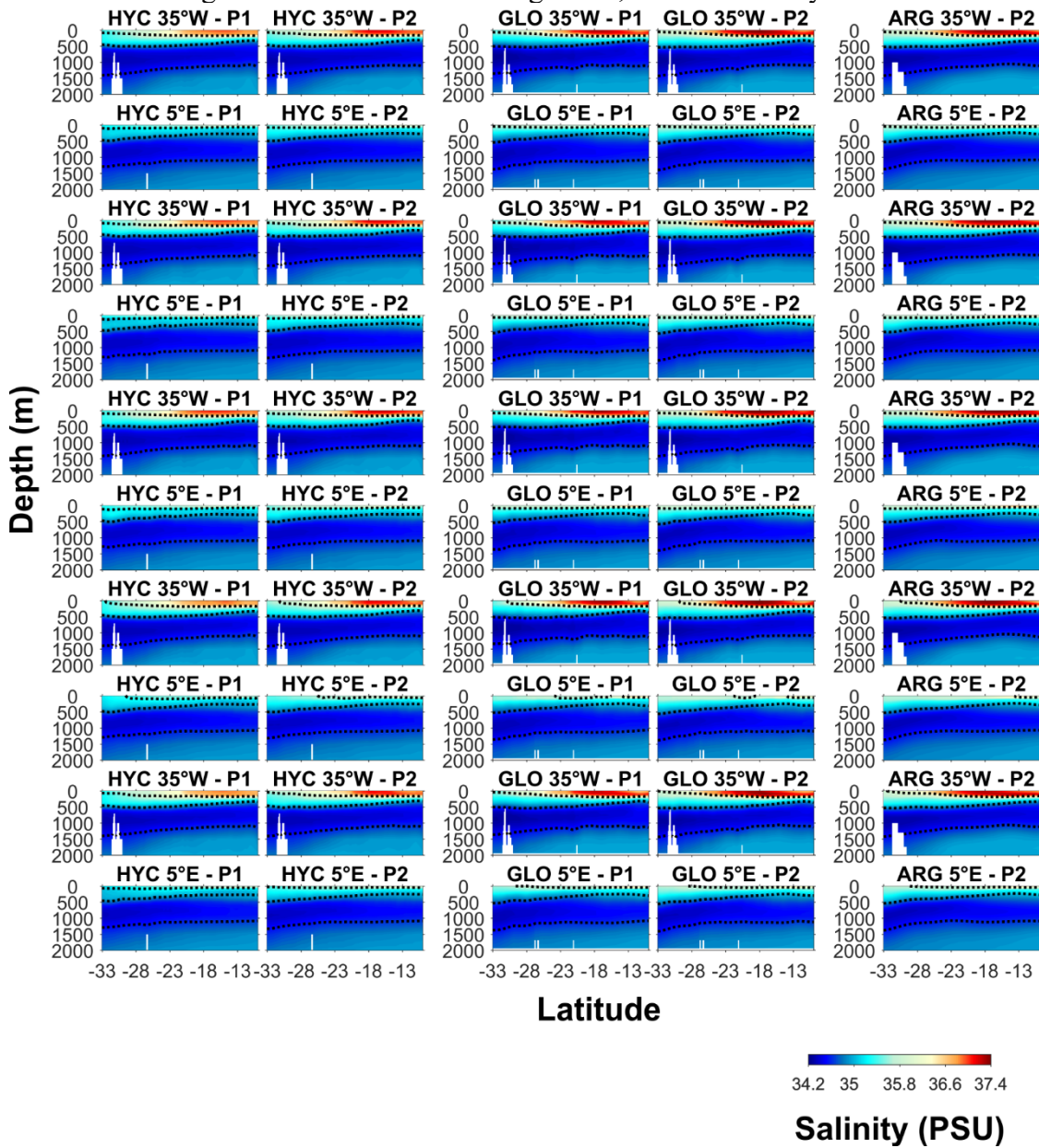
<b>Water mass</b>	<b>Period</b>	<b>HYCOM</b>		<b>GLORYS</b>		<b>ARGO</b>
		S <sub>35°W-5°E</sub> P1 (PSU)	S <sub>35°W-5°E</sub> P2(PSU)	S <sub>35°W-5°E</sub> P1 (PSU)	S <sub>35°W-5°E</sub> P2 (PSU)	S <sub>35°W-5°E</sub> P2 (PSU)
SW	Annual	0.79	0.76	0.70	0.84	0.77
SW	Summer	0.72	0.72	0.67	0.80	0.74
SW	Autumn	0.81	0.76	0.65	0.81	0.75
SW	Winter	0.82	0.80	0.75	0.85	0.56
SW	Spring	0.75	0.76	0.70	0.84	0.80
SACW	Annual	0.30	0.17	0.09	0.19	0.14
SACW	Summer	0.32	0.21	0.09	0.20	0.16
SACW	Autumn	0.32	0.23	0.14	0.24	0.18
SACW	Winter	0.27	0.06	-0.06	0.00	0.00
SACW	Spring	0.28	0.10	-0.03	0.09	0.08
AAIW	Annual	-0.09	-0.07	-0.11	-0.07	-0.06
AAIW	Summer	-0.09	-0.08	-0.10	-0.07	-0.06
AAIW	Autumn	-0.09	-0.08	-0.11	-0.07	-0.06
AAIW	Winter	-0.06	-0.06	-0.11	-0.07	-0.04
AAIW	Spring	-0.09	-0.07	-0.10	-0.06	-0.05

The AAIW showed few differences in the values of  $\theta$  and S between the two longitudinal sections, however, in all seasons the average salinity at 5°E was higher than at 35°W. Through reanalysis data, it was also established that the second decade was more saline than the first in almost all cases.

Although the differences are in the order of approximately 0.07PSU, this data differs from the AAIW refreshing results obtained in the trend analysis. However, it reaffirms the process of entering more saline waters from the Indian Ocean in the SAO, highlighted by Yao et al. (2017), which characterizes higher salinity values on the eastern border of the SAO.

The intermediate water core was well demarcated in the two types of data (Figure 13), however, the lowest values were observed in the GLORYS data (SEC\_35°W=34.26PSU and SEC\_5°E=34.34PSU) and ARGO (SEC\_35°W=34.27PSU and SEC\_5°E=34.33PSU), highlighting the difficulty of HYCOM data (SEC\_35°W=34.31PSU and SEC\_5°E=34.36PSU) in simulating salinity values in agreement with the float data.

Figure 13 – The same as in Figure 12, for PSU salinity data.

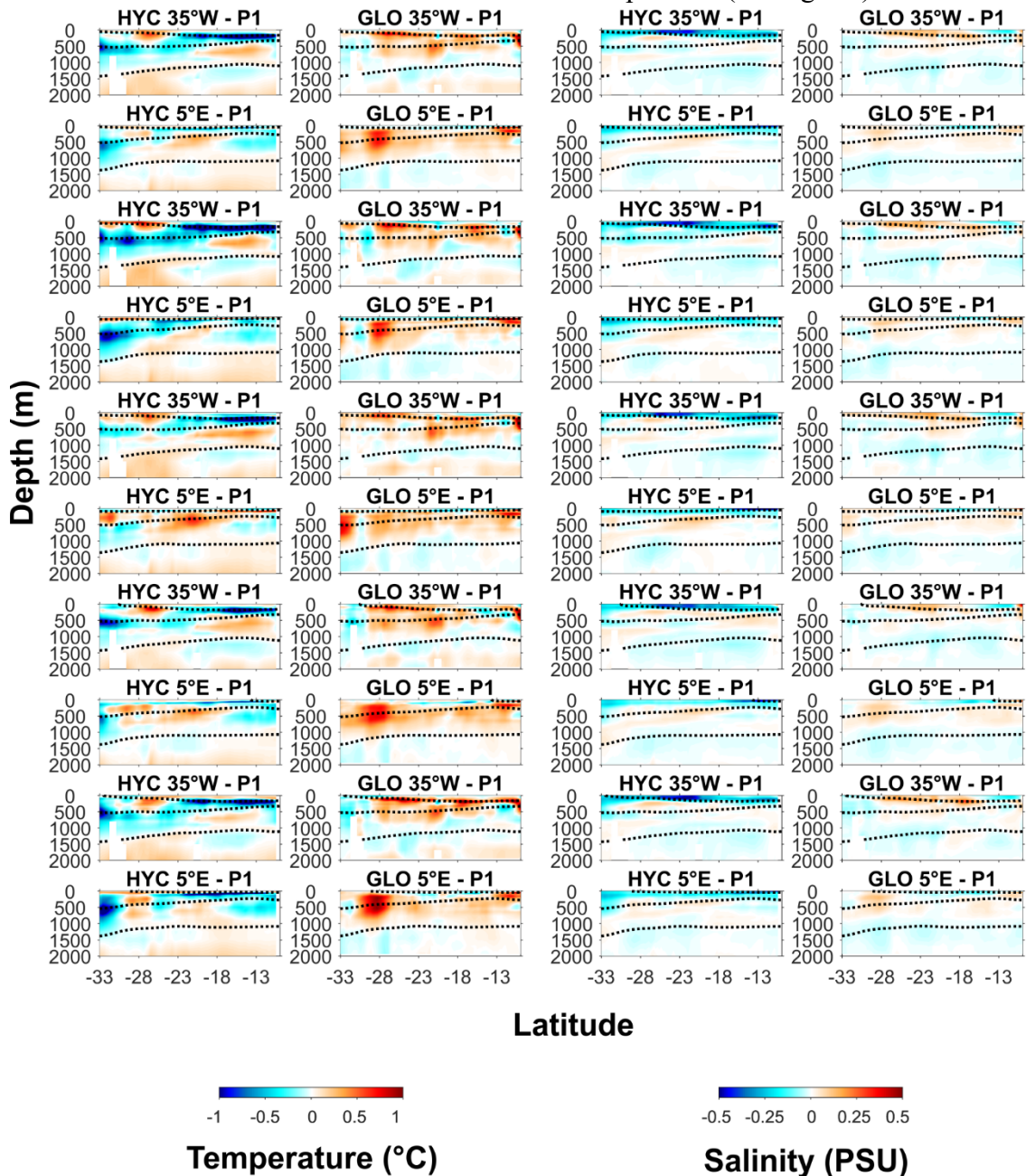


The main divergence between the two longitudinal sections in this layer was related to the latitudinal reach of the minimum salinity core, characteristic of this water mass. In all stations, the maximum range of this core varied between 15°S and 33°S on the east border of SAO, while on the west border this variation occurred up to 2° latitude further north.

Given the differences in  $\theta$  and S between reanalysis and ARGO data, the bias (Figure 14) and RMSE (Table 5) of the analyzes were calculated. From the bias, it was inferred that HYCOM data on the western border were on average warmer (less saline) than ARGO, in all seasons for SW, with a greater difference of  $\theta$  (S) during summer (winter), equal to 0.08°C (-0.26PSU). According to the average values of GLORYS, the results of  $\theta$  (S) were warmer (more

saline) than the ARGO data for this region, with the greatest differences of variables during autumn, equal to 0.14°C and 0,04PSU.

Figure 14 – Representation of the bias for the longitudinal sections of temperature ( $^{\circ}\text{C}$ ) and salinity at  $35^{\circ}\text{W}$  (Brazilian coast) and  $5^{\circ}\text{E}$  (African coast), data from HYCOM (HYC) about ARGO and GLORYS (GLO) about ARGO, during the period between 2002–2012, divided into annual average (panels of line 1), summer (panels of line 2), autumn (panels of line 3), winter (panels of line 4), and spring (line 5 panels). Dashed lines show the potential density of the interface between Surface Water (SW) and South Atlantic Central Water (SACW) ( $25.7\text{kg.m}^{-3}$ ), between SACW and Antarctic Intermediate Water (AAIW) ( $26.8\text{kg.m}^{-3}$ ), and between AAIW and North Atlantic Deep Water ( $27.5\text{kg.m}^{-3}$ ).



On the eastern border of SAO, the average behavior of HYCOM was similar to that of  $35^{\circ}\text{W}$ , however, the average  $\theta$  data was colder ( $-0.15^{\circ}\text{C}$ ) than the ARGO data, during the winter. In this season, the salinity differences were also higher than at  $35^{\circ}\text{W}$ , equal to  $-0.4\text{PSU}$ .

For GLORYS, the  $\theta$  bias behavior was similar to the western border in all seasons, with a higher average value equal to  $-0.11^{\circ}\text{C}$  (summer). Regarding the salinity bias, different aspects were observed for  $5^{\circ}\text{E}$  in all seasons, except in autumn, which presented an average bias more saline than the data from the floats ( $0.07\text{PSU}$ ).

For SACW, the behavior of the two reanalyses was homogeneous in the two transects, with mean values of  $\theta$  colder for HYCOM and warmer for GLORYS, with greater differences occurred on the western border of SAO ( $-0.51^{\circ}\text{C}$  and  $0.24^{\circ}\text{C}$ ).

In the salinity data the only data that was not similar to the others, occurred in the winter of GLORYS ( $-0.02\text{PSU}$ ), in the other seasons the values in the two borders were less saline in HYCOM and more saline in GLORYS. The biggest difference between HYCOM and ARGO data occurred at  $5^{\circ}\text{E}$  ( $-0.13\text{PSU}$ ). Between GLORYS and ARGO ( $0.04\text{PSU}$ ), it occurred at  $35^{\circ}\text{W}$ .

In AAIW, HYCOM  $\theta$  values were mostly cooler than ARGO, except during autumn at  $35^{\circ}\text{W}$  ( $0.02^{\circ}\text{C}$ ). In GLORYS, the data were hotter in all seasons for the two sections, with a greater difference equal to  $0.21^{\circ}\text{C}$ , when compared to the value of  $-0.14^{\circ}\text{C}$  from HYCOM.

The two reanalyses well represented the salinity behavior at  $35^{\circ}\text{W}$ , with mean bias values approximately equal to 0 in all seasons, except in the summer of HYCOM ( $0.01\text{PSU}$ ). At  $5^{\circ}\text{E}$ , the biggest differences were equal to  $0.02\text{PSU}$  for the two reanalyses.

In general, the temperature RMSE values were always higher than those of salinity. The representation of the data at  $5^{\circ}\text{E}$  was better than at  $35^{\circ}\text{W}$ , and although this behavior occurred for both models, GLORYS had lower values than the indices observed for HYCOM. Since the RMSE measurement starts at 0 and increases as the errors are greater, that is, the closer to 0 the better the comparison, the salinity representations at  $5^{\circ}\text{E}$  from GLORYS were better, while the temperature data at  $35^{\circ}\text{W}$  of HYCOM were the worst results, as can be seen in Table 5.

Table 5 – Representation of the Root Mean Square Error for the longitudinal sections of temperature ( $^{\circ}\text{C}$ ) and salinity (PSU) in 35°W (Brazilian coast) and 5°E (African coast), from HYCOM data in comparison with ARGO, and GLORYS with ARGO, during the period between 2002–2012, divided into annual, summer, autumn, winter, and spring averages.

<b>Parameter</b>	<b>Period</b>	<b>HYCOM</b>		<b>GLORYS</b>	
		<b>35°W</b>	<b>5°E</b>	<b>35°W</b>	<b>5°E</b>
$\theta$	Annual	0.29	0.19	0.19	0.21
$\theta$	Summer	0.44	0.29	0.24	0.29
$\theta$	Autumn	0.29	0.22	0.24	0.25
$\theta$	Winter	0.27	0.24	0.23	0.23
$\theta$	Spring	0.29	0.38	0.26	0.23
S	Annual	0.21	0.15	0.07	0.05
S	Summer	0.21	0.15	0.08	0.06
S	Autumn	0.21	0.18	0.09	0.06
S	Winter	0.20	0.16	0.08	0.06
S	Spring	0.22	0.15	0.08	0.05

### 10.3 INTERFACE DEPTHS AND LAYER THICKNESS OF WATER MASSES

Given the differences in the depth of interface between the water masses, on opposite sides of the SAO, and the influence of these changes in the limits of each layer in the water column, variations in the depth of reach of the SW, SACW, and the AAIW, were assessed for the periods P1 and P2, in each station.

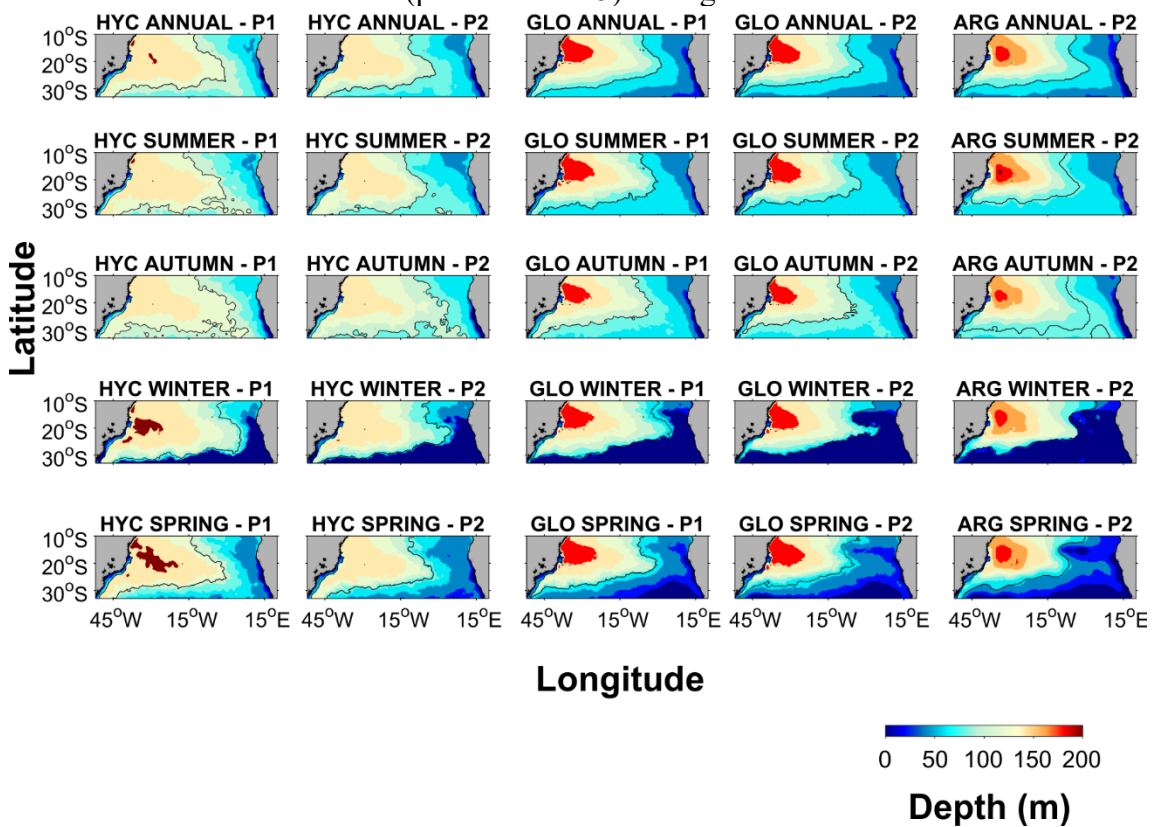
The base of the surface layer, occupied by the SW, was at depths (z) between 0m and 200m in all data and periods. However, the average HYCOM data were higher than GLORYS in all seasons during P1, with the lowest average values during winter, equal to  $z=90.05\text{m}$  and  $z=71.49\text{m}$ , for both data. In the reanalysis data from P2, all mean depths were more superficial than that observed in P1.

The comparison between GLORYS and ARGO data was better, when compared to HYCOM and ARGO. The highest differences in mean values occurred during winter and were equivalent to 23.94m (HYCOM) and 8.66m (GLORYS). During P1, the maximum depth of the SW base (Figure 15 – panels in row 5) obtained a greater spatial distribution in the spring, in comparison with the other seasons. In HYCOM data, the maximum depth ( $z=200\text{m}$ ) was distributed in the region between 10°S–25°S and 37°W–15°W. For GLORYS these maximum ( $z=186.13\text{m}$ ) were between 10°S–22°S and 40°W–22°W.

In the P2 period, maximum values as high as in the first decade for HYCOM data ( $z_{\max}=150\text{m}$ ) were not observed. In the GLORYS data, the maximum depth of the SW base was equivalent to 186.13m, occupying the region between 10°S–22°S and 40°W–22°W in most

seasons, except during the autumn when this area was between 12°S–20°S and 40°W–23°W. In the ARGO data, the maximum value was equal to 200m and occurred only during the summer (Figure 15 – line 2 panels), at approximately 18°S and 35°W. At the other stations, the maximum value was 190m with a distribution similar to the one recorded in the GLORYS data.

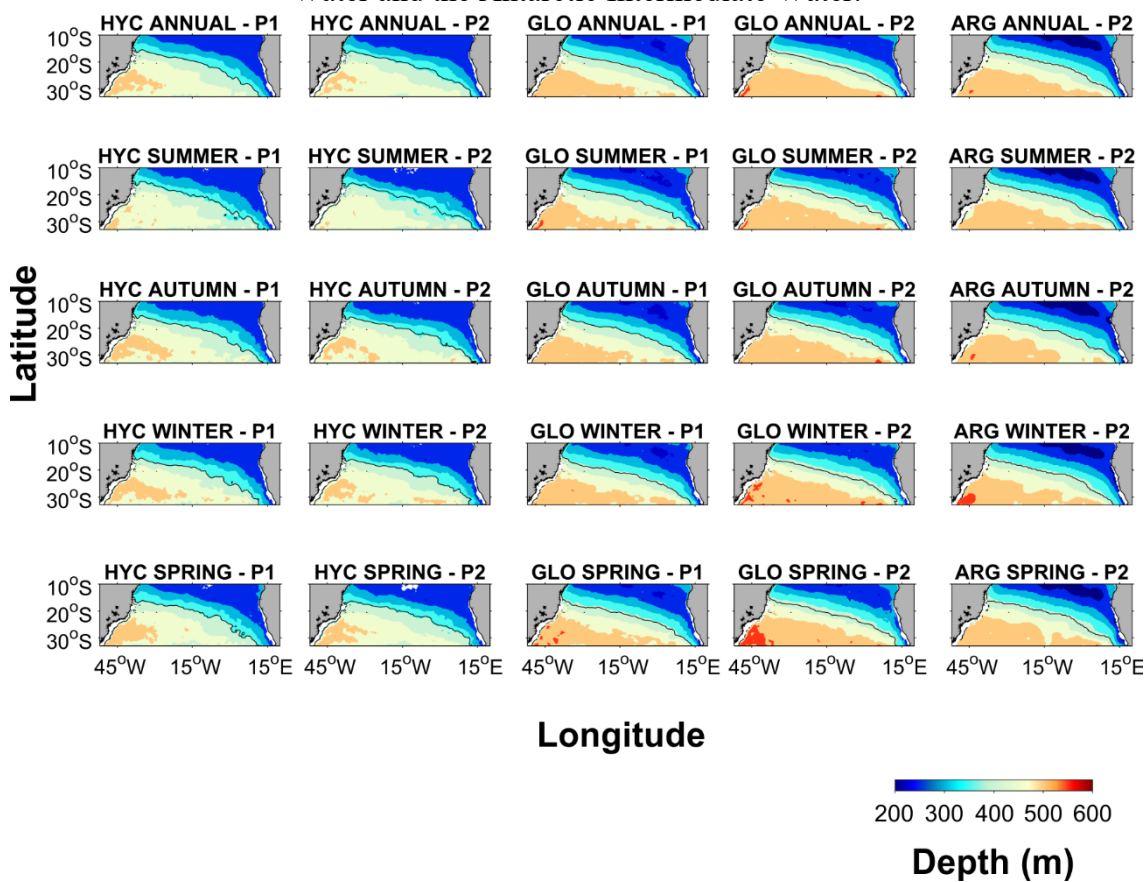
Figure 15 – Representation of interface depth between Surface Water and South Atlantic Central Water, for data from HYCOM (HYC), GLORYS (GLO), and ARGO (ARG), during the periods 1993–2001 (P1) and 2002–2012 (P2), divided into annual (panels of line 1), summer (panels of line 2), autumn (panels of line 3), winter (panels of line 4), and spring (panels of line 5) averages.



The interface depth between SW–SACW showed intense seasonal variability in the SAO, mainly in the region adjacent to the African coast, in the summer and winter seasons. On the surface, the SW occupation was verified throughout the South Atlantic during the summer. In winter, there was no presence of SW on the eastern border of SAO south of 15°S, due to the entry of cold waters into the South Atlantic, transported by SAC to the south of SAO.

For SACW (Figure 16), the interface depth was shallower in the north of the South Atlantic and deeper in the south. In the two analysis periods, the interface data of GLORYS were deeper, in relation to HYCOM, while the highest values were observed during summer and spring (561.76m in P1 and 594.89m in P2).

Figure 16 – The same as in Figure 15 for the interface between the South Atlantic Central Water and the Antarctic Intermediate Water.



In the average data of HYCOM, the values of P1 ( $z_{\max}=401.02\text{m}$ ) were higher than those observed during P2 ( $z_{\max}=395.74\text{m}$ ), while in the GLORYS data, P2 obtained the highest values ( $z_{\max}=426.11\text{m}$ ). As in SW, for SACW the GLORYS was better than HYCOM, in comparison with the ARGO data. The biggest differences between the two reanalyses for the floats were equal to 15.24m and 23.73m, respectively.

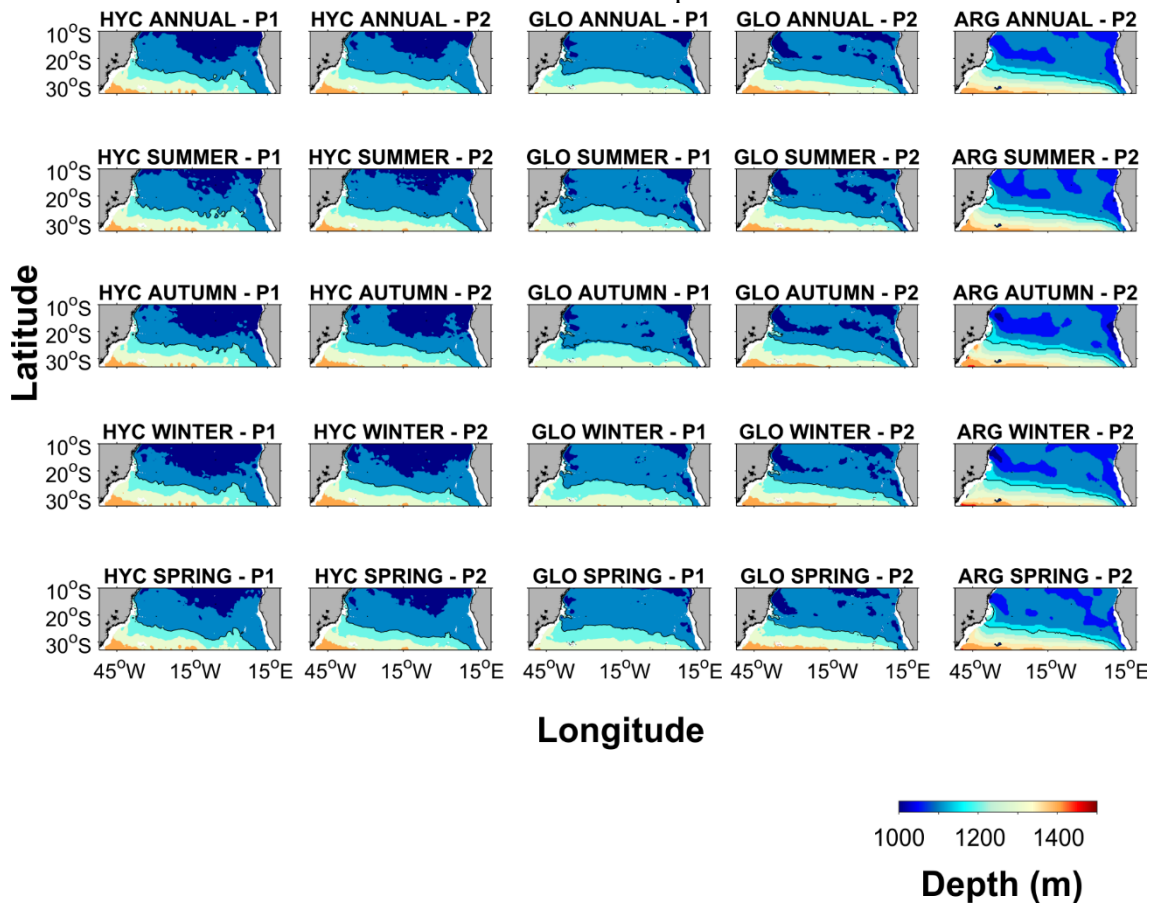
However, the maximum seasonal depth was not well represented by either model, since the data measured in *in situ* indicated that the SACW base was deeper during the winter ( $z_{\max}=600\text{m}$ ) in the period 2002–2012, differently than what was shown in the two reviews.

The spatial distribution of the maximum depth values was greater during P1 in the HYCOM data, and during P2, in the GLORYS data. In both, as in ARGO, the spatial distribution of half of the SAO is occupied by SACW reaching approximately 600m.

The region of the water column occupied by the AAIW (Figure 17) was deeper in the HYCOM data during P1 (1202.78m), and in the GLORYS data during P2 (1206.31m). However, in contrast, for the water masses above the AAIW, the ARGO data were better

represented by HYCOM in the characterization of the second decade, with a maximum difference between the two data equal to 11.28m. For GLORYS this value reached 18.38m.

Figure 17 – The same as in Figure 15 for the interface between Antarctic Intermediate Water and North Atlantic Deep Water.



Seasonally, the springs of the two types of data and the periods P1 and P2 were the seasons in which the AAIW base was at its deepest. Despite the seasonal similarity, the data from the P2 period shows deeper intermediate waters, when compared to what was verified during the first decade.

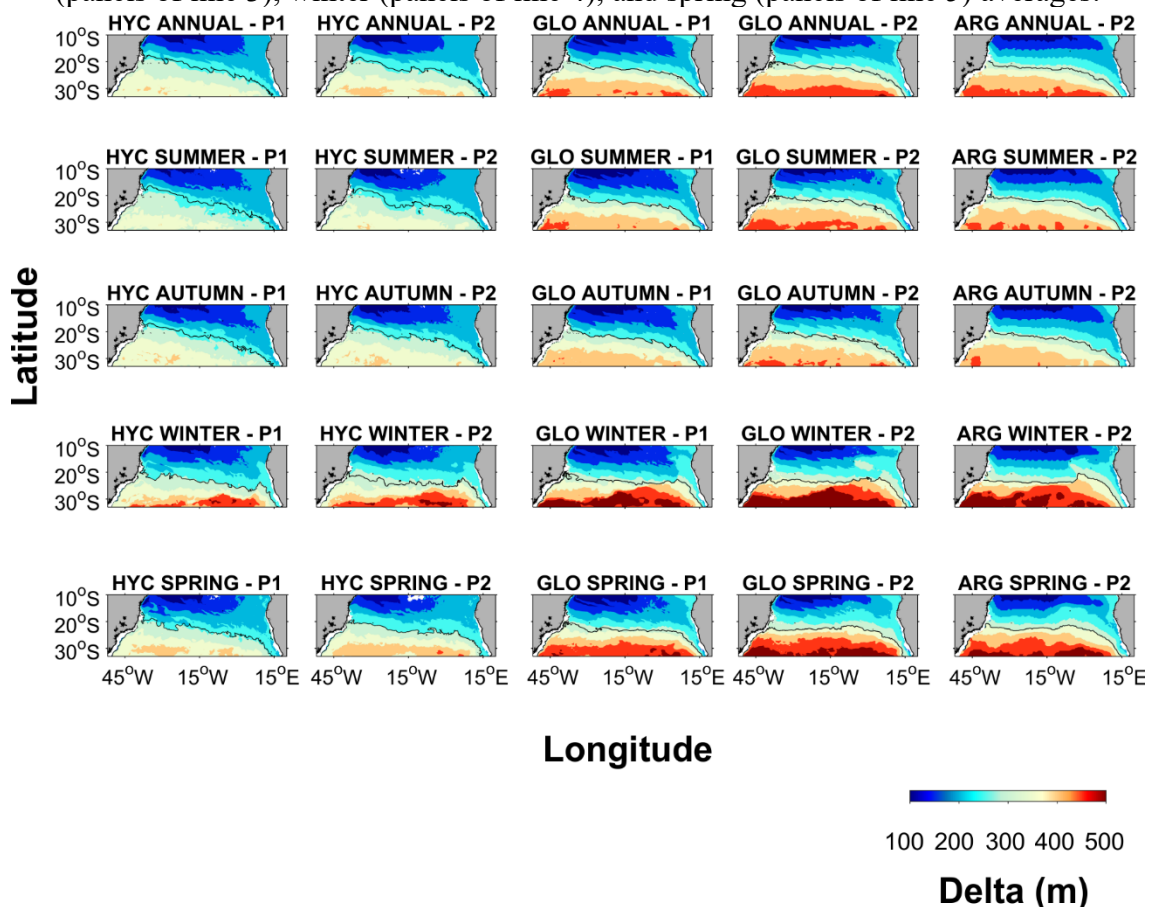
During the colder seasons (winter and spring) the contribution of the waters formed in Antarctica and the flow through the DP favored the intrusion of cooler intermediate waters in the SAO (SWINGEDOUW et al., 2009; RÜHS et al., 2019).

The spatial distribution of these maximum depth levels was greater in the HYCOM data, mainly during autumn and winter, in latitudes northern of 22°S. Spatially, GLORYS better characterized the ARGO data, since the location of these depth maxima was more widely spaced and with a different distribution than what was observed in the HYCOM data.

The variations found in the interface depth of the water masses influence the thickness of the layers and their arrangement in the water column. Also, the properties and transport of these alter the AMOC and the flow of heat and salt to the North Atlantic.

Figures 18 and 19 characterize the variations in the thickness of SACW and AAIW, over the two analyzed periods and seasonally. The variations that occurred in the SW were represented in Figure 15 since any variation in the thickness of this layer would interfere in the depth of its interface with the SACW.

Figure 18 – Representation of the South Atlantic Central Water layer thickness, for data from HYCOM (HYC), GLORYS (GLO), and ARGO (ARG), during the periods 1993–2001 (P1) and 2002–2012 (P2), divided into annual (panels of line 1), summer (panels of line 2), autumn (panels of line 3), winter (panels of line 4), and spring (panels of line 5) averages.



In Figure 18, it can be seen that the SAO was divided diagonally into thickness values less than 300m to the north and thickness values greater than 300m to the south. In HYCOM data, results of  $\Delta \geq 500$ m only occurred during the winter, equivalent to 508.53m for P1 and 524.03m for P2, in the other seasons the thickness of the SACW decreased as the temperature increased, with a lower maximum value during the summer ( $\Delta=402.32$ m).

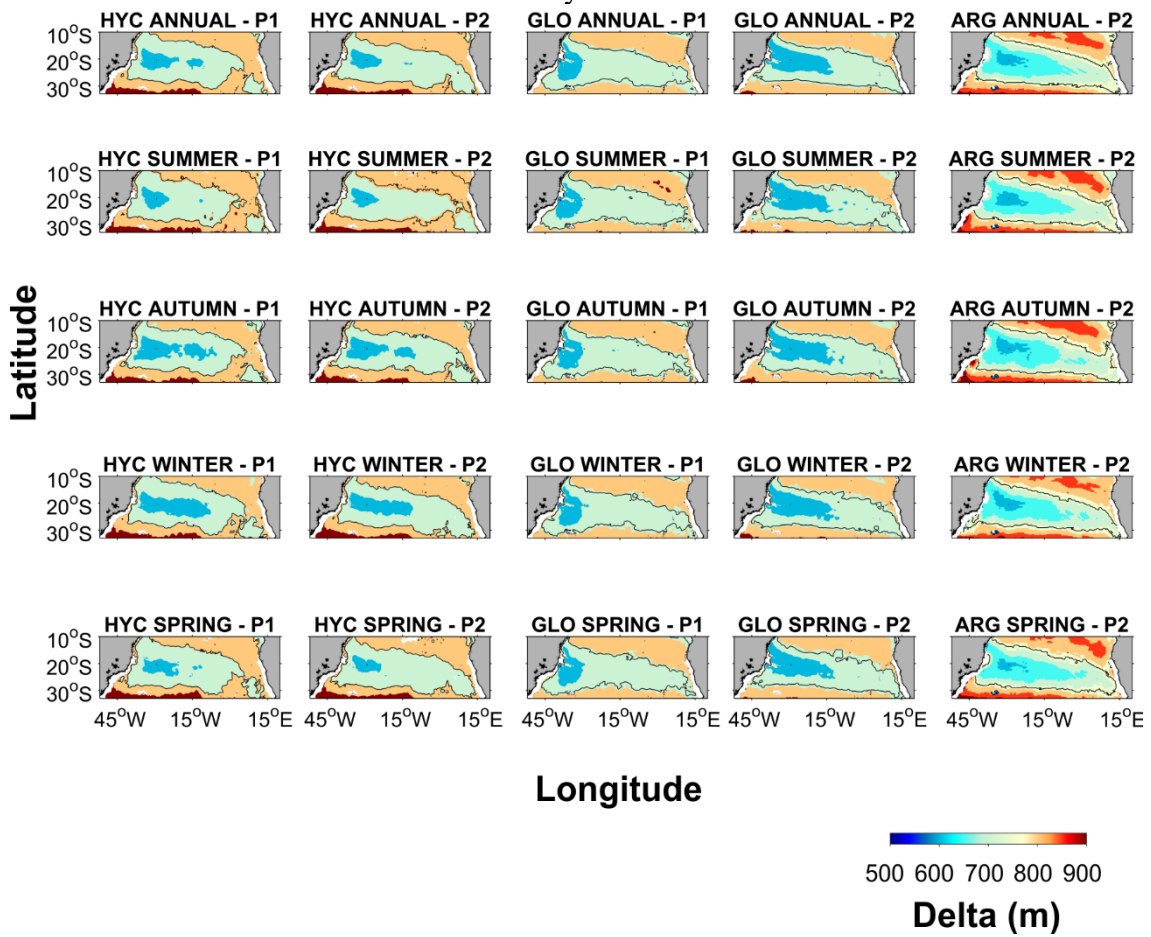
This occupation of SACW is defined by the superior circulation of the SASG, the heat exchange between the equator and the poles and the bifurcation of the SEC at depths between 100m and 500m. The variations in the layers below the SW, mainly in the SACW, are mostly associated with the process of ventilation of the interior of the ocean, which depends on the ocean-atmosphere interactions in the surface layer (BINDOFF; MCDOUGALL, 1994; BLANKE et al., 2002).

The comparison between the two periods showed that in all seasons the maximum thickness values were higher in P2 than in P1, for both reanalyses. However, unlike HYCOM, during P2, maximum values  $\Delta > 500$ m were observed in all stations from GLORYS. Also, the average GLORYS values for each station were more significant in relation to the ARGO data, with a maximum difference equal to 7.45m, compared to the maximum difference that is equal to 44.41m from HYCOM to ARGO.

In contrast to HYCOM, the lowest values of the maximum thickness of the GLORYS and ARGO data were observed during the fall (318.11m and 312.42m). For these results, the average values of summer, autumn, winter, and spring were all over 300m thick. For HYCOM, average results above 300m occurred only in winter and spring.

Despite the good quantitative representation of GLORYS compared to ARGO, spatially, the two reanalyses did not represent well the distribution of SACW thickness values.

Figure 19 – The same as in Figure 18 for the thickness of the Antarctic Intermediate Water layer.



The  $\Delta$  results of the AAIW (Figure 19) were higher in HYCOM than in GLORYS during the two periods, for all seasons. Between the decades, the values of P1 were higher than those of P2 and, as observed in SACW, the maximum thicknesses occurred in the springs of the two reanalysis ( $\Delta=1059.95\text{m}$  and  $\Delta=1048.94\text{m}$  for P1 and P2 of the HYCOM, and  $\Delta=1007.15\text{m}$  and  $\Delta=968.90\text{m}$  for GLORYS P1 and P2).

In comparison to the ARGO data, HYCOM overestimated the AAIW  $\Delta$  values in the period of 2002–2012. Thus, the GLORYS data were more similar to ARGO, with the maximum difference between them equal to 9.82m, while this value was 37.79 for HYCOM.

Spatially, the flow of AAIW from southern Africa towards Brazil was represented by a range of values of  $\Delta \sim 600\text{m}$ , with a core of minimum values located close to the Cabo Frio region, on the Brazilian coast. The longitudinal occupation of this core was similar for the two periods of the HYCOM data. However, for GLORYS during P1 this core was restricted to the longitudes of  $35^\circ\text{W}$  and  $40^\circ\text{W}$ , while in P2 it reached the longitude of  $13^\circ\text{W}$ . In the ARGO data, the spatial distribution of the minimum thickness was more restricted to longitudes west of  $20^\circ\text{W}$ .

Gordon (1986) and Rintoul (1991) studies support the importance of hot and cold water routes for changes in the properties of water masses in SAO. During P2, the Indo-Atlantic connection, or hot water route, shows the region of the lesser thickness of the intermediate waters crossing the South Atlantic.

The waters that flow through the Pacific-Atlantic connection may have been incorporated at the level of intermediate waters, strengthening the occupation of this water mass in the SAC flow towards the region adjacent to Africa. On the other hand, in the second decade, the central waters seem to have been expanded due to the contribution of the waters of the Indian Ocean, through the Indo-Atlantic connection.

Rühs et al. (2019) highlight the interdecadal variations in the volumetric contribution of these routes within the South Atlantic and infer greater contribution from the Indian Ocean in recent decades. However, they also highlight the contribution of 40% of the flow through the Pacific-Atlantic connection. The more saline waters of the Indian Ocean support the increase in salinity at the level of SACW, causing variations in the density and stratification of SAO waters. On the other hand, the entry of fewer saline waters, originated from the AAIW formation area, reaffirm the reduction in salinity values, causing the cooling trends observed in the AAIW.

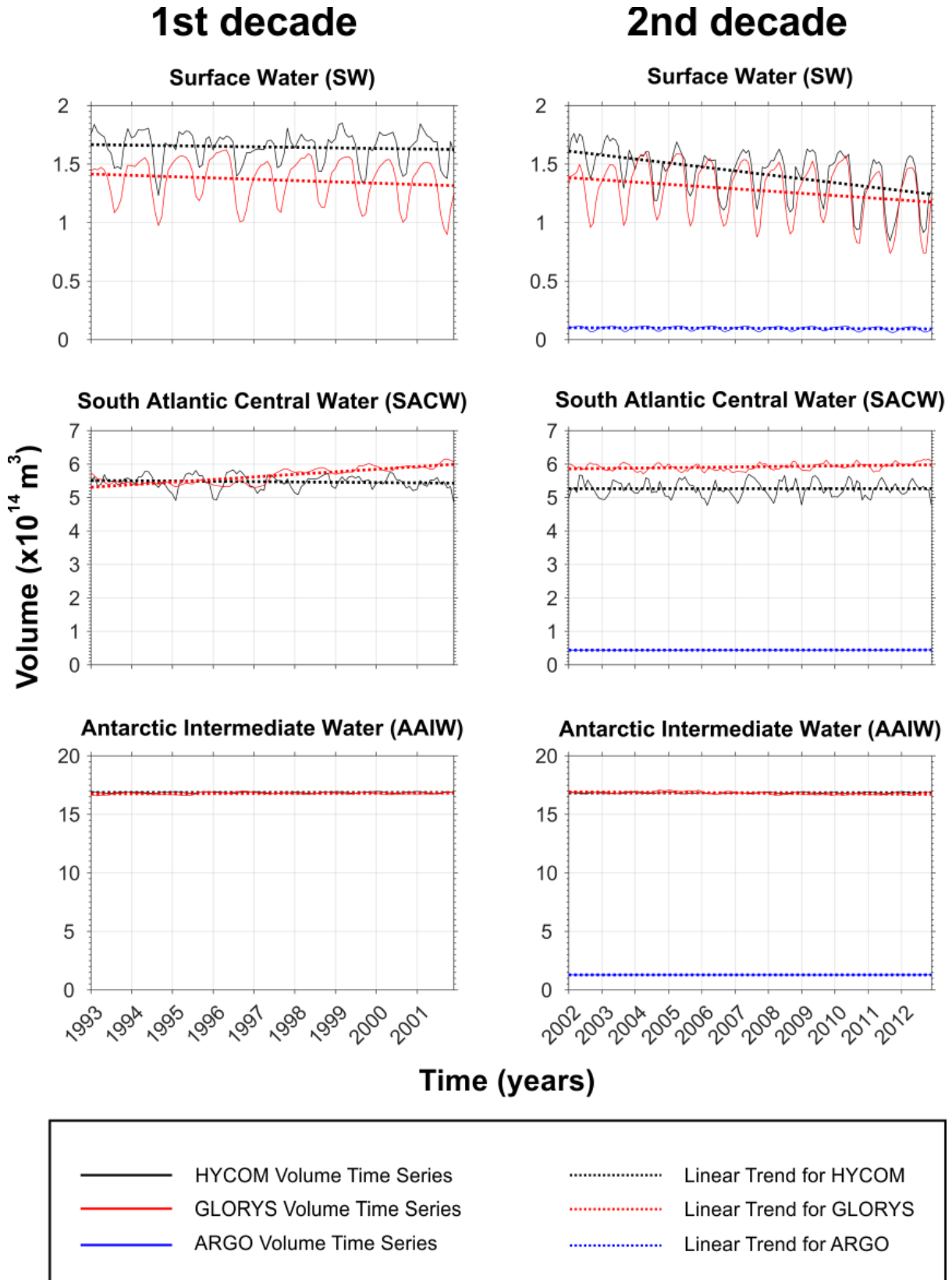
To investigate the interdecadal differences in the contribution of each water mass to the SAO, the mean time series of volume anomalies were generated (Figure 20) for the entire South Atlantic, divided between periods P1 and P2. The mean volume values of SW, SACW, and AAIW can be seen in Table 6.

Table 6 – Average volume values (in  $\times 10^{14} \text{m}^3$ ) for the South Atlantic Ocean (SAO). The data are from the HYCOM and GLORYS reanalyses, and ARGO floats, during the periods 1993–2001 (P1) and 2002–2012 (P2). The analyzes were divided for each water mass of the upper circulation of the SAO, represented by Surface Water (SW), South Atlantic Central Water (SACW), and Antarctic Intermediate Water (AAIW).

	<b>HYCOM</b>		<b>GLORYS</b>		<b>ARGO</b>
<b>Water mass</b>	<b>Volume P1</b>	<b>Volume P2</b>	<b>Volume P1</b>	<b>Volume P2</b>	<b>Volume P2</b>
SW	1.645	1.426	1.364	1.279	0.096
SACW	5.468	5.263	5.647	5.915	0.440
AAIW	16.853	16.830	16.780	16.807	1.273

The trends calculated for the individual layers pointed out that the surface waters are in a process of volumetric reduction, observed in all data for the two periods. Despite the agreement between the results for the behavior of SW, HYCOM overestimated the trend values ( $-0.0111 \times 10^{14} \text{m}^3$ ) when compared to the ARGO data ( $-0.0003 \times 10^{14} \text{m}^3$ ). For the second decade, on the other hand, the results of GLORYS ( $-0.0062 \times 10^{14} \text{m}^3$ ) were closer to those verified in the float data.

Figure 20 – Average time series of average volume ( $\times 10^{14}$ ) in  $\text{m}^3$ , of each water mass for the South Atlantic. For data from HYCOM (continuous line in black), GLORYS (continuous line in red) and ARGO (continuous line in blue), during the periods 1993–2001 (panels on the left), for reanalysis, and 2002–2012 (panels on the right), for both types of data. The first row of panels shows the results for Surface Water (SW), the second row of panels shows the results for South Atlantic Central Water (SACW), and the third row of panels shows the results for Antarctic Intermediate Water (AAIW). The dashed lines represent the linear trend ( $\text{m}^3 \cdot \text{decade}^{-1}$ ), with 95% statistical significance, of the data from HYCOM, GLORYS, and ARGO, respectively.



In the results for P2, the reverse process happened at SACW. For this layer, the reanalysis and measured *in situ* data pointed to an expansion of central waters, with a greater

result in the GLORYS data equal to  $0.0036 \times 10^{14} \text{m}^3$ . The HYCOM values were lower than the others ( $0.00001 \times 10^{14} \text{m}^3$ ) and the ARGO data were different from the two reanalyses ( $0.0001 \times 10^{14} \text{m}^3$ ), in this layer of the water column.

The trend towards AAIW was not similar between any of the two types of data analyzed, however, the values calculated from the ARGO indicate expansion of the AAIW by  $0.00003 \times 10^{14} \text{m}^3$ . About what was observed for ACAS, these values are low, but still represent an expansion of this water mass.

The interdecadal variations in the average volume of each water mass were on average in the order of  $0.1 \times 10^{14} \text{m}^3$  for the two reanalyses. The trend data showed that the surface waters are in a process of retraction, summarily giving way to the expansion of the central and intermediate waters below them.

Since, the structure of the water masses of the SAO, form the upper arm of the AMOC, the intensification of the exchanges of the SAO with the Indian Ocean and the Pacific Ocean are altering the properties of the water masses transported to the Northern Hemisphere. In the long run, the continuous intensification of these processes could cause unbalance within this Circulation.

Biastoch et al. (2008) conclude in their study that the effects of AL dynamics on AMOC, act mainly on the decadal variability of this Circulation. According to them, a decadal transport signal from the AL region, in the depth of the thermocline, gradually decreases in intensity from south to north but reaches the NAO with a magnitude comparable to the effect of the deep water formation processes in the Northern Hemisphere.

In agreement with that presented by Biastoch et al. (2008), the average increase in the volume of SACW in SAO, associated with the trends of heating and salinization of this water mass, as a result of the increase in the Leakage of the Rings of the Agulhas, would be incorporated over the decades into the NAO. With the transport of warmer water in the depth of the thermocline, in the upper arm of AMOC. On the other hand, the salinization of SACW would be compensated by the cooling of the AAIW, below it.

The effects of changes in the properties of water masses exported from SAO to NAO have been addressed in several studies (WEIJER et al., 2002; HAWKINS et al., 2011; MIGNAC et al., 2019). Among the studied scenarios, the collapse of AMOC was mainly related to the heating and cooling of the waters transported to the Northern Hemisphere. These modifications would difficult convective processes in the region of bottom water formation, transported to the SAO, reducing the intensity of the entire Circulation, which would cause climate changes on a global scale (JACKSON et al., 2015).

## 11 CONCLUSIONS

The interdecadal differences in the variations of heat and salt in the SAO and changes in the volume of the upper water masses were investigated from reanalysis data generated by numerical modeling and measured *in situ* by ARGO floats. The period from 1993 to 2001 was used for analyzes of the first decade, while from 2002 to 2012 was used for the second, the latter also covering the ARGO data. Interdecadal changes and changes in volume were explored as a function of the potential density of the interface between the layers and in the sections of the SAO.

On interannual and longitudinal scales, it was observed through the diagrams of temperature versus salinity that variations of  $\theta$  and S were greater on the eastern border of SAO. In the comparison between the two decades, the interannual variability was lower during the second decade, because of the possibility of assimilation of ARGO data in numerical modeling data from the 21st century starting. The time series of temperature and salinity anomalies also pointed out results of different trends between the decades analyzed, since in the trend analysis for P2 some observations were the opposite of what was verified for the 20 years of analysis.

Seasonally, the divergences in the vertical distribution of water masses on the two borders of the SAO become more evident. The summer season highlights the warm and saline waters adjacent to the Brazilian coast, transported from the equator towards the poles by the Brazil Current. The winter season highlights the cooler and fresher waters, resulted from the Southern Ocean flows incorporated into SAC and partly transported by BeC, in the region adjacent to the African coast.

The variability identified by the high-resolution models overestimated the data measured *in situ* by the ARGO floats, mainly in the representation of the  $\theta$ -S diagrams. However, the observations made by GLORYS were satisfactory in most of the results of this work, such as, for example, in the identification of the Benguela Upwelling System extension along the eastern border of SAO.

On the other hand, the observations made by HYCOM underestimated the values obtained for  $\theta$  and S in the cross-sections on the western and eastern borders of the SAO. Also, in the results of the occupation of the water masses and the thickness of the layers, GLORYS has always presented results more similar to ARGO, than HYCOM.

In general, the seasonal variability of the depth of the base of the SW had strong oscillations in the SAO, mainly in the region adjacent to the African coast during the summer

and winter seasons. During the summer the SW was distributed over the entire length of the South Atlantic in the open ocean, and in the winter the SW was not observed at the eastern border of the SAO south of 15°S, due to the entry of cold waters into the South Atlantic, transported from the Southern Ocean.

The occupation of SACW in SAO is well defined and did not show significant seasonal variability, SAO was divided diagonally from approximately 15°S to the Brazilian coast, to 32°S of the African coast, with a greater contribution from SACW to the north than to the south. Seasonally, the coldest seasons were the period when the AAIW base was at its deepest (1202.78m and 1206.31m). Due to the contribution of the waters formed in Antarctica and the flow through the DP, the intrusion of intermediate waters in the SAO is favored in winter and spring.

Finally, the analyses support the existence of temporal and spatial variability in the SAO, which define trends in water heating and salinization and changes in the volume of water masses, with an increase in the contribution of SACW and AAIW in the upper circulation.

The increase in the volume of central waters after the intensification of AL, injects hot and salty waters into the SAO, and the volume of intermediate waters increases, due to the entry of cold and less saline waters through the DP. The participation of these processes in the formation of the upper branch of AMOC, which transports hot water from SAO to NAO, is subject to the unbalance of this Circulation, as a result of the intensification of the transport of warmer and saline waters to the Northern Hemisphere.

## **ACKNOWLEDGMENT**

We thank the support of the Agência Nacional do Petróleo, Gás Natural e Biocombustíveis (ANP) and PETROBRAS (project number 2015/00515-6), for the financing of this work. To the National Ocean Partnership Program (NOPP) for the development and availability of HYCOM-NCODA data, as part of the US Global Ocean Data Assimilation Experiment (GODAE), to the Mercator Ocean System for the availability and support of GLORYS12V1 data on the Copernicus Marine Environment platform Monitoring Service (CMEMS) and Coriolis Operational Oceanography for making ARGO data available (<http://www.coriolis.eu.org>).

## REFERENCES

- Biastoch A, Böning CW, Lutjeharms JRE (2008) Agulhas leakage dynamics affects decadal variability in Atlantic overturning circulation. *Nature* 456:489–492.  
<https://doi.org/10.1038/nature07426>
- Bindoff NL, McDougall TJ (1994) Diagnosing climate change and ocean ventilation using hydrographic data. *J Phys Oceanogr* 24:1137–1152. [https://doi.org/10.1175/1520-0485\(1994\)024<1137:DCCAOV>2.0.CO;2](https://doi.org/10.1175/1520-0485(1994)024<1137:DCCAOV>2.0.CO;2)
- Blanke B, Speich S, Madec G, Maugé R (2002) A global diagnostic of interior ocean ventilation: A global diagnostic of interior ocean ventilation. *Geophys Res Lett* 29:108-1–108-4. <https://doi.org/10.1029/2001GL013727>
- Brown E, Colling A, Park D, et al (2001). The North Atlantic Gyre: Observations and theories. In: Brown E, Colling A, Park D (ed) *Ocean Circulation*, 2rd edn. Oxford, Butterworth-Heinemann, pp 79–142.
- Bryden HL (2003) Changes in Ocean Water Mass Properties: Oscillations or trends? *Science* 300:2086–2088. <https://doi.org/10.1126/science.1083980>
- Capuano TA, Speich S, Carton X, Laxenaire R (2018) Indo-Atlantic exchange, mesoscale dynamics, and Antarctic Intermediate Water. *J Geophys Res Oceans* 123:3286–3306. <https://doi.org/10.1002/2017JC013521>
- Chassignet E, Hurlburt H, Metzger EJ, et al (2009) US GODAE: Global ocean prediction with the HYbrid Coordinate Ocean Model (HYCOM). *Oceanog* 22:64–75.  
<https://doi.org/10.5670/oceanog.2009.39>
- Colberg F, Reason CJC (2006) A model study of the Angola Benguela Frontal Zone: Sensitivity to atmospheric forcing. *Geophys Res Lett* 33:L19608.  
<https://doi.org/10.1029/2006GL027463>
- COPERNICUS MARINE ENVIRONMENT MONITORING SERVICE (2018) Ocean Products. <http://marine.copernicus.eu/services-portfolio/access-to-products/>. Accessed 22 January 2018.
- Curry R, Dickson B, Yashayaev I (2003) A change in the freshwater balance of the Atlantic Ocean over the past four decades. *Nature* 426:826–829.  
<https://doi.org/10.1038/nature02206>
- de Ruijter WPM, Biastoch A, Drijfhout SS, et al (1999) Indian-Atlantic interocean exchange: Dynamics, estimation and impact. *J Geophys Res* 104:20885–20910.  
<https://doi.org/10.1029/1998JC900099>
- Donners J, Drijfhout SS, Hazeleger W (2005) Water mass transformation and subduction in the South Atlantic. *J Phys Oceanogr* 35:1841–1860. <https://doi.org/10.1175/JPO2782.1>
- Fennel W (1999) Theory of the Benguela Upwelling System. *J Phys Oceanogr* 29:177–190.  
[https://doi.org/10.1175/1520-0485\(1999\)029<0177:TOTBUS>2.0.CO;2](https://doi.org/10.1175/1520-0485(1999)029<0177:TOTBUS>2.0.CO;2)

- Gabioux M, Costa VS da, Azevedo Correia de Souza JM, et al (2014) Modeling the South Atlantic Ocean from medium to high resolution. *Rev Bras Geof* 31:229–242. <https://doi.org/10.22564/rbgf.v31i2.27>
- Gaillard F, Reynaud T, Thierry V, et al (2016) In Situ-Based Reanalysis of the Global Ocean Temperature and Salinity with ISAS: Variability of the Heat Content and Steric Height. *J Climate* 29:1305–1323. <https://doi.org/10.1175/JCLI-D-15-0028.1>
- Garzoli SL, Matano R (2011) The South Atlantic and the Atlantic Meridional Overturning Circulation. *Deep-Sea Research Part II: Topical Studies in Oceanography* 58:1837–1847. <https://doi.org/10.1016/j.dsr2.2010.10.063>
- Goes M, Christoffersen J, Dong S, et al (2018) An updated estimate of salinity for the Atlantic Ocean sector using temperature-salinity relationships. *J Atmos Oceanic Technol* 35:1771–1784. <https://doi.org/10.1175/JTECH-D-18-0029.1>
- Goes M, Wainer I, Signorelli N (2014) Investigation of the causes of historical changes in the subsurface salinity minimum of the South Atlantic. *J Geophys Res Oceans* 119:5654–5675. <https://doi.org/10.1002/2014JC009812>
- Gordon AL (1986) Intercean exchange of thermocline water. *J Geophys Res* 91:5037–5046. <https://doi.org/10.1029/JC091iC04p05037>
- Hawkins E, Smith RS, Allison LC, et al (2011) Bistability of the Atlantic overturning circulation in a global climate model and links to ocean freshwater transport. *Geophys Res Lett* 38:L10605. <https://doi.org/10.1029/2011GL047208>
- Hazeleger W, Drijfhout S (2006) Subtropical cells and meridional overturning circulation pathways in the tropical Atlantic. *J Geophys Res* 111:C03013. <https://doi.org/10.1029/2005JC002942>
- Holfort JR, Siedler G (2001) The meridional oceanic transports of heat and nutrients in the South Atlantic. *J Phys Oceanogr* 31:5–29. [https://doi.org/10.1175/1520-0485\(2001\)031<0005:TMOTOH>2.0.CO;2](https://doi.org/10.1175/1520-0485(2001)031<0005:TMOTOH>2.0.CO;2)
- Huang B, Xue Y, Behringer DW (2008) Impacts of Argo salinity in NCEP Global Ocean Data Assimilation System: The tropical Indian Ocean. *J Geophys Res* 113:C08002. <https://doi.org/10.1029/2007JC004388>
- HYBRID COORDINATE OCEAN MODEL (2017) HYCOM System Description. <https://www.hycom.org/>. Accessed 15 September 2017.
- Lagerloef G, Schmitt R, Schanze J, Kao H-Y (2010) The ocean and the global water cycle. *Oceanog* 23:82–93. <https://doi.org/10.5670/oceanog.2010.07>
- Lass HU, Schmidt M, Mohrholz V, Nausch G (2000) Hydrographic and Current Measurements in the Area of the Angola–Benguela Front. *J Phys Oceanogr* 30:21–2609. [https://doi.org/10.1175/1520-0485\(2000\)030<2589:HACMIT>2.0.CO;2](https://doi.org/10.1175/1520-0485(2000)030<2589:HACMIT>2.0.CO;2)
- Lima MO, Cirano M, Mata MM, et al (2016) An assessment of the Brazil Current baroclinic structure and variability near 22°S in distinct ocean forecasting and analysis systems. *Ocean Dynamics* 66:893–916. <https://doi.org/10.1007/s10236-016-0959-6>
- Maamaatauaiahutapu K, Provost C, Andrié C, Vigan X (1999) Origin and ages of mode waters in the Brazil–Malvinas Confluence region during austral winter 1994. *J Geophys Res* 104:21051–21061. <https://doi.org/10.1029/1999JC900177>

- Marcello F, Wainer I, Rodrigues RR (2018) South Atlantic Subtropical Gyre late twentieth century changes. *J Geophys Res Oceans* 123:5194–5209.  
<https://doi.org/10.1029/2018JC013815>
- McDonagh EL, King BA (2005) Oceanic fluxes in the South Atlantic. *J Phys Oceanogr* 35:109–122. <https://doi.org/10.1175/JPO-2666.1>
- MERCATOR OCEAN (2017) GLORYS. <https://www.mercator-ocean.fr/sciences-publications/glorys/>. Accessed 01 October 2017.
- Mignac D, Ferreira D, Haines K (2018) South Atlantic meridional transports from NEMO-based simulations and reanalyses. *Ocean Sci* 14:53–68. <https://doi.org/10.5194/os-14-53-2018>
- Mignac D, Ferreira D, Haines K (2019) Decoupled Freshwater Transport and Meridional Overturning in the South Atlantic. *Geophys Res Lett* 46:2178–2186.  
<https://doi.org/10.1029/2018GL081328>
- Pedlosky J (1990) The dynamics of the Oceanic Subtropical Gyres. *Science* 248:316–322.  
<https://doi.org/10.1126/science.248.4953.316>
- Pereira J, Gabiou M, Almeida MM, et al (2014) The bifurcation of the Western Boundary Current System of the South Atlantic Ocean. *Rev Bras Geof* 32:241–257.  
<https://doi.org/10.22564/rbgf.v32i2.456>
- Rimaud J, Speich S, Blanke B, Grima N (2012) The exchange of Intermediate Water in the southeast Atlantic: Water mass transformations diagnosed from the Lagrangian analysis of a regional ocean model: AAIW in the Southeast Atlantic. *J Geophys Res* 117:C08034.  
<https://doi.org/10.1029/2012JC008059>
- Rintoul SR (1991) South Atlantic interbasin exchange. *J Geophys Res* 96:2675–2692.  
<https://doi.org/10.1029/90JC02422>
- Rodrigues RR, Rothstein LM, Wimbush M (2007) Seasonal variability of the South Equatorial Current Bifurcation in the Atlantic Ocean: A numerical study. *J Phys Oceanogr* 37:16–30. <https://doi.org/10.1175/JPO2983.1>
- Rodrigues RR, Wimbush M, Watts DR, et al (2010) South Atlantic mass transports obtained from subsurface float and hydrographic data. *J Mar Res* 68:819–850.  
<https://doi.org/10.1357/002224010796673858>
- Roemmich D, Church J, Gilson J, et al (2015) Unabated planetary warming and its ocean structure since 2006. *Nature Clim Change* 5:240–245.  
<https://doi.org/10.1038/nclimate2513>
- Roemmich D, Gilson J, Sutton P, Zilberman N (2016) Multidecadal change of the South Pacific Gyre Circulation. *J Phys Oceanogr* 46:1871–1883. <https://doi.org/10.1175/JPO-D-15-0237.1>
- Rühs S, Schwarzkopf FU, Speich S, Biastoch A (2019) Cold vs. warm water route – sources for the upper limb of the Atlantic Meridional Overturning Circulation revisited in a high-resolution ocean model. *Ocean Sci* 15:489–512. <https://doi.org/10.5194/os-15-489-2019>
- Schmidtko S, Johnson GC (2012) Multidecadal warming and shoaling of Antarctic Intermediate Water. *J Climate* 25:207–221. <https://doi.org/10.1175/JCLI-D-11-00021.1>

- Schmitt RW (1995) The ocean component of the global water cycle. *Rev Geophys* 33:1395–1409. <https://doi.org/10.1029/95RG00184>
- Shillington FA, Reason CJC, Duncombe Rae CM, et al (2006) Large scale physical variability of the Benguela Current Large Marine Ecosystem (BCLME). In: Shannon V, Hempel G, Malanotte-Rizzoli P (ed) *Large Marine Ecosystems*, 14vol. Elsevier, pp 49–70.
- Silveira ICA, Schmidt ACK, Campos EJD, et al (2000) A Corrente do Brasil ao largo da costa leste brasileira. *Rev Bras Oceanog* 48:171–183. <http://dx.doi.org/10.1590/S1413-77392000000200008>
- Soto-Navarro FJ, Criado-Aldeanueva F (2012) Model thermohaline trends in the Mediterranean Sea during the last years: A change with respect to the last decades? *The Scientific World Journal* 2012:1–8. <https://doi.org/10.1100/2012/365698>
- Storto A, Alvera-Azcárate A, Balmaseda MA, et al (2019) Ocean reanalyses: Recent advances and unsolved challenges. *Front Mar Sci* 6:1–10. <https://doi.org/10.3389/fmars.2019.00418>
- Stramma L (1991) Geostrophic transport of the South Equatorial Current in the Atlantic. *J Mar Res* 49:281–294. <https://doi.org/10.1357/002224091784995864>
- Stramma L, England M (1999) On the water masses and mean circulation of the South Atlantic Ocean. *J Geophys Res* 104:20863–20883. <https://doi.org/10.1029/1999JC900139>
- Stramma L, Peterson RG (1990) The South Atlantic Current. *J Phys Oceanog* 20:846–859. [https://doi.org/10.1175/1520-0485\(1990\)020<0846:TSAC>2.0.CO;2](https://doi.org/10.1175/1520-0485(1990)020<0846:TSAC>2.0.CO;2)
- Swingedouw D, Fichefet T, Goosse H, Loutre MF (2009) Impact of transient freshwater releases in the Southern Ocean on the AMOC and climate. *Clim Dyn* 33:365–381. <https://doi.org/10.1007/s00382-008-0496-1>
- THERMODYNAMIC EQUATION OF SEAWATER-2010 (2018) TEOS-10 Software. <http://www.teos-10.org/>. Accessed 13 March 2018.
- Thresher R, Morrongiello J, Sloyan BM, et al (2014) Parallel decadal variability of inferred water temperatures for Northern and Southern Hemisphere intermediate water masses. *Geophys Res Lett* 41:1232–1237. <https://doi.org/10.1002/2013GL058638>
- Tim N, Zorita E, Schwarzkopf FU, et al (2018) The impact of Agulhas Leakage on the Central Water Masses in the Benguela Upwelling System from a high-resolution ocean simulation. *J Geophys Res Oceans* 123:9416–9428. <https://doi.org/10.1029/2018JC014218>
- Walsh G (1982) On the relation between sea-surface heat flow and thermal circulation in the ocean. *Tellus* 34:187–195. <https://doi.org/10.3402/tellusa.v34i2.10801>
- Weijer W (2002) Response of the Atlantic overturning circulation to South Atlantic sources of buoyancy. *Global and Planetary Change* 34:293–311. [https://doi.org/10.1016/S0921-8181\(02\)00121-2](https://doi.org/10.1016/S0921-8181(02)00121-2)
- Wu L, Cai W, Zhang L, et al (2012) Enhanced warming over the global subtropical western boundary currents. *Nature Clim Change* 2:161–166. <https://doi.org/10.1038/nclimate1353>
- Yao W, Shi J, Zhao X (2017) Freshening of Antarctic Intermediate Water in the South Atlantic Ocean in 2005–2014. *Ocean Sci* 13:521–530. <https://doi.org/10.5194/os-13-521-2017>

## 12 CONCLUSÃO

O presente trabalho investigou, através dos produtos de reanálise HYCOM e GLORYS, durante o período de 20 anos (1993–2012), padrões nas variações espaciais e sazonais na velocidade da componente meridional e no transporte de volume da Corrente do Brasil, ao largo da região sudeste brasileira.

Além disso, também foram analisadas as diferenças interdecadais nas variações de calor e salinidade no OAS e alterações no fluxo do volume das massas d'água superiores, a partir destas duas reanálise e dados medidos *in situ* por flutuadores ARGO, utilizando o período de 1993 a 2001 para análises da primeira década e de 2002 a 2012 para a segunda, essa última abrangendo os dados do ARGO. As alterações interdecadais e as mudanças no volume foram exploradas em função da densidade potencial de interface entre as camadas e na setorização do Oceano Atlântico Sul.

A partir dos resultados e dos trabalhos já realizados, foram apontadas duas principais causas para a existência do ciclo anual do transporte da CB, identificado na região estudada, e para as variações espaciais ao longo do seu fluxo. Uma das possibilidades é a variação anual do rotacional do vento, causado pelo deslocamento sazonal da posição do ASAS, responsável pelo GSAS. Esta variabilidade sazonal do ASAS é discutida em Reboita et al. (2019).

Outra possibilidade, está relacionada as alterações no volume transportado, devido a existência de células de recirculação ao longo da CB e pela incorporação de Anéis das Agulhas na altura de Cabo Frio. Além disso, a intensidade das variáveis velocidade e transporte também pode estar sendo alterada durante a primavera e o verão, em decorrência das mudanças sazonais na circulação atmosférica e na posição da bifurcação da CSE.

Para as variações nas massas d'água da circulação superior do OAS, em escalas interanuais e longitudinais, foi observado através dos diagramas de temperatura *versus* salinidade que variações de  $\theta$  e S foram maiores na fronteira leste do OAS. Na comparação entre as duas décadas, a variabilidade interanual foi menor durante a segunda década, em vista da possibilidade de assimilação dos dados ARGO nos dados de modelagem numérica a partir do século 21, agregar valores realísticos aos resultados obtidos. As séries temporais de anomalias de temperatura e salinidade também apontaram resultados de tendência diferentes entre as décadas analisadas, uma vez que nas análises de tendência para P2 algumas observações foram o oposto do verificado para os 20 anos de análise.

Sazonalmente, ficam mais evidentes as divergências na distribuição vertical das massas de água nas duas fronteiras do OAS. A estação de verão destaca as águas quentes e salinas adjacente à costa brasileira, transportada do equador em direção aos pólos pela Corrente do Brasil. A estação de inverno realça as águas frias e mais frescas, resultado dos fluxos do oceano Austral, que entram na Corrente do Atlântico Sul e são transportadas pela Corrente da Benguela, na região adjacente a costa africana.

As variabilidades identificadas pelos modelos de alta resolução superestimaram os dados medidos *in situ* pelos flutuadores ARGO, principalmente na representação dos diagramas  $\theta$ -S. No entanto, as observações realizadas pelo GLORYS foram satisfatórias na maioria dos resultados deste trabalho, como por exemplo, na identificação da extensão Sistema de Ressurgência da Benguela ao longo da fronteira leste do OAS.

Por outro lado, as observações realizadas pelo HYCOM subestimaram os valores obtidos para  $\theta$  e S nas seções transversais nas fronteiras oeste e leste do OAS. Além disso, nos resultados da ocupação das massas d'água e da espessura das camadas, o GLORYS sempre apresentou resultados mais similares ao ARGO, do que o HYCOM.

De modo geral, a variabilidade sazonal da profundidade da base da AS teve oscilações intensas no OAS, principalmente na região adjacente à costa africana durante as estações de verão e inverno. Durante o verão a AS esteve distribuída em toda a extensão do Atlântico Sul em oceano aberto, e no inverno a AS não foi observada na fronteira leste do OAS ao sul de 15°S, devido a entrada de águas frias no Atlântico Sul, transportadas do Oceano Austral.

A ocupação da ACAS no OAS é bem definida e não apresentou variabilidades sazonais significativas, o OAS foi dividido diagonalmente de aproximadamente 15°S até da costa brasileira à 32°S da costa africana, com maior contribuição da ACAS ao norte e menor ao sul. Sazonalmente, as estações mais frias foram o período em que a base da AIA esteve mais profunda. Em função da contribuição das águas formadas na Antártica e o fluxo através da Passagem de Drake, a intrusão de águas intermediárias no OAS é favorecida nestas estações.

Por fim, as análises sustentam a existência de variabilidades temporais e espaciais no OAS, que definem tendências de aquecimento e salinização das águas e alteração no volume das massas de água, com aumento da contribuição de ACAS e AIA na circulação superior.

O aumento de volume das águas centrais a partir da intensificação do Vazamento das Agulhas, injeta águas quentes e salgadas no OAS, enquanto que, em menor intensidade o volume das águas intermediárias aumenta, pela entrada de águas frias e menos salinas através da Passagem de Drake. A participação desses processos na formação do braço superior da CRMA, que transporta águas quentes do OAS para o OAN, sujeita o desequilíbrio dessa célula,

como resultado da intensificação do transporte de águas mais quentes e salinas para o Hemisfério Norte.

## REFERÊNCIAS

- AGÊNCIA NACIONAL DO PETRÓLEO, GÁS NATURAL E BIOCOMBUSTÍVEIS (ANP). **Anuário Estatístico do Petróleo, Gás Natural e Biocombustíveis**. Rio de Janeiro: ANP, 2016. 264 p.
- BEAL, L. M. *et al.* On the role of the Agulhas system in ocean circulation and climate. **Nature**, v. 472, n. 7344, p. 429–436, 2011.
- BIASTOCH A.; BÖNING C. W.; LUTJEHARMS J. R. E. Agulhas leakage dynamics affects decadal variability in Atlantic overturning circulation. **Nature**, v. 456, p. 489–492, 2008.
- BILÓ, T. C. *et al.* Methods for estimating the velocities of the Brazil Current in the pre-salt reservoir area off southeast Brazil (23°S–26°S). **Ocean Dynamics**, v. 64, n. 10, p. 1431–1446, 2014.
- BINDOFF, N. L.; MCDOUGALL, T. J. Diagnosing climate change and ocean ventilation using hydrographic data. **Journal of Physical Oceanography**, v. 24, p. 1137–1152, 1994.
- BLANKE, B. *et al.* A global diagnostic of interior ocean ventilation: A global diagnostic of interior ocean ventilation. **Geophysical Research Letters**, v. 29, n. 8, p. 108–1–108–4, 2002.
- BROWN E. *et al.* The north atlantic gyre: Observations and theories. In: BROWN E. *et al.* **Ocean Circulation**, 2. ed. Oxford: Butterworth-Heinemann, 2001. p. 79–142.
- BRYDEN, H. L. Changes in ocean water mass properties: Oscillations or trends? **Science**, v. 300, n. 5628, p. 2086–2088, 2003.
- CAMPOS, E. J. D.; GONÇALVES, J. E.; IKEDA, Y. Water mass characteristics and geostrophic circulation in the South Brazil Bight: Summer of 1991. **Journal of Geophysical Research**, v. 100, n. C9, p. 18537, 1995.
- CAMPOS, E. J. D.; VELHOTE, D.; DA SILVEIRA, I. C. A. Shelf break upwelling driven by Brazil Current Cyclonic Meanders. **Geophysical Research Letters**, v. 27, n. 6, p. 751–754, 2000.
- CAPUANO, T. A. *et al.* Indo-Atlantic exchange, mesoscale dynamics, and Antarctic Intermediate Water. **Journal of Geophysical Research: Oceans**, v. 123, n. 5, p. 3286–3306, 2018.
- CHASSINET, E. *et al.* US GODAE: Global ocean prediction with the HYbrid Coordinate Ocean Model (HYCOM). **Oceanography**, v. 22, n. 2, p. 64–75, 2009.
- COLBERG, F.; REASON, C. J. C. A model study of the Angola Benguela Frontal Zone: Sensitivity to atmospheric forcing. **Geophysical Research Letters**, v. 33, n. 19, p. L19608, 2006.

COPERNICUS MARINE ENVIRONMENT MONITORING SERVICE. **Ocean Products**. 2018. Disponível em: <http://marine.copernicus.eu/services-portfolio/access-to-products/>. Acesso em: 22 January 2018.

CURRY, R.; DICKSON, B.; YASHAYAEV, I. A change in the freshwater balance of the Atlantic Ocean over the past four decades. **Nature**, v. 426, n. 6968, p. 826–829, 2003.

DE RUIJTER, W. P. M. *et al.* Indian-Atlantic interocean exchange: Dynamics, estimation and impact. **Journal of Geophysical Research: Oceans**, v. 104, n. C9, p. 20885–20910, 1999.

DERECHYNSKY, C. P., OLIVEIRA, J. S., MACHADO, C. O. Climatologia da precipitação no município do Rio de Janeiro. **Revista Brasileira de Meteorologia**, v. 24, n. 1, p. 24-38, 2009.

DONNERS, J.; DRIJFHOUT, S. S.; HAZELEGER, W. Water mass transformation and subduction in the South Atlantic. **Journal of Physical Oceanography**, v. 35, n. 10, p. 1841–1860, 2005.

FENNEL, W. Theory of the Benguela Upwelling System. **Journal of Physical Oceanography**, v. 29, p. 14, 1999.

FLORENCIE, P.; VERRON, J. South Atlantic Ocean circulation: Simulation experiments with a quasi-geostrophic model and assimilation of TOPEX/POSEIDON and ERS 1 altimeter data. **Journal of Geophysical Research: Oceans**, v. 103, n. C11, p. 24737–24758, 1998.

GABIOUX, M. *et al.* Modeling the South Atlantic Ocean from medium to high resolution. **Revista Brasileira de Geofísica**, v. 31, n. 2, 2014.

GAILLARD, F. *et al.* In Situ-Based Reanalysis of the Global Ocean Temperature and Salinity with ISAS: Variability of the Heat Content and Steric Height. **Journal of Climate**, v. 29, p. 1305–1323, 2016.

GARFIELD, N. **The Brazil Current at subtropical latitudes**. 1990. 122 f. Tese (Doutorado em Filosofia da Oceanografia) - University of Rhode Island, Rhode Island, 1990.

GARZOLI, S. L.; MATANO, R. The South Atlantic and the Atlantic Meridional Overturning Circulation. **Deep Sea Research Part II: Topical Studies in Oceanography**, v. 58, n. 17–18, p. 1837–1847, 2011.

GOES, M. *et al.* An updated estimate of salinity for the Atlantic Ocean sector using temperature–salinity relationships. **Journal of Atmospheric and Oceanic Technology**, v. 35, n. 9, p. 1771–1784, 2018.

GOES, M.; WAINER, I.; SIGNORELLI, N. Investigation of the causes of historical changes in the subsurface salinity minimum of the South Atlantic. **Journal of Geophysical Research: Oceans**, v. 119, n. 9, p. 5654–5675, 2014.

GOES, M.; CIRANO, M.; MATA, M. M.; MAJUMDER, S. Long-Term Monitoring of the Brazil Current Transport at 22° S From XBT and Altimetry Data: Seasonal, Interannual, and

Extreme Variability. **Journal of Geophysical Research: Oceans**, v. 124, p. 3645–3663, 2019.

GORDON, A. L. Intercean exchange of thermocline water. **Journal of Geophysical Research**, v. 91, n. C4, p. 5037, 1986.

GORDON, A. L.; GREENGROVE, C. L. Geostrophic circulation of the Brazil-Falkland Confluence. **Deep Sea Research Part A**. Oceanographic Research Papers, v. 33, n. 5, p. 573–585, 1986.

GUERRA, L. A. A. Vórtices das Agulhas colidem com a Corrente do Brasil? 2011. 88 f. Tese (Doutorado em Engenharia Oceânica) - Universidade Federal do Rio de Janeiro, Rio de Janeiro, 2011.

GUERRA, L. A. A.; PAIVA, A. M.; CHASSIGNET, E. P. On the translation of Agulhas rings to the western South Atlantic Ocean. **Deep Sea Research Part I: Oceanographic Research Papers**, v. 139, p. 104–113, 2018.

HAWKINS E. *et al.* Bistability of the Atlantic overturning circulation in a global climate model and links to ocean freshwater transport. **Geophysical Research Letters**, v. 38, p. L10605, 2011.

HAZELEGER, W.; DRIJFHOUT, S. Subtropical cells and meridional overturning circulation pathways in the tropical Atlantic. **Journal of Geophysical Research**, v. 111, n. C3, p. C03013, 2006.

HOLFORT, J. R.; SIEDLER, G. The meridional oceanic transports of heat and nutrients in the South Atlantic. **Journal of Physical Oceanography**, v. 31, p. 25, 2001.

HUANG, B.; XUE, Y.; BEHRINGER, D. W. Impacts of Argo salinity in NCEP Global Ocean Data Assimilation System: The tropical Indian Ocean. **Journal of Geophysical Research**, v. 113, n. C8, p. C08002, 2008.

HYBRID COORDINATE OCEAN MODEL. **HYCOM**: System Description. 2017. Disponível em: <https://www.hycom.org/>. Acesso: 15 September 2017.

LAGERLOEF, G. *et al.* The ocean and the global water cycle. **Oceanography**, v. 23, n. 4, p. 82–93, 2010.

LASS, H. U. *et al.* Hydrographic and current measurements in the area of the Angola–Benguela Front. **Journal of Physical Oceanography**, v. 30, p. 21, 2000.

LIMA, J. A. M. **Oceanic circulation on the Brazilian Shelf- break and Slope at 22°S**. 1997. 164 f. Tese (Doutorado em Matemática Aplicada) - University of New South Wales, Kensington.

LIMA, M. O. *et al.* An assessment of the Brazil Current baroclinic structure and variability near 22°S in distinct ocean forecasting and analysis systems. **Ocean Dynamics**, v. 66, n. 6–7, p. 893–916, 2016.

- MAAMAATUAIAHUTAPU, K. *et al.* Origin and ages of mode waters in the Brazil-Malvinas Confluence region during austral winter 1994. **Journal of Geophysical Research: Oceans**, v. 104, n. C9, p. 21051–21061, 1999.
- MANO, M. F. *et al.* Energy flux to a cyclonic eddy off Cabo Frio, Brazil. **Journal of Physical Oceanography**, v. 39, n. 11, p. 2999–3010, 2009.
- MARCELLO, F.; WAINER, I.; RODRIGUES, R. R. South Atlantic Subtropical Gyre late twentieth century changes. **Journal of Geophysical Research: Oceans**, v. 123, n. 8, p. 5194–5209, 2018.
- MCDONAGH, E. L.; KING, B. A. Oceanic fluxes in the South Atlantic. **Journal of Physical Oceanography**, v. 35, n. 1, p. 109–122, 2005.
- MERCATOR OCEAN. **GLORYS**. 2017. Disponível em: <https://www.mercator-ocean.fr/sciences-publications/glorys/>. Acesso em: 01 October 2017.
- MIGNAC, D.; FERREIRA, D.; HAINES, K. South Atlantic meridional transports from NEMO-based simulations and reanalyses. **Ocean Science**, v. 14, n. 1, p. 53–68, 2018.
- MIGNAC D.; FERREIRA D.; HAINES K. Decoupled Freshwater Transport and Meridional Overturning in the South Atlantic. **Geophysical Research Letters**, v. 46, p. 2178–2186, 2019.
- MÜLLER, T. *et al.* Direct measurements of western boundary currents off Brazil between 20°S and 28°S. **Journal of Geophysical Research**, v. 103, p. 5429-5437, 1998.
- PEDLOSKY, J. The dynamics of the oceanic Subtropical Gyres. **Science**, v. 248, n. 4953, p. 316–322, 1990.
- PEREIRA, J. *et al.* The bifurcation of the Western Boundary Current System of the South Atlantic Ocean. **Revista Brasileira de Geofísica**, v. 32, n. 2, p. 241, 2014.
- REBOITA, M. S. *et al.* The South Atlantic Subtropical Anticyclone: Present and Future Climate. **Frontiers in Earth Science**, v. 7, p. 1-8, 2019.
- RIMAUD, J. *et al.* The exchange of Intermediate Water in the southeast Atlantic: Water mass transformations diagnosed from the lagrangian analysis of a regional ocean model. **Journal of Geophysical Research: Oceans**, v. 117, n. C8, p. C08034, 2012.
- RINTOUL, S. R. South Atlantic interbasin exchange. **Journal of Geophysical Research: Oceans**, v. 96, n. C2, p. 2675–2692, 1991.
- RODRIGUES, R. R.; ROTHSTEIN, L. M.; WIMBUSH, M. Seasonal variability of the South Equatorial Current Bifurcation in the Atlantic Ocean: A numerical study. **Journal of Physical Oceanography**, v. 37, n. 1, p. 16–30, 2007.
- RODRIGUES, R. R. *et al.* South Atlantic mass transports obtained from subsurface float and hydrographic data. **Journal of Marine Research**, v. 68, n. 6, p. 819–850, 2010.

- ROEMMICH, D. *et al.* Unabated planetary warming and its ocean structure since 2006. **Nature Climate Change**, v. 5, n. 3, p. 240–245, 2015.
- ROEMMICH, D. *et al.* Multidecadal change of the South Pacific Gyre Circulation. **Journal of Physical Oceanography**, v. 46, n. 6, p. 1871–1883, 2016.
- ROSSBY, T. On gyre interactions. **Deep Sea Research Part II: Topical Studies in Oceanography**, v. 46, n. 1–2, p. 139–164, 1999.
- RÜHS, S. *et al.* Cold vs. warm water route – sources for the upper limb of the Atlantic Meridional Overturning Circulation revisited in a high-resolution ocean model. **Ocean Science**, v. 15, n. 3, p. 489–512, 2019.
- SCHMID, C.; MAJUMDER, S. Transport variability of the Brazil Current from observations and a data assimilation model. **Ocean Science**, v. 14, p. 417–436, 2018.
- SCHMIDTKO, S.; JOHNSON, G. C. Multidecadal warming and shoaling of Antarctic Intermediate Water. **Journal of Climate**, v. 25, n. 1, p. 207–221, 2012.
- SCHMITT, R. W. The ocean component of the global water cycle. **Reviews of Geophysics**, v. 33, n. S2, p. 1395–1409, 1995.
- SHILLINGTON, F. A. *et al.* Large scale physical variability of the Benguela Current Large Marine Ecosystem (BCLME). In: SHANNON, V.; HEMPEL, G.; MALANOTTE-RIZZOLI, P. **Large Marine Ecosystems**. 14. ed. Elsevier, 2006. p. 49–70.
- SILVEIRA I. C. A. *et al.* A corrente do Brasil ao largo da costa leste brasileira. **Revista Brasileira de Oceanografia**, v. 48, p. 171–183, 2000.
- SOTO-NAVARRO, F. J.; CRIADO-ALDEANUEVA, F. Model thermohaline trends in the Mediterranean Sea during the last years: A change with respect to the last decades? **The Scientific World Journal**, v. 2012, p. 1–8, 2012.
- STORTO, A. *et al.* Ocean reanalyses: Recent advances and unsolved challenges. **Frontiers in Marine Science**, v. 6, p. 1–10, 2019.
- STRAMMA, L. Geostrophic transport of the South Equatorial Current in the Atlantic. **Journal of Marine Research**, v. 49, n. 2, p. 281–294, 1991.
- STRAMMA, L.; ENGLAND, M. On the water masses and mean circulation of the South Atlantic Ocean. **Journal of Geophysical Research: Oceans**, v. 104, n. C9, p. 20863–20883, 1999.
- STRAMMA, L.; IKEDA, Y.; PETERSON, R. G. Geostrophic transport in the Brazil current region north of 20°S. **Deep Sea Research Part A. Oceanographic Research Papers**, v. 37, n. 12, p. 1875–1886, 1990.
- STRAMMA, L.; PETERSON, R. G. The South Atlantic Current. **Journal of Physical Oceanography**, v. 20, p. 846–859, 1990.

- SWINGEDOUW, D. *et al.* Impact of transient freshwater releases in the Southern Ocean on the AMOC and climate. **Climate Dynamics**, v. 33, n. 2–3, p. 365–381, 2009.
- TALLEY, L. D. Ocean Circulation. In: MUNN, R. E. **Encyclopedia of global environmental change**, 1. ed. New York: Wiley, 2002, p. 557-579.
- TAYLOR, K. E. Summarizing multiple aspects of model performance in a single diagram. **Journal of Geophysical Research: Atmospheres**, v. 106, n. D7, p. 7183–7192, 2001.
- THERMODYNAMIC EQUATION OF SEAWATER-2010. **TEOS-10 Software**. 2018. Disponível em: <http://www.teos-10.org/>. Acesso em: 13 March 2018.
- THOMPSON, A. F.; RAHMSTORF, S. Ocean circulation. In: LE QUÉRÉ, C., SALTZMAN, E. S. **Surface Ocean - Lower Atmosphere Processes**. Washington: American Geophysical Union, 2009. p. 99-118.
- THRESHER, R. *et al.* Parallel decadal variability of inferred water temperatures for Northern and Southern Hemisphere intermediate water masses. **Geophysical Research Letters**, v. 41, n. 4, p. 1232–1237, 2014.
- TIM, N. *et al.* The impact of Agulhas Leakage on the Central Water Masses in the Benguela Upwelling System from a high-resolution ocean simulation. **Journal of Geophysical Research: Oceans**, v. 123, n. 12, p. 9416–9428, 2018.
- VIANA, A. R. *et al.* Evidence of bottom current influence on the Neogene to Quaternary sedimentation along the Northern Campos Slope, SW Atlantic Margin. **Geological Society**, v. 22, p. 249–259, 2002.
- WALIN, G. On the relation between sea-surface heat flow and thermal circulation in the ocean. **Tellus**, v. 34, n. 2, p. 187–195, 1982.
- WEIJER W. Response of the Atlantic overturning circulation to South Atlantic sources of buoyancy. **Global and Planetary Change**, v. 34, p. 293–311, 2002.
- WU, L. *et al.* Enhanced warming over the global subtropical western boundary currents. **Nature Climate Change**, v. 2, n. 3, p. 161–166, 2012.
- YAO, W.; SHI, J.; ZHAO, X. Freshening of Antarctic Intermediate Water in the South Atlantic Ocean in 2005–2014. **Ocean Science**, v. 13, n. 4, p. 521–530, 2017.

## ANEXO A – Comprovante de submissão na revista *Ocean Dynamics*

03/03/2020 Gmail - ODYN-D-20-00033 - Ocean Dynamics: Submission Confirmation for Spatial and Temporal Variability of Water Masses in th...



Yhaohannah Lima <yhaohannah@gmail.com>

---

**ODYN-D-20-00033 - Ocean Dynamics: Submission Confirmation for Spatial and Temporal Variability of Water Masses in the Upper Circulation of the South Atlantic**

1 mensagem

---

ODYN Editorial Office <em@editorialmanager.com> 3 de março de 2020 18:20  
Responder a: ODYN Editorial Office <xavier.castanos@springernature.com>  
Para: Antônia Pamela Yhaohannah de Lima <yhaohannah@gmail.com>

Dear Mrs. de Lima,

Your submission entitled "Spatial and Temporal Variability of Water Masses in the Upper Circulation of the South Atlantic" has been received by journal Ocean Dynamics

The submission id is: ODYN-D-20-00033

Please refer to this number in any future correspondence.

You will be able to check on the progress of your paper by logging on to Editorial Manager as an author. The URL is <https://www.editorialmanager.com/odyn/>.

Thank you for submitting your work to this journal.

Kind regards,

Editorial Office  
Ocean Dynamics

PS: If there would be any concern regarding authorship, please contact the Editorial Office.

Now that your article will undergo the editorial and peer review process, it is the right time to think about publishing your article as open access. With open access your article will become freely available to anyone worldwide and you will easily comply with open access mandates. Springer's open access offering for this journal is called Open Choice (find more information on [www.springer.com/openchoice](http://www.springer.com/openchoice)). Once your article is accepted, you will be offered the option to publish through open access. So you might want to talk to your institution and funder now to see how payment could be organized; for an overview of available open access funding please go to [www.springer.com/oafunding](http://www.springer.com/oafunding). Although for now you don't have to do anything, we would like to let you know about your upcoming options.

Recipients of this email are registered users within the Editorial Manager database for this journal. We will keep your information on file to use in the process of submitting, evaluating and publishing a manuscript. For more information on how we use your personal details please see our privacy policy at <https://www.springernature.com/production-privacy-policy>. If you no longer wish to receive messages from this journal or you have questions regarding database management, please contact the Publication Office at the link below.

---

In compliance with data protection regulations, you may request that we remove your personal registration details at any time. (Use the following URL: <https://www.editorialmanager.com/odyn/login.asp?a=r>). Please contact the publication office if you have any questions.